

Acid etching as a surface pre-treatment step for PVD coatings on high strength steels

Manikandan Balasubramanian

Acid etching as a surface pre-treatment step for PVD coatings on high strength steels

by

Manikandan Balasubramanian

to obtain the degree of Master of Science
at the Delft University of Technology
to be defended publicly on January 24, 2020 at 10:00 am

Student number: 4741102
Project duration: December 1, 2018 – January 24, 2020
Thesis committee: Dr. ir. W.G. Sloof, TU Delft, supervisor
Dr. R.J. Westerwaal, TATA Steel-IJmuiden, supervisor
Prof. dr. ir. J. Sietsma, TU Delft
Dr. S.J. Garcia, TU Delft

Acknowledgement

Coming from a mechanical engineering background, this thesis was a novel experience for me. Without the encouragement and constant support from many people, this research wouldn't have been possible. It is with my utmost gratitude that I acknowledge their contributions.

Firstly, I am grateful to my supervisor from TATA Steel, Dr. Ruud Westerwaal. His invaluable guidance through every step of my research work was extremely vital. He has constantly made himself available for discussions regarding every little aspects of my research work, which helped me progress profusely. I would like to express my sincere gratitude towards my supervisor in TU Delft, Dr. Wim Sloof for his faith in me to conduct the research. His positive feedback and suggestions to improve my thesis motivated me to work even harder. His guidance on carrying out the SEM/EDX techniques and XPS analyses was essential in the successful completion of my thesis. I would also like to thank Kees Kwakernaak (TU Delft) to help me clear any doubts on SEM/EDX techniques. I would like to extend my gratitude towards Piet Stoffels and Ruud Pattiasina who helped me conduct the etching experiments and the PVD team, Erwin Bouwens and Christiaan Boelsma, to help me work with the Emely and with whom I had fun discussing football during breaks. Also, special thanks to Jan Pool who conducted SEM/EDX analyses in TATA Steel and the two great 'Winters', Hans and Marcel, who carried out GDOES and contact angle measurements for my work.

They say when you really wish for something from the bottom of your heart, the universe conspires to have it delivered to you. What they mean by universe is the people who support you and push you forward in life, to the path that you always wanted to take. I take this as an opportunity to dedicate this thesis to my parents who are the sole reason why I'm here, at Delft, living my dream. They worked extremely hard to make it possible for me to pursue my dreams and I'm glad that I've made them proud. I'm also eternally grateful to my friends who have stood by me throughout and who have been my family in a land where I would have otherwise been alone.

*Manikandan Balasubramanian
Delft, January 2020*

Abstract

Coating deposition by Physical Vapour Deposition (PVD) on high strength steels is an important research project at TATA Steel - IJmuiden. The research is aimed at replacing the conventional hot-dip galvanisation process to obtain a defect-free coating without affecting their well engineered properties. However, the annealing treatment of the steel, performed to obtain these properties, affects the coating adhesion properties. This is a result of the selective oxidation process, which forms external oxides of alloying elements at the surface. Therefore, a pre-treatment process is required to remove these surface oxides from the steel strips before they are coated. Plasma sputtering is currently being used for the pre-treatment to remove any contaminants and surface oxides from the steel. To obtain a good coating adhesion, a relative large amount of surface oxides needs to be removed by sputtering. Also, the removed material is known to contaminate the vacuum chamber in the PVD deposition line, for which frequent maintenance of the chamber might be necessary. Thus, an additional surface pre-treatment step was investigated in this study to reduce the sputter process inside the vacuum as much as possible. A combination of electrolytic alkaline cleaning and sulphuric acid etching pre-treatment steps was proposed as a surface pre-treatment step in this study.

In the present work, the effect of both direct current electrolytic alkaline cleaning and sulphuric acid etching on the surface of a DP800 steel was investigated. Two different baths were considered for this purpose; a 27 g/L NaOH bath with some additive at 60°C and a 50 g/L H₂SO₄ bath at 25°C and 50°C. A current density of 1.5 A/dm² was applied during the electrolytic cleaning for which both cathodic and anodic polarisation methods were investigated. Also, a range of acid etching times (10s to 120s) was investigated for the given concentration and temperatures of the acid bath to study its effect on the surface. The effect of adding a corrosion inhibitor into the acid bath on the rest of the coating deposition process was also investigated. Various surface characterisation techniques were used to study the effect of this surface pre-treatment step on the surface morphology and surface composition. Surface wettability tests using sessile drop experiments were performed to provide information on how coating adhesion properties vary as a function of the pre-treatment steps. Finally, coating adhesion tests were performed after zinc deposition to investigate the adhesion performance of the steel after the pre-treatment steps.

Initial surface analysis during electrolytic alkaline cleaning showed that the anodic polarisation was more effective than cathodic polarisation of the sample, as the latter tends to reduce the surface wettability by additional deposits of iron fines over the surface. A subsequent acid etching provided a reduction in the minimum required sputter intensity to obtain a good adhesion from 2300 kJ/m² to about 800 kJ/m². A further reduction was achieved to a sputter intensity of only 214 kJ/m² after retarding the effects of surface reoxidation by vacuum sealing the samples. Acid etching at 25°C provided bad coating adhesion at lower etching times, attributed to the partial dissolution of surface oxides and absence of an initial grain roughening. Good coating adhesion was either obtained at higher etching times or by increasing the temperature of the acid bath to 50°C. Addition of a corrosion inhibitor was considered impractical as high sputter intensities (> 321 kJ/m²) were required to remove the adsorbed inhibitor molecules from the surface. Thus, a reduction in the required sputter intensity was achieved by more than a factor of 10 after acid etching, only if the effects of surface reoxidation during the transfer time between acid etching and entering the PVD installation can be minimized.

Contents

List of Figures	ix
List of Tables	xi
1 Introduction	1
1.1 Automotive steels	1
1.2 Processing of automotive steels	1
1.3 Problem definition - Surface pretreatment for PVD	3
1.4 Research questions	4
1.5 Structure of the report	5
2 Theory	7
2.1 Surface treatment processes	7
2.1.1 Electrolytic alkaline cleaning	7
2.1.2 Acid etching	8
2.1.3 Argon ion sputtering	10
2.2 Physical Vapour Deposition - Coating process	10
3 Experimental setup and analysis techniques	13
3.1 Experimental setup	13
3.2 PVD coating chamber setup	14
3.2.1 Schematic of the PVD chamber	15
3.2.2 Coating deposition	15
3.3 Methods used for surface characterisation of the steel	17
3.3.1 SEM and EDX analyses	17
3.3.2 GDOES depth profile analysis	18
3.3.3 XPS analysis	19
3.3.4 IR spectroscopy	19
3.4 Surface wettability analysis	19
3.5 Adhesion tests	20
3.5.1 OT bending test	20
3.5.2 BMW crash test	22
4 Results and Discussion	25
4.1 Analysis of surface-treated DP800 samples	25
4.1.1 Characterisation of degreased DP800 substrate	25
4.1.2 Effect of electrolytic alkaline cleaning	30
4.1.3 Effect of sulphuric acid etching	37
4.1.4 Effect of corrosion inhibitor	51
4.2 Analysis of coated DP800 samples	55
4.2.1 Minimum required sputter intensity	55
4.2.2 Effect of substrate temperature on coating adhesion	56
4.2.3 Effect of surface pre-treatment process on coating adhesion	59

4.2.4	Effect of corrosion inhibitor during the pre-treatment process on coating adhesion	67
5	Conclusions	71
6	Recommendations	73
A	Ellingham diagram and Diffusion of alloying elements	75
A.1	Ellingham diagram - Possible region for RTF process	75
A.2	Diffusion of alloying elements	76
B	EDX results	79
C	Contact angle vs Exposure Time measurements	87
	Bibliography	89

List of Figures

1.1	Growth and reduction of Wüstite scale during annealing	2
1.2	Material removal rate as a function of strip speed	4
2.1	Changes in coating microstructure as a function of substrate temperature	11
3.1	Experimental setup for surface pre-treatment process	14
3.2	Schematic of the PVD coating chamber	15
3.3	Two steel strips placed on carts equipped with magnets	16
3.4	Final zinc coated DP800 substrate using PVD coating deposition	17
3.5	Depth of analysis for different signals emitted from the surface of the sample	18
3.6	Schematic of sessile drop experiment	20
3.7	Bended OT test specimen	21
3.8	OT test specimens showing OK and NOK adhesion	21
3.9	Bended part of a BMW crash test specimen	22
3.10	BMW test specimens showing OK and NOK adhesion	23
4.1	SEM image of an untreated DP800 sample	26
4.2	Presence of particles and a cluster of particles on an untreated DP800 sample	26
4.3	GDOES depth profile plots of an untreated DP800 sample at different scales	27
4.4	XPS spectrum of an untreated DP800 substrate (BE - 500 to 750 eV)	28
4.5	XPS spectrum of an untreated DP800 substrate (BE - 40 to 120 eV)	29
4.6	Comparative IR spectra of untreated, anodic cleaned and cathodic cleaned DP800 samples	31
4.7	Discolouration of a cathodic cleaned DP800	31
4.8	SEM image on the discoloured part over a cathodic cleaned DP800 substrate	32
4.9	Comparative surface morphologies of electrolytic alkaline cleaned DP800 substrates	33
4.10	Comparative GDOES depth profile results of untreated and anodic cleaned DP800 substrates	34
4.11	Comparative XPS spectra of untreated DP800 and anodic cleaned DP800 substrates (BE - 500 to 750 eV)	35
4.12	Comparative XPS spectra of untreated DP800 and anodic cleaned DP800 substrates (BE - 40 to 120 eV)	36
4.13	Weight loss of acid etched DP800 substrates with temperature and concentration	38
4.14	Surface changes taking place in a DP800 substrate with increasing etching time in a 25°C dilute H ₂ SO ₄ bath	40
4.15	Disappearance of particles and clusters taking place with increasing etching time	41
4.16	Non-uniform surface roughness observed in a DP800 substrate with increasing etching time	43
4.17	Variations in surface roughness between two different grains in a 30s acid etched DP800 substrate	43
4.18	Charge transfer taking place across the Helmholtz double layer	45
4.19	Comparative GDOES depth profile results of untreated, anodic cleaned and acid etched DP800 substrates	47

4.20	Low temperature oxidation mechanism in metals	48
4.21	Comparative XPS spectra of anodic cleaned DP800, untreated DP800 and acid etched DP800 taken 20 days after the treatment (BE - 500 to 750 eV)	49
4.22	Comparative XPS spectra of anodic cleaned DP800, untreated DP800 and acid etched DP800 taken 20 days after the treatment (BE - 40 to 120 eV)	50
4.23	Comparative weight loss results for inhibited and uninhibited samples etched in dilute H ₂ SO ₄ bath at 50°C	51
4.24	Comparative analysis of uninhibited and inhibited DP800 samples	53
4.25	Presence of nano-scale particles over the surface after etching with dilute H ₂ SO ₄ at 50°C with 150 µL/L inhibitor for 120s	54
4.26	GDOES plots of carbon and sulphur between uninhibited and inhibited DP800 samples	54
4.27	Temperature evolution of the substrate with increasing sputter time for a sputter power of 200 W	57
4.28	Microstructural evolution of the coating material with increasing substrate temperature	58
4.29	Etching time vs Sputter intensity plots for DP800 samples etched in a 25°C dilute H ₂ SO ₄ bath	60
4.30	Comparative acid etching time vs Sputter intensity plots for adhesion tests with and without vacuum sealing	62
4.31	Delaminated part of the BMW test results of a strip etched for 10s in a 25°C acid bath and sputtered at 214 kJ/m ²	63
4.32	SEM images of the delaminated parts	63
4.33	SEM image of a flake-like substance over the adhesive part	64
4.34	SEM image of the substrate part at higher magnifications	64
4.35	Etching time vs sputter intensity plots for vacuum sealed for DP800 samples etched in a 50°C dilute H ₂ SO ₄ bath	66
4.36	Surface morphology of the final coated microstructure of DP800 substrates etched at different etching times	67
4.37	Acid etching time vs Sputter intensity plots for inhibited samples	68
4.38	Inhibited samples etched for 120s in dilute H ₂ SO ₄ bath at 50°C with 150 µL/L inhibitor with increasing sputter intensity	70
A.1	Ellingham diagram	76
B.1	EDX analysis of untreated DP800 sample	79
B.2	EDX analysis of a cathodic cleaned DP800 sample	80
B.3	EDX analysis of an anodic cleaned DP800 sample	81
B.4	EDX analysis of an acid etched DP800 sample etched for 10s in a 25°C dilute H ₂ SO ₄ bath	82
B.5	EDX analysis of an acid etched and inhibited DP800 sample etched for 120s in a 50°C dilute H ₂ SO ₄ bath with 150 µL/L inhibitor added	83
B.6	EDX analysis of a flake-like substance over the adhesive part of the delamination	84
B.7	EDX analysis of the substrate part of the delamination	85
C.1	Contact angle vs Exposure time for DP800 samples etched in a 25°C dilute H ₂ SO ₄ bath for 60s	87
C.2	Contact angle vs Exposure time for DP800 samples etched in a 25°C dilute H ₂ SO ₄ bath for 60s without a rinsing step	88

List of Tables

3.1	Composition of alloying elements in DP800 HCT780X	13
3.2	Specifications for 0T bending test	21
3.3	Specifications for BMW crash test	23
4.1	Binding energies of the corresponding XPS spectra of individual elements	29
4.2	Variations in contact angle measured between an untreated DP800 substrate with electrolytically cleaned DP800 substrates	32
4.3	Comparative binding energies of the spectra obtained in Figure 4.11	35
4.4	Comparative binding energies of the spectra obtained in Figure 4.12 (Si and Cr)	36
4.5	Dissolution rates for acid etched DP800 substrates with increasing acid bath temperature (in °C)	39
4.6	Dissolution rates for acid etched DP800 substrates with increasing acid concentration (in g/L)	39
4.7	Variations in contact angle with increasing etching time for DP800 substrates etched in a 25°C dilute H ₂ SO ₄ bath	44
4.8	Binding energies of Fe 2p _{3/2} and O 1s on an acid etched DP800 substrate etched for 60s in a 25°C dilute H ₂ SO ₄ bath	49
4.9	Binding energies of alloying elements on an acid etched DP800 substrate etched for 60s in a 25°C dilute H ₂ SO ₄ bath	50
4.10	Variations in contact angle with increasing etching time for DP800 substrates etched in a 25°C dilute H ₂ SO ₄ bath with 150 μL/L inhibitor	52
4.11	Adhesion test results on coated DP800 substrates pre-treated with decreasing plasma sputter intensity	56
4.12	Adhesion test results of DP800 substrates coated at increasing substrate temperatures	57
A.1	Gibbs free energy of oxide formation for major alloying elements	76
B.1	Atomic fractions (At%) of major elements for points in Figure B.1	79
B.2	Atomic fractions (At%) of major elements for points in Figure B.2	80
B.3	Atomic fractions (At%) of major elements for points in Figure B.3	81
B.4	Atomic fractions (At%) of major elements for points in Figure B.4	82
B.5	Atomic fractions (At%) of major elements for points in Figure B.5	83
B.6	Atomic fractions (At%) of major elements for points in Figure B.6	84
B.7	Atomic fractions (At%) of major elements for points in Figure B.7	85

1

Introduction

1.1. Automotive steels

Advanced high strength steels (AHSS) are a typical classification of low-carbon steels with an exceptional combination of formability, weldability and strength [1]. Research studies on AHSS are fulfilling the state-of-the-art requirements of a light-weight, efficient, economic and a crash resistant vehicles in recent years.

Typical AHSS are classified as Dual phase (DP) steels, Transformation-Induced plasticity assisted (TRIP) Steels, bainitic steels, martensitic steels, and Twinning-Induced plasticity (TWIP) steels [2]. Among these AHSS, Dual phase steels are the most conventionally used steels in the automotive body panels. The microstructure of DP steels consists of a soft ferrite matrix surrounded by uniformly distributed islands of a secondary phase. The secondary phase can be martensitic or a combination of martensitic and retained austenitic or bainitic phases [3], depending upon their heat treatment and the amount of alloying elements added during steel-making. Thus, combination of better elongation at higher tensile strength with excellent formability, attributed to its high work hardening rates, and excellent crash resistance and toughness can be achieved using DP steels [2][4].

This research study is limited to a typical DP steel, which has an ultimate tensile strength of about 780 MPa and yield strength of about 480 MPa. The major alloying elements present in the steel are Mn, Si and Cr. These alloying elements promote the growth and stabilisation of different phases in the steel [5][6], leading to enhancements in microstructural and mechanical properties of the steel. However, these alloying elements pose a challenge to the coatability of the steel substrate by forming additional surface oxides during the annealing process, which will be discussed further in Section 1.2.

1.2. Processing of automotive steels

Processing of DP steels generally involve hot rolling of the steel strips, surface treatment to remove thick oxides, cold rolling for thickness reduction, a continuous annealing process to refine the grains and to obtain the desired microstructure, and then an optional coating process on the steel substrate. The coating processes may involve hot dip galvanisation or galvannealing process in a hot zinc melt alloyed with some aluminium or a Galfan process involving additions of magnesium in the zinc-aluminium melt [7]. Of all these five processes, annealing plays a major role in our study as it is known to influence the final surface morphology and surface composition of the steel substrate, which might further influence the coatability of the steel.

Annealing is generally performed in two steps as explained by Mao et al. [8] in his study. First, the steel strips are subjected to an oxidising atmosphere in a Direct flame Furnace (DFF) where a layer of Wüstite (FeO) forms over the surface due to high temperature oxidation. Then the strips are transferred into a Radiant Tube Furnace (RTF) where a reducing atmosphere, composed of nitrogen (N_2) mixed with hydrogen (H_2), is maintained to remove the Wüstite layer from the surface. In some cases, a full RTF process is performed during annealing without a DFF step, where the strips will be subjected to a reducing atmosphere to remove an initially formed iron oxide layer over the substrate after cold rolling. A certain dew point is maintained during the RTF process by introducing water vapour in the furnace, which can also assist in the decarburising of the steel strips.

The reducing atmosphere for iron oxide inside the RTF will not be reducing other alloying element oxides (Figure A.1). Depending upon the dew point atmosphere maintained in the RTF, oxides of alloying elements tend to form over the surface of the steel strips as external oxides or within the sub-surface layers of the bulk as internal oxides as explained by Wagner's model for selective oxidation [9][10][11]. This happens due to variations in the flux of oxygen atoms at the surface of the steel strips which is related to the oxygen partial pressure and thus the dew point temperature maintained within the furnace. The higher the dew point temperature, the higher the partial pressure of oxygen and thus the higher the flux of oxygen atoms at the surface of the steel strips. This will initiate a faster inward flow of oxygen towards the steel surface from a high concentration region to a low concentration region within the bulk, diffusing oxygen atoms into the bulk to react with alloying elements to form internal oxides at sub-surface layers. At lower dew point atmospheres, a reverse diffusion process can take place where outward flow of alloying elements is faster, which tend to diffuse towards the surface due to thermal activation to react with oxygen atoms at the surface forming external surface oxides. Figure 1.1 shows a schematic of the internal or external surface oxides formed during the annealing step.

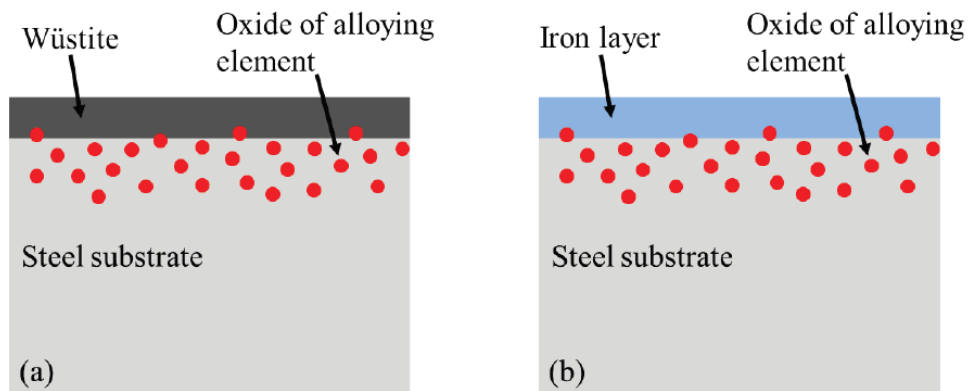


Figure 1.1: (a) Growth of Wüstite scale and internal oxides of alloying elements after the DFF step in the annealing process (b) Reduction of Wüstite scale and segregation of other alloying elements to form external or internal oxides after the RTF step in the annealing process - Mao et al. [8]

In general, after the annealing process, the steel strips can be galvanised, which will be done by a conventional hot dip galvanising (HDG) line or an electroplating line. However, these conventional coating processes have their limitations,

- Hot dip galvanisation involves immersing the steel strips in a hot zinc melt, which is maintained at temperatures of about 460°C . This may lead to microstructural changes in the steel substrate, which may further influence its mechanical properties. Furthermore, studies by

Fernandes et al. [12] and Carpio et al. [13] suggest the possibilities of liquid metal embrittlement during hot dipping processes which induces intergranular cracking within the steel substrate after further processing.

- Electroplating involves high energy consumption and environmental pollution [14] as the electrolytic solution used during the process has to be readily disposed off, which causes environmental concerns. Also concerns regarding diffusion of hydrogen into the steel substrates to cause hydrogen embrittlement were also evident from studies reported by Carr et al. [15].
- Further coating developments by alloying pure zinc with magnesium and implementing bilayered Zn - Zn-Mg coatings to improve corrosion resistant properties cannot be achieved with these conventional coating techniques due to heavy dross formation and difficulties in implementing multilayered coating using HDG and high costs involved in electrodeposition techniques. [16].

Thus, an alternative coating technology was developed, namely the Physical Vapour Deposition (PVD) process, which is a low temperature coating technique, allowing the possibilities of multilayered coatings with a large variety of coating compositions on the steel substrate and minimizing the drawbacks of conventional hot dip galvanising and electroplating techniques.

1.3. Problem definition - Surface pretreatment for PVD

Prior to the PVD zinc coating deposition over the surface of the steel substrate, a proper surface treatment needs to be applied to remove any contaminants or external surface oxides present on its surface. This will activate the steel surface to obtain a proper coating with no delamination. Currently, the PVD coating process uses an argon ion sputtering process, which produces plasma through ionisation of argon gas in a plasma sputter unit. The argon ions bombard over the target material at high energies to remove any contaminants or oxides present on the surface of the material. However, the sputtering process has certain drawbacks. The material to be coated requires high sputter intensities for surface oxides or contaminants to be removed, as the sputter rate used during the process is low (about 0.2 nm/s [17]). Also, the removed material from the plasma sputter unit is known to contaminate the vacuum chamber, due to which the treatment process may not be feasible enough in a continuous process line for large scale coating of steel strips. Borst et al. [18] calculated the rate of material removal with respect to the sputter depth, for a strip length of 1.75 m in length which was sputtered at various strip speeds. Figure 1.2 shows the rate of material removal of the 1.75 m strip vs the strip speed as a function of surface thicknesses being removed.

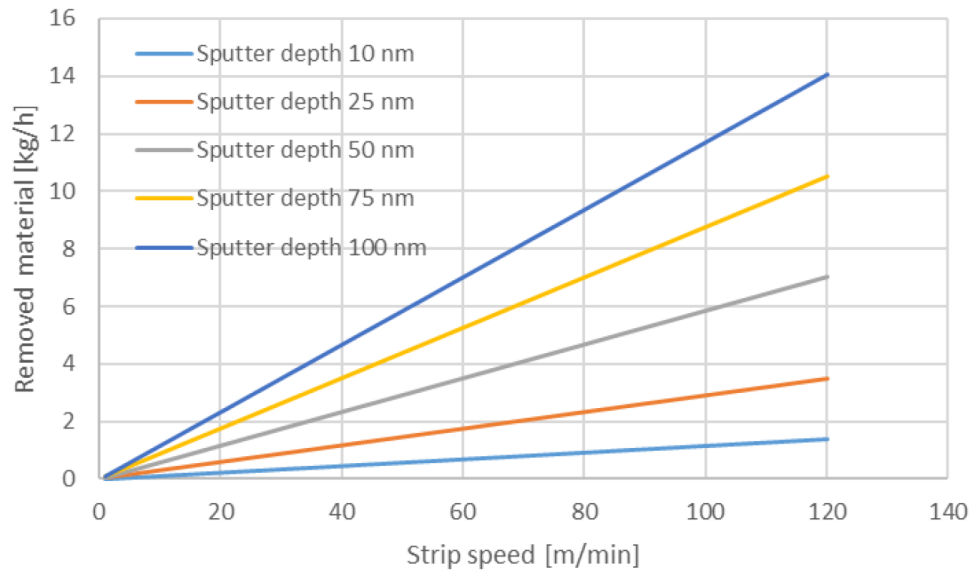


Figure 1.2: Material removal rate as a function of strip speed - Borst et al. [18]

For a sputter depth of about 100 nm and a strip speed of about 50 m/min, 6 kg of material is being removed per hour of sputtering. Thus, in one day, about 144 kg of material may settle as residues inside the PVD coating chamber. This may not be feasible in a continuous production line as frequent maintenance of the PVD deposition line will be required to remove the residues off the chamber to reduce the effects of contamination inside the chamber.

Thus, a surface pre-treatment needs to be developed prior to the sputtering process to reduce the minimum required intensity of sputtering as much as possible. A possible pre-treatment step might involve the application of acid etching after an electrolytic alkaline cleaning step to chemically dissolve the oxides and contaminants present on the surface. Acid etching will dissolve the surface oxides present over the steel after the annealing process. An alkaline cleaning pre-treatment will be integrated as a preliminary step to remove organic contaminants from the surface. Thus a combination of both will be investigated for their effect on the surface characteristics of the steel substrate for their effect on the surface characteristics of the steel substrate prior to the PVD coating deposition process.

1.4. Research questions

Since two different processes, namely, electrolytic alkaline cleaning and sulphuric acid etching will be investigated in this work, the aim of the study is answering the main research question:

Is a combination of electrolytic alkaline cleaning and sulphuric acid etching an effective surface pre-treatment step for PVD coating deposition process?

To answer the main research question, the following sub-questions must be addressed:

- How do the different types of electrolytic alkaline cleaning influence the surface of a DP800 steel substrate?
- How does acid etching process influence the microstructure and surface chemical composition of a DP800 substrate? How do they change with changes in the acid parameters?
- How does the addition of a corrosion inhibitor to the acid etching bath influence the PVD coating deposition process?

- What are the challenges involved in transferring the substrate from the pre-treatment step to the PVD coating chamber?
- What are the surface changes taking place in the final coating microstructure due to the proposed treatment?
- Does temperature of the substrate before the coating deposition play a role on the coating properties?

1.5. Structure of the report

The report is divided into 5 chapters. Chapter 2 discusses the theoretical information regarding different surface treatment processes and the PVD coating method. Chapter 3 describes the required experimental setup for surface treatment processes and PVD coating as well as the analysis techniques used for surface characterisation of the treated and coated samples. Chapter 4 describes the results obtained through these analysis techniques for both coated and uncoated substrates and discussions as to why these results are obtained. Chapter 5 covers the conclusions for the study and Chapter 6 expanding on the conclusions by suggesting some recommendations.

2

Theory

In this chapter, relevant theoretical information about various surface treatment processes such as electrolytic alkaline cleaning, acid etching and magnetron sputtering will be discussed to study their basic methodology and their applications. Also, the process of Physical Vapour Deposition (PVD) will be discussed and its application of coating deposition on dual-phase steels will be discussed in this chapter.

2.1. Surface treatment processes

Three different surface treatment processes will be discussed in this study,

- Electrolytic alkaline cleaning
- Acid etching
- Argon ion sputtering

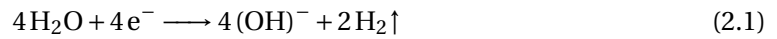
2.1.1. Electrolytic alkaline cleaning

Alkaline cleaning is a preliminary step for cleaning steel strips to remove iron fines and organic residues present on the surface of the strip as contaminants. Residues such as grease and waxes during processing or preservation oils to prevent corrosion during transportation are common sources by which organic contaminants are present over the steel surface. Removal of these contaminants is a necessary pre-cleaning step as they are known to affect the coating adhesion properties of the base metal by intruding during the application of any external metallic or polymeric coating over the base material.

A dilute solution of sodium hydroxide (NaOH) is the most commonly used alkali solution during the cleaning process of general low carbon steel strips [19]. Electrolysis is often introduced during the alkaline cleaning process to increase the cleaning efficiency. Electrolysis is a process of application of a direct current through an ionic solution to induce a chemical change. It induces a scrubbing action on the surface of the metal by evolution of gases at the surface, which removes the contaminants more effectively. Two methods were derived from the electrolytic cleaning process by the application of a direct current [19] [20],

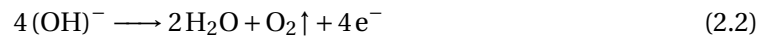
- Cathodic cleaning - Cathodic cleaning is done by applying a negative potential to the sample immersed in the electrolyte, the anode being the counter electrode. Since it is a cathodic reaction, the surface gains electrons from the solution to liberate hydrogen gas at the surface,

which helps in the removal of contaminants,



A major drawback of the cathodic cleaning process is the possible redeposition of iron fines on the surface of the substrate after the treatment, as the substrate tends to attract ferrous ions which might be present as contaminants in the alkaline bath [21]. Also, due to the release of hydrogen at the surface, hydrogen embrittlement within the substrate is possible [19][22].

- Anodic cleaning - Anodic cleaning or reverse current cleaning is done by applying a positive potential to the strip immersed in an alkaline electrolyte; the cathode being the counter electrode. In this process, oxygen liberation takes place at the surface due to the action of hydroxyl ions, which discharge electrons at the surface from the following anodic reaction,



Thus, it assists in the removal of smuts and hydrocarbon residues from the metal surface by the scrubbing action of oxygen liberated at the surface, which removes the organic residues from the surface [19]. Proper control of current density is required to avoid excessive oxidation effects on the surface.

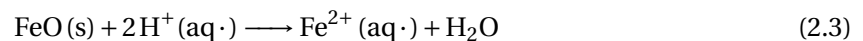
Even though the volume of gas released for the scrubbing action is more for the cathodic cleaning process, anodic cleaning is preferred under standard industrial conditions as problems due to redeposition of iron fines over the surface can be prevented in the latter case [19][21].

A third method is also derived from electrolysis where alternating current is used instead of direct current to alternate the polarisation of samples between anodic and cathodic at regular intervals of time. This method is also called periodic reverse current cleaning and it was proven to be more efficient than direct current electrolytic cleaning processes as it combines the advantages of both anodic and cathodic direct current cleaning [21][19].

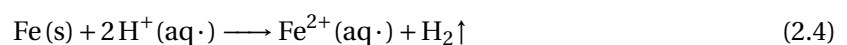
This study focuses on the application of direct current electrolytic cleaning processes and hence the effect of anodic and cathodic cleaning on the surface characteristics of steel substrates will be studied.

2.1.2. Acid etching

Acid cleaning or acid etching is a common technique used for the removal of oxide scales from the metal surface either by immersing the sample in an acid bath or by spraying them on the surface at a certain concentration and temperature of the acid solution [20]. Acid etching of steel generally involves a reductive dissolution mechanism of iron oxides present at the surface, where attack of H^+ ions over these oxides lead to the formation of aqueous ferrous ions which further dissolves into the acid solution as studied by Gines et al. [23],



After oxide dissolution, the acid attack prolongs by attacking the base metal substrate as follows,



In the present work, acid etching is performed after the electrolytic alkaline cleaning step. This was done because the residues present as oil or grease over the surface of the sample cannot be dissolved

effectively only by acid etching.

The dissolution rate during the etching step can be calculated by the weight loss taking place per unit surface area at a given time period for which the equation appears to be similar to corrosion rate equation for general weight loss measurement techniques,

$$k = \frac{W_o - W_f}{\rho A t} \quad (2.5)$$

where,

k = Reaction rate (cm/s)

W_o = Original weight of the substrate (g)

W_f = Final weight of the substrate (g)

ρ = Density of the substrate (g/cm³)

A = Surface area of the acid treated substrate (cm²)

t = Etching time (s)

Gines et al. [23] studied the pickling kinetics of hot-rolled mild steel in hydrochloric acid and reported that the rate of dissolution of surface oxides varied exponentially with the acid temperature and polynomially with the acid concentration. However, in the present work, a cold rolled and annealed DP steel substrate will be used, where the surface oxides are inhomogeneous and their morphologies tend to vary (will be discussed in Section 4.1.1). Also the thickness of these oxides tends to be low (nano-scale oxides). Therefore, the study investigates whether these methods can also be applied for cold rolled and annealed DP steels.

Effect of corrosion inhibitors on acid etching

Over-etching can occur during the etching process when the acid attacks the base metal after complete dissolution of oxides from the steel surface (Equation 2.5). In case of steels with non-uniform oxide thickness, the acid attack on the metal substrate may even occur after partial dissolution of surface oxides. The effect of over-etching might be disadvantageous to the steel substrates due to possible diffusion of H⁺ ions into the grain boundary regions which may induce hydrogen embrittlement and intergranular corrosion within the steel substrates. The attack of H⁺ ions on the grains might even initiate grain dissolution on the steel substrate, making the steel more rough. Thus, the addition of a corrosion inhibitor in the acid bath is necessary to prevent over-etching and to achieve proper control over oxide dissolution.

Inhibitors act as a protective layer on the metal surface by adsorption. The mechanism of adsorption of organic inhibitors on the metal surface is by a substitution process between the inhibitor molecules dissolved in the acid bath and the water molecules adsorbed over the metal surface within the bath [24][25]. This prevents the metal atoms to react with the adsorbed water molecules to dissolve as cations in the aqueous solution.



The adsorption of the inhibitor molecules on the surface can be physical or chemical, depending upon the chemical structure of the molecule, nature and distribution of charge, pH of the solution and other chemical factors.

Studies show that the derivatives of functional groups such as amines, triazoles and pyridine are effective against corrosion of steels in a hydrochloric acid media [25]. Thiourea derivatives are known to be effective against corrosion in a sulphuric acid media [24][26]. The study uses a thiourea derivative (N,N'-diethylthiourea) as a corrosion inhibitor.

2.1.3. Argon ion sputtering

Sputtering is a process by which physical vaporisation of atoms from the surface of a target material takes place due to the bombardment of ionised gaseous atoms (typically Argon ions) [27]. In this study, argon gas supplied between an anode and a grounded cathode is ionised by the application of a potential difference between them. These ions then bombard the steel surface by high momentum transfer between the argon ions and the atoms at the surface, which knocks out the surface atoms and removes the topmost layer.

This study implements a magnetron sputtering unit which uses magnetic bars attached to the copper box to create a magnetic field that traps the free electrons near the surface of the substrate to create a dense electron cloud [28]. This increases the efficiency of the sputtering process as they tend to increase the concentration of ionised Ar atoms to bombard the surface of the substrate.

The sputter unit is implemented internally in the PVD process as a surface pre-treatment process for the steel substrate before coating deposition. This activates the surface by removing the surface oxides and contaminants just before the coating deposition takes place. Also, the temperature of the substrate increases due to energy transfer from the bombarding argon ions to the substrate before the coating process takes place. This will further affect the final coating microstructure and its adhesion properties, which will be discussed in detail in Section 2.2 and Section 4.2.

2.2. Physical Vapour Deposition - Coating process

Physical Vapour Deposition (PVD) is a low temperature coating process, where a metal (or an alloy) is vaporized from a solid or a liquid state and transported through vacuum to deposit on a substrate (steel substrate) and condense, forming a thin uniform layer on the surface of the substrate [27]. The process can offer better coating properties for higher grades of steel such as the deposition of multi-layered coatings, coatings with large compositional variations, better adherence to the steel substrate, better surface finish and corrosion resistance compared to the conventional hot dipping and electroplating techniques [14][16].

TATA Steel develops a PVD coating deposition process, where the source material is placed in a crucible to melt and vaporise in an induction coil. Then the vapours rise towards a Vapour Deposition Box (VDB), which distributes the vapours uniformly along the surface of the target material to be coated. The vapours then condense immediately over the surface to form a thin uniform coating over the target.

Several factors are involved in this process that affects the coating adhesion properties of the material to be coated. One of the major factors involved is the effect of substrate temperature, which will be investigated in this study. Vapour atoms which are incident on the target material during deposition, tend to occupy lattice sites over its surface by a hopping diffusion mechanism. This requires that the target material is at a high energy state to facilitate the diffusion of the vapour atoms to occupy those sites. At lower substrate temperatures, the energy available for the atoms to overcome the activation barrier for diffusion is not enough. This might influence the flux of the atoms distributed over the surface, thus growing local asperities, which results in flux shadowing to form pores at the interface [29]. Studies by Thornton et al. [30] also reported changes in the final microstructure of coatings deposited on metal substrates as a function of the substrate temperature as shown in Figure 2.1. The study observed smaller grains with open grain boundaries at lower substrate temperatures, which was explained by the lower surface diffusibility of the vapour atoms.

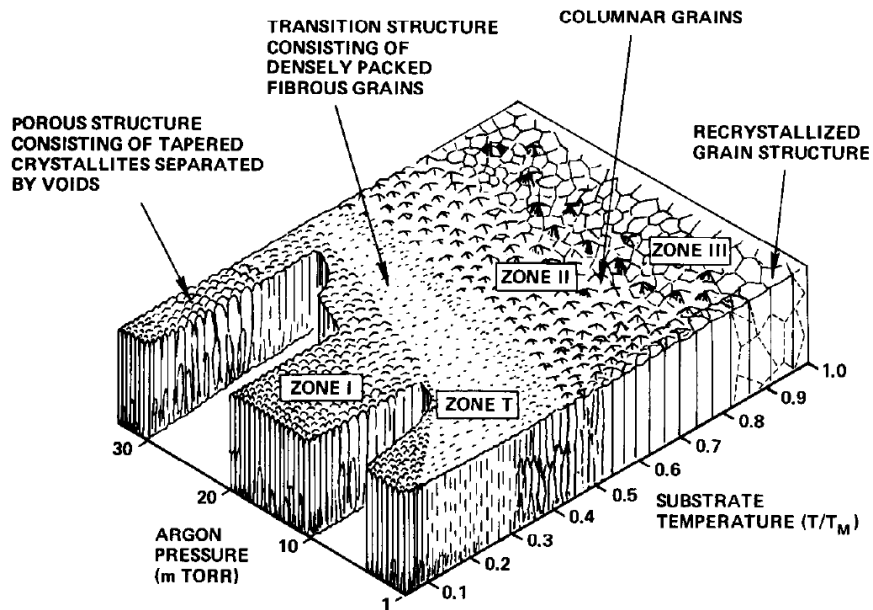


Figure 2.1: Changes in coating microstructure as a function of substrate temperature - Thornton et al. [30]

Thus, the substrate temperature plays a crucial role in the surface diffusion process of the vapour atoms and growth of the microstructure of the coating. The higher the substrate temperature, the higher will be the energy available for the atoms to diffuse towards the lattice sites and better will be the coating adhesion over the target material.

In this study, the effect on the final coating microstructure with the substrate temperature will be investigated and its effect on the adhesion of the coating material over the substrate will be studied accordingly.

3

Experimental setup and analysis techniques

The steel used for this research purpose is a dual phase steel with a thickness of 0.9 mm, an ultimate tensile strength of about 780 MPa and a yield strength of about 480 MPa [31]. It also known as a cold-rolled DP800 UC (uncoated DP800 (HCT 780X)) with the composition of major alloying elements given in Table 3.1 (determined using GDOES depth profile analysis at larger depths),

Table 3.1: Composition of alloying elements in DP800 HCT780X

Element	Mn	Si	Cr	Al
Wt%	1.8	0.2	0.6	0.04

The steel substrate was then cut into strips of dimensions 16.5 cm x 10 cm x 0.09 cm for coating deposition using the PVD setup.

3.1. Experimental setup

The experimental setup consists of an alkaline bath and an acid bath. The alkaline bath contains a standard 27g/L NaOH solution with 8.1mL/L Unisurfa KB-35 additive as a surfactant. Two stainless steel plates were immersed in the alkaline solution, which act as electrodes in the electrolysis process. A DC power source was used for electrolytic cleaning of the sample with a standard current density of 1.5 A/dm². Heaters were equipped for the bath which maintains a standard temperature of about 60°C. The acid bath was a dilute solution of sulphuric acid (H₂SO₄) maintained at a standard concentration of about 50 g/L. Figure 3.1 shows the setup for electrolytic alkaline cleaning and acid etching.

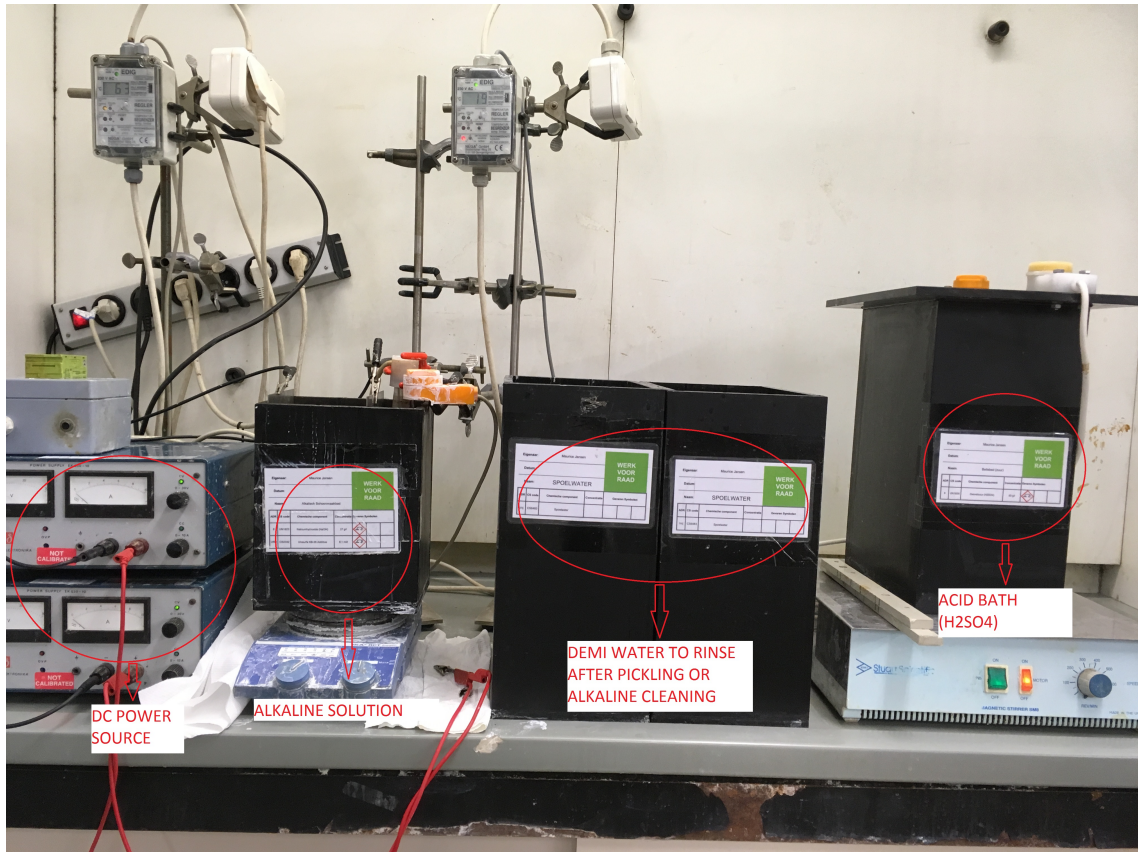


Figure 3.1: Experimental setup for surface pre-treatment process

To investigate the effect of corrosion inhibitor, a separate glass beaker was used to prepare an acid bath with $150\mu\text{L}/\text{L}$ Leuzolit 282-S-6/50 inhibitor for which the main component was $\text{N,N}'$ -diethylthiourea. The concentration was based on the results obtained by Singh (1993) [26] who reports an inhibition efficiency of about 90% for $\text{N,N}'$ -diethylthiourea on pickling of mild steel substrates in a 1N H_2SO_4 solution at 40°C . In this study, the inhibition efficiency might vary with the type of steel substrates used and variations in the acid bath parameters.

DP steel samples of dimensions $16.5\text{ cm} \times 10\text{ cm} \times 0.09\text{ cm}$ were first degreased with isopropanol and treated electrolytically in the alkaline solution by the application of either positive or negative potential, corresponding to either anodic or cathodic polarisation of the sample respectively. A rinsing step using demineralised water was then followed to remove the remnants of the alkaline solution over the steel surface. After choosing an appropriate alkaline cleaning method (which will be discussed in Section 4.1), the steel strips were dipped for various acid etching times in dilute sulphuric acid bath for which the acid bath temperature was maintained at 25°C and 50°C . The etching times varied between 10s to 120s. After the immersion in the acid bath, the strips were immediately dipped in a very dilute solution of NaOH to neutralise any remaining acid over the surface and then rinsed using demineralised water. The strips were then dried by a flowing air jet over the surface.

3.2. PVD coating chamber setup

The PVD setup used in this study was discussed as reported by Westerwaal et al. [28] and [17] and the following descriptions are based on these reports.

3.2.1. Schematic of the PVD chamber

TATA Steel uses Emely, a PVD coating chamber which uses a thermal evaporation method to deposit the coating material over the steel substrates. A schematic of the PVD coating chamber is depicted in Figure 3.2. It mainly consists of a plasma sputter unit, a coating deposition unit and continuously traversing steel strips assisted by rollers, over which the coating deposition takes place. In the present work, the steel samples to be coated are placed on individual carts which are transported through the rollers via a thin traversing strip. The chamber is maintained at a very high vacuum environment of about 10^{-4} mbar.

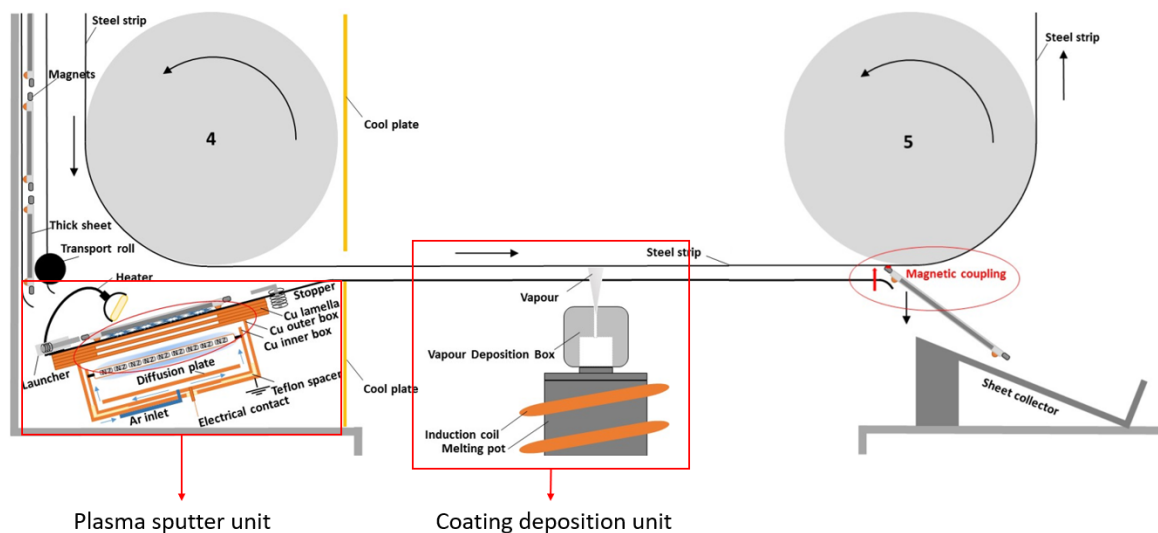


Figure 3.2: Schematic of the PVD coating chamber - Ref Source - Bouwens et al. [28]

The plasma sputter unit consists of an inner and outer copper box, for which the inner box acts as an anode and the outer box being grounded. Argon gas inlet is provided for plasma generation within the box and a diffusion plate is provided underneath to distribute the argon gas evenly throughout the box. Magnets are placed in certain orientation to trap the free electrons, which increases the concentration of Ar^+ ions after the ionisation process to increase the efficiency of sputtering. Sputter rates between 0.15 ± 0.07 nm/s to 0.33 ± 0.07 nm/s can be achieved during the process [17]. An infrared heater is provided over the sputter unit as an optional pre-heating source for the substrate before coating deposition. The heater will be used in case of low sputter intensities to increase the substrate temperature, which will be discussed later in Chapter 4.

The coating deposition unit consists of a crucible in which the zinc is placed. The pot is heated using an induction coil which then melts and vaporises the zinc. Coating deposition on the steel substrate is performed using a Vapour Deposition Box (VDB) placed above the pot which distributes the zinc vapours evenly over the surface. The VDB is pre-heated to temperatures above the zinc melting point to prevent vapour condensation. Ideal zinc coatings were obtained at melt temperatures of about 650°C for which the VDB was pre-heated to about 750°C to 900°C .

3.2.2. Coating deposition

Acid etched steel strips were placed on carts of dimensions 33 cm x 17 cm and the coating was deposited on two steel strips simultaneously as shown in Figure 3.3.

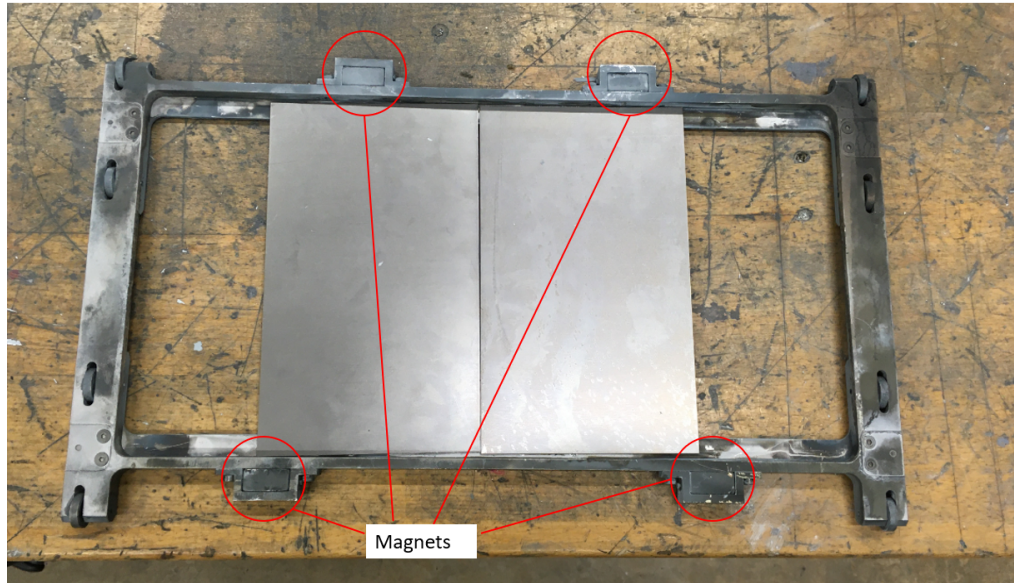


Figure 3.3: Two steel strips placed on carts equipped with magnets

The gaps on the carts were covered using other steel strips and sealed using a metallic tape. Magnets were equipped on the carts, which assist in the transportation of the cart from the plasma sputter unit to the coating deposition unit via magnetic coupling with the thin steel strip, which is constantly traversing inside the PVD chamber. A thermocouple was welded to one of the substrates to track its temperature during the infrared heating or sputtering process. The cart with the substrates was then placed over the plasma sputter unit. The chamber was then closed and evacuated to pressures of about 10^{-4} mbar.

The Vapour Deposition Box (VDB) was pre-heated using heating filaments attached within the box. After the VDB has reached a high enough temperature, the induction heater was switched on for heating the zinc melting pot. Meanwhile, the strip was typically set at a speed of about 1 m/min. At this moment, the steel substrate placed over the sputter unit can be pre-heated using an infrared heater if desired. After the optional pre-heating, the Ar gas inlet was opened and the sputtering was then initiated (mostly at 200 W) and the sputter time was tracked using a stopwatch. Eventually, the temperature of the zinc melt reaches about 650°C . After the sputtering was done, the cart was launched towards the moving steel strip (Refer Figure 3.2) which is then attached to the steel strip by the magnets. The moving steel strip then transports the cart over the VDB. The final coated steel is depicted in Figure 3.4.

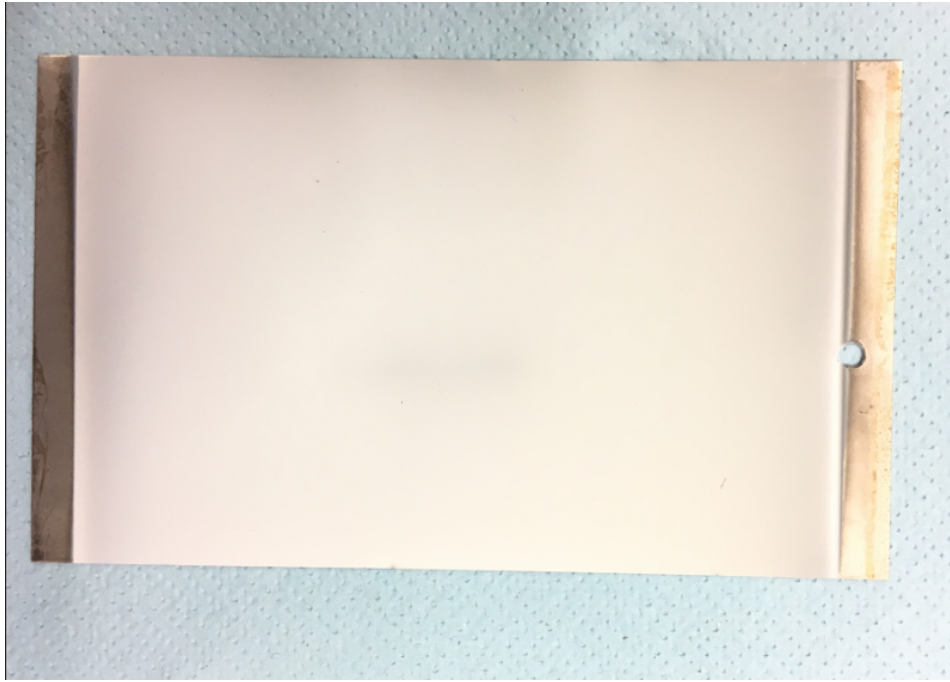


Figure 3.4: Final zinc coated DP800 substrate using PVD coating deposition

3.3. Methods used for surface characterisation of the steel

Four different surface characterisation techniques were used in this study to investigate the changes in the surface morphology and composition taking place after the pre-treatment steps -

- SEM analyses were used to observe changes in surface morphologies of the DP800 steel after the pre-treatment steps. EDX analyses were performed to determine the surface compositions at certain locations on the substrate (Appendix B).
- GDOES depth profile measurements were performed to track variations in surface compositions of individual elements on the DP800 steel with respect to its depth from the surface.
- XPS analyses were used to identify the types of oxides over the surface of the steel.
- IR spectroscopy was performed to detect the presence of hydrocarbon impurities over the surface before and after the electrolytic alkaline cleaning steps.

A brief description on the techniques used are discussed in the following sections.

3.3.1. SEM and EDX analyses

Scanning Electron Microscopy (SEM) is a surface characterisation technique used to produce high magnification images of samples to investigate their surface morphology and topology. The technique uses a beam of primary electrons which are incident upon the sample surface and are scattered elastically or inelastically. This will in-turn emit back-scattered (due to elastic collisions) and secondary electrons (due to inelastic collisions) which are detected using a detector that produces a signal which is further amplified to create an image.

Energy Dispersive X-ray spectroscopy (EDX) is a characterisation technique, often integrated with SEM, used to determine the elemental composition at the surface of the sample under analysis. It uses information from X-ray photons emitted during the transfer of electrons from the outer shell of an atom to a vacancy produced in an ionised atom during the collision of primary electrons with

the atoms at the surface.

These characterisation techniques provide information upto a certain depth from the surface of the samples, which depends on the interaction volume of the characteristic electrons or X-ray photons emitted from the surface. A schematic representation of this interaction volume is depicted in Figure 3.5.

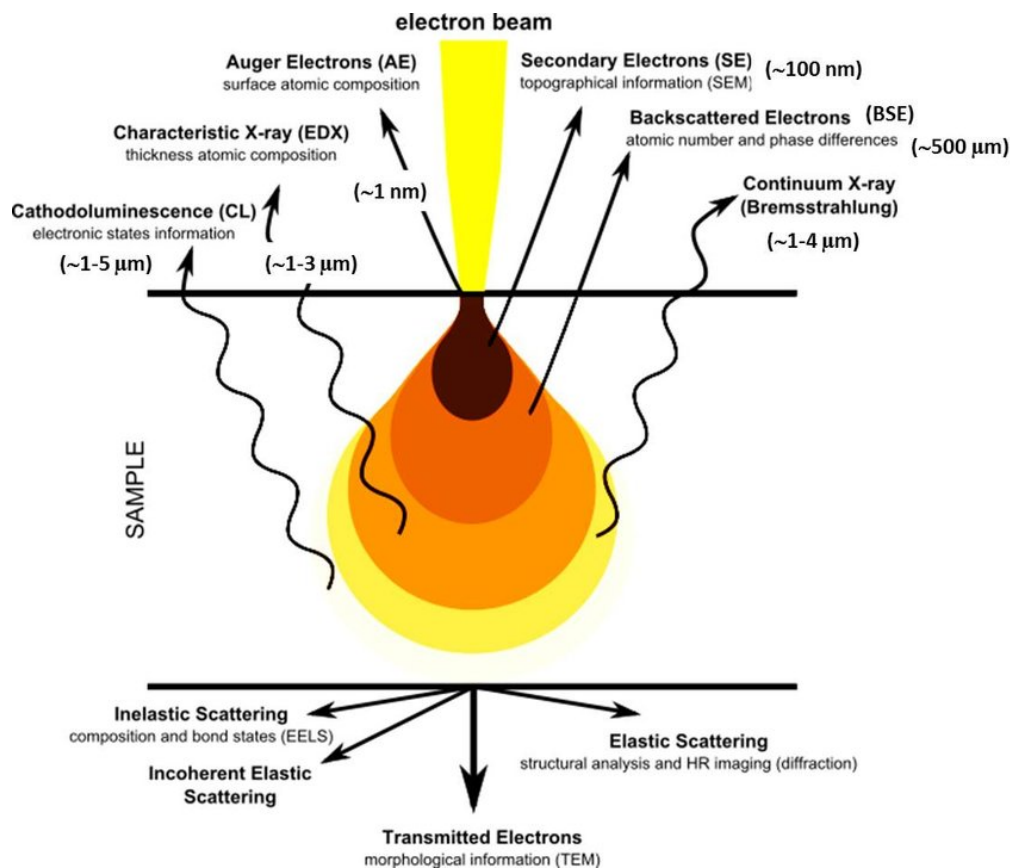


Figure 3.5: Depth of analysis for different signals emitted from the surface of the sample

This study uses secondary electrons emitted from the sample surface to obtain topographical information to study the morphological changes on the surface. Secondary electrons provide information depths up to 100 nm below the surface (see Figure 3.5). EDX is used to obtain surface compositional information up to a depth of about 1 μm below the surface. Also, point and line analyses were used during EDX analyses to determine the surface composition at certain specific points over the surface.

3.3.2. GDOES depth profile analysis

Glow Discharge Optical Emission Spectroscopy (GDOES) was used as a surface characterisation technique to determine the average surface composition of different elements. Depth profiling method was used to determine the chemical composition as a function of depth from the surface. This method is based on a glow discharge plasma created between an anode and a cathodic work-piece. The argon ions bombard the surface of the sample and thereby removing the surface atoms. The removed atoms are excited and tend to emit radiation at characteristic wavelengths. The corresponding spectrum is detected using an optical spectrometer and the concentration of each element is determined by the intensities of their characteristic spectral lines. A depth resolution of about 1 nm can be achieved using GDOES analysis.

A type JY-5000RF GDOES analyser was used in this study, operated at a sputter power of 30 W at 3 mbar pressure of argon gas. A spot size of about 5 mm in diameter was analysed during the study.

3.3.3. XPS analysis

X-ray Photoelectron Spectroscopy (XPS) is a surface characterisation technique used in the quantitative determination of the elemental composition at the surface as well as the qualitative determination of electronic states of different elements. The technique uses a monochromatic X-ray beam source (Al- K_{α} or Mg- K_{α} X-rays) incident on the surface of the sample to emit electrons at different kinetic energies from the sample. Depending upon the number of electrons released, different elements produce a characteristic set of spectral peaks at different binding energy values which helps to identify the elements. These spectral peaks correspond to the electronic configurations of the electrons within each atom, thus providing information on the electronic state and thus the oxidation states of each elements. Difference in oxidation states are accompanied by chemical shifts in the binding energy values.

This study uses the binding energy of different metals at different electronic states to determine the possible type of oxides or composition present at the surface of the samples. A PHI 5400 ESCA XPS analyser was used with an Al- K_{α} X-ray beam source having a photon energy of 1486.6 eV. A take off angle of 45° was used for an elliptical spot size of 1.55 mm major diameter and 1.1 mm minor diameter. The photoelectron spectra were recorded using a spherical capacitor analyser (SCA) operated with a pass energy of 71.55 eV, in the binding energy range of 0-1000 eV with a step size of 0.25 eV and a dwell time of 2 s per step. The energy scale of the SCA was calibrated according to the procedure described in [American Society for Testing and Materials, Surface and Interface Analysis, 17 (1991) 889 [32]]. The spectrum was shifted such that the C 1s peak correspond to 284.8 eV to correct for any charging of the sample. Further the spectra were corrected for satellites due to non-monochromatic X-ray source.

3.3.4. IR spectroscopy

Infrared (IR) spectroscopy is a qualitative analysis technique used in the detection of functional groups in different molecules (typically organic compounds) present on the surface of a sample. The bonds of different functional groups vibrate at different frequencies when IR radiation is incident on the sample. When these frequencies match the resonant frequency of the IR, absorption occurs. This generates an electromagnetic spectrum at different frequencies (or wavelength) to determine the possible functional groups.

In this study, the technique is used as a preliminary analysis to check whether organic residues are present over the surface of the substrate before and after the electrolytic alkaline cleaning step. A Bruker Tensor 2 spectrometer with a diamond macro ATR-crystal was used with a spectral resolution of 4 cm^{-1} with 32 scans recorded for each sample.

3.4. Surface wettability analysis

Surface wettability analyses were performed on steel substrates to investigate the variations in surface free energy of the steel substrates with respect to changes in the surface pre-treatment methods. This might provide information on how changes in the surface can influence the coating adhesion properties of the samples. Surface wettability of the steel can be analysed by performing sessile drop experiments, where the contact angle of a certain liquid droplet on the steel substrate will be measured and its variation with respect to the exposure times will be tracked. The analysis consists

of a syringe with a capillary, through which the liquid droplet is placed on the sample and a CCD camera used to monitor the contact angle variation with respect to time [33]. A schematic of the sessile drop experiment is given in Figure 3.6.

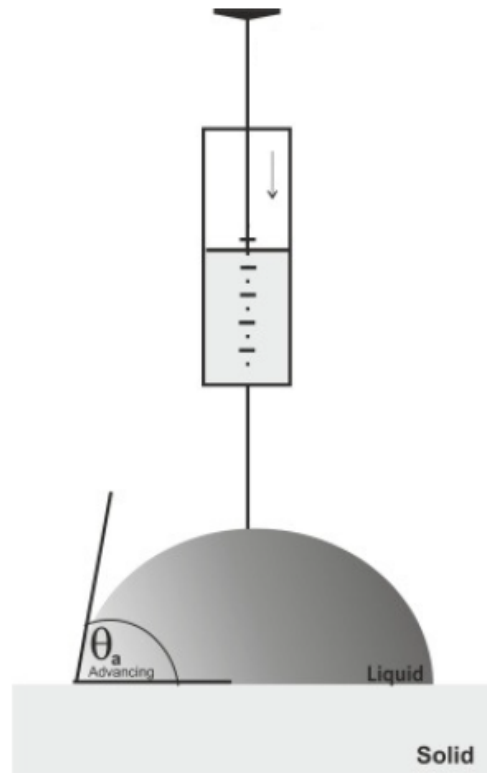


Figure 3.6: Schematic of sessile drop experiment [33]

For a solid-liquid interaction, the extent of adhesion of the liquid droplet with the surface of the solid was determined by the work of adhesion (W_a) of the substrate which is the reversible work required to separate the two phases in contact with each other. It is determined using the contact angle (θ_a) of the liquid droplet and its surface tension (γ_l) related by the Young-Dupre's equation given in Equation 3.1 [34],

$$W_a = \gamma_l (1 + \cos\theta_a) \quad (3.1)$$

A smaller contact angle of the liquid with respect to the solid surface indicates the solids' ability to adhere effectively with the liquid droplet, as the work of adhesion of the solid with the liquid droplet depends on the cosine of the contact angle measured.

3.5. Adhesion tests

Two different adhesion test procedures were followed to qualitatively assess the adhesion performance of PVD deposited Zn coatings on the DP800 substrates, namely, the 0T bending test and the BMW crash test [16].

3.5.1. 0T bending test

The 0T test procedure involves the adhesion performance of PVD coated steel strips under high bending stresses. Here, the coated steel strips were cut into smaller strips of dimensions 10 cm x 2.5 cm and bent till the two ends of the strips touch each other as shown in Figure 3.7.

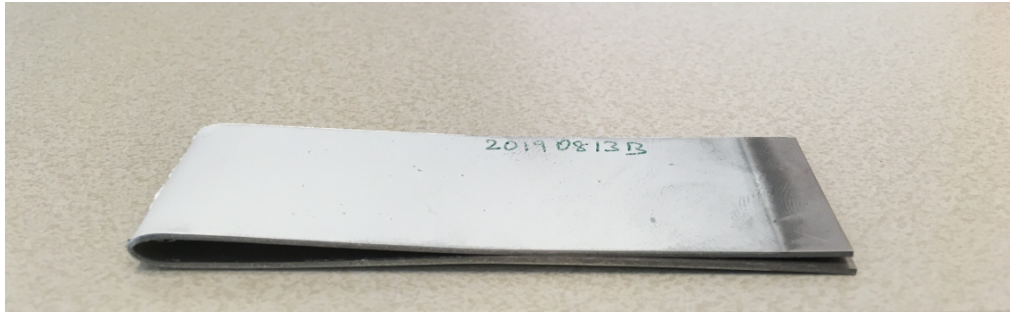


Figure 3.7: Bended OT test specimen

Then a duct tape is stuck onto the bended side of the steel strip and pulled off quickly. Proper care was taken during the bending of the steel strips as slivers of steel might come off the surface when bended too far, which mimics the coating delamination. The quality of the coating is determined by the specifics of OT test as given in Table 3.2.

Table 3.2: Specifications for OT bending test

Results	Specifications
OK	Zn coating is not visible on the pulled off duct tape suggesting good adhesion under bending
NOK	Zn coating is visible on the pulled off duct tape suggesting bad adhesion under bending

Figure 3.8 depicts the bended part of the specimens which show OK and NOK adhesion results respectively.



(a)



(b)

Figure 3.8: OT test specimens showing (a) OK adhesion, (b) NOK adhesion

3.5.2. BMW crash test

The BMW test procedure is used to assess the adhesion performance of coated steel substrate under crash-like conditions. Here, the coated steel strips were cut into smaller strips of dimensions 10 cm x 2.5 cm. An epoxy adhesive was used for this test (Betamate from DOW chemicals). First, it was pre-heated in a furnace at 175°C for about 3 to 4 min to increase the viscosity and apply it over the coated steel strips. Then the strips were placed in the same furnace for about 20 min. This further increases the viscosity of the adhesive to achieve proper adhesion with the coated steel strip. The adhesive is then cooled at room temperature for about 15 min to cure and consolidate over the steel strip. After cooling, the strips were quickly bent over 90° with the adhesive on the exterior using a bending tool, which breaks the adhesive at the bended part. Figure 3.9 depicts the bended part where the adhesive is broken.

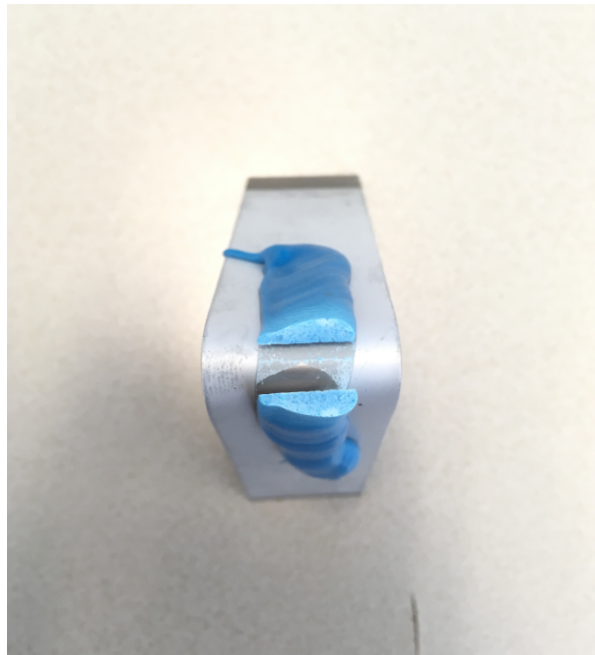


Figure 3.9: Bended part of a BMW crash test specimen

If zinc coating is visible on the broken part of the resin, the coating adhesion was considered NOK (bad adhesion). If the zinc coating is not visible on the resin, the coating adhesion was considered OK (good adhesion). This was represented by codes (0,1,2,3 and 4) as depicted in Table 3.3.

Table 3.3: Specifications for BMW crash test

Results	Specifications
0	No zinc delamination visible on the resin
1	Zn coating has fully or on large parts delaminated (visible clearly on the resin)
2	Zn coating has delaminated on one or more small spots (visible as small spots on the resin)
3	Zn coating has delaminated when bending further than 90°
4	Zn coating has delaminated but the coating is still visible on the substrate

Generally, the results which do not correspond to the code 0 are considered as a NOK coating adhesion as delamination took place regardless of the bending method. Figure 3.10 depicts the BMW test specimens which provided good and bad adhesion results.



(a)



(b)

Figure 3.10: BMW test specimens showing (a) OK adhesion results, (b) NOK adhesion results

4

Results and Discussion

Investigations of the surface morphology, composition and wettability of various surface treated samples were of utmost importance in this study. Microscopic images were obtained to study the changes in the surface morphologies of the substrate as a function of the pre-treatment step. Qualitative and quantitative compositional analyses were performed by spectroscopic techniques (EDX/GDOES/XPS). Wettability analyses were performed by contact angle measurements from sessile drop experiments. Adhesion performance of the coated steel was determined by adhesion tests. Thus, in this chapter, the results of these analyses will be presented and discussed.

4.1. Analysis of surface-treated DP800 samples

In this section, analyses on surface changes due to two different treatments, namely the electrolytic cleaning and acid etching processes, will be discussed.

4.1.1. Characterisation of degreased DP800 substrate

An untreated sample (only degreased with isopropanol) was considered as a reference to compare its surface characteristics with the treated samples. Figure 4.1 shows a SEM image of a DP800 substrate degreased in isopropanol. The surface appeared irregular with plateaus and valleys. The plateaus were the flatter regions and the valleys were the irregularities in between the plateaus.

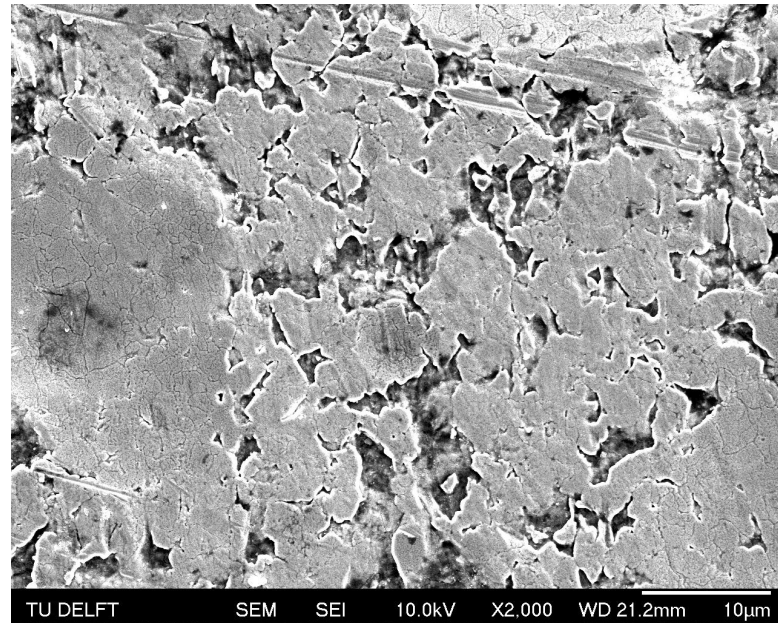


Figure 4.1: SEM image of an untreated DP800 sample

Further magnifications revealed the presence of uniformly dispersed particles over the grains with clusters of particles along the grain boundaries (Figure 4.2).

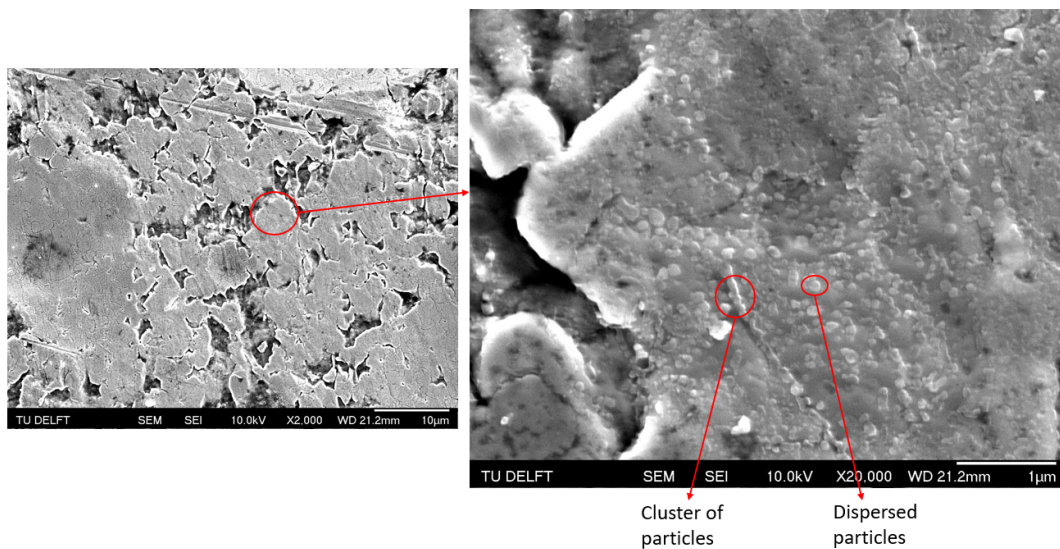
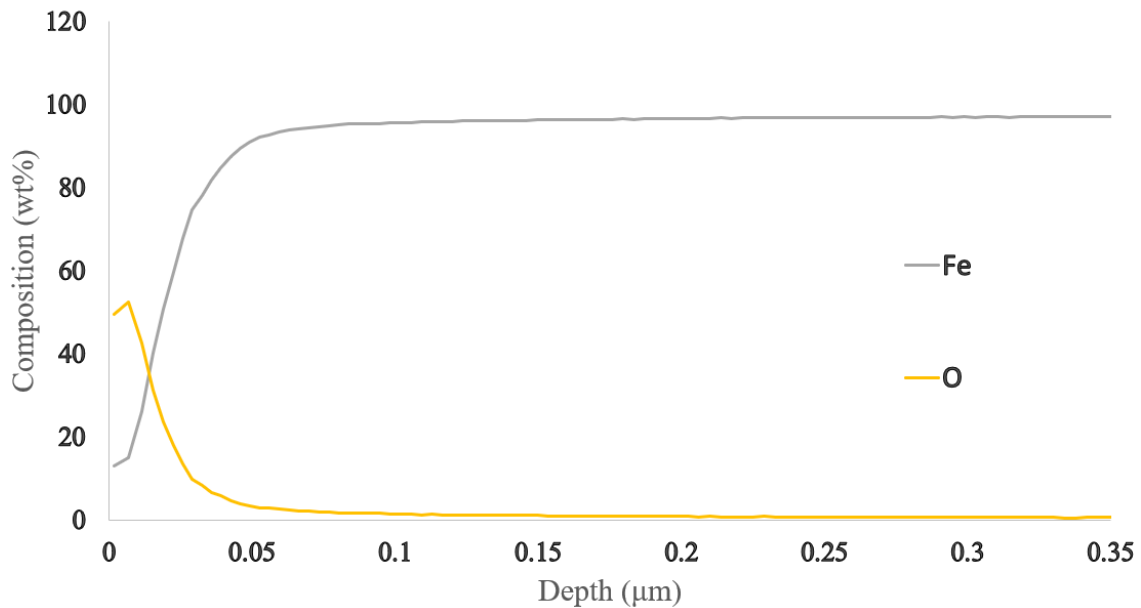


Figure 4.2: Presence of particles and a cluster of particles observed on an untreated DP800 sample

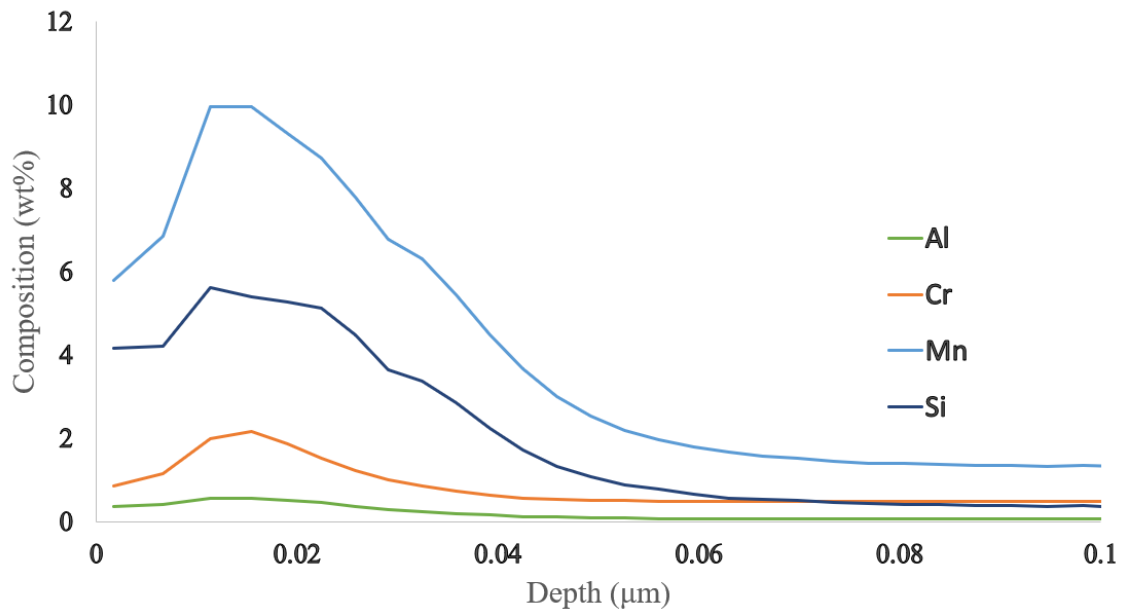
EDX analyses confirmed that the clusters had higher atomic fractions of Mn, Si and O and the particles had higher Mn and O atomic fractions (Figure B.1). This might suggest that Mn-Si rich oxides are present as clusters of particles and the Mn-rich oxides as dispersed particles over the surface. However, the EDX analyses performed on these particles and clusters may not reveal their exact composition due to the interaction volume of the characteristic X-rays used for the analysis which goes up to 1 μm in depth. Thus, other surface compositional analysis techniques like GDOES and XPS were performed to detect the surface compositions of major alloying elements over the surface.

GDOES depth profiling was performed on an untreated DP800 sample to determine the concentrations and the depth up to which the enrichments of alloying elements were present. Figure 4.3

shows the results of GDOES depth profile analysis for the same. Average results were taken for every 10 nm for the first 200 nm to reduce measurement noise.



(a)



(b)

Figure 4.3: GDOES depth profile plots of an untreated DP800 sample at different scales - (a) Fe and O, (b) Mn, Si, Cr and Al

GDOES measurements confirm the enrichments of Mn and Si upto depths of about 40 to 50 nm over the surface. However, the enrichment of oxygen extends up to depths of about 120 nm with higher concentrations at the first 50 nm of depth (see Figure 4.3a). Other alloying elements such as Cr and Al have lower surface enrichments compared to Mn and Si (see Figure 4.3b).

Enrichments of Mn at the surface tend to reach values up to 10 wt% even though its composition

in the bulk is around 1.8 wt%. Another interesting comparison that can be made from the GDOES plot (see Figure 4.3b) is the difference between the surface enrichments of Si and Cr. Si and Cr have comparable compositions in the bulk (0.2 wt% and 0.6 wt% respectively). However, a higher enrichment of Si (6 wt%) was observed compared to Cr (2 wt%). The same can be observed in case of Al where it reaches concentration levels of about 0.5 wt% even though its concentration in the bulk is only about 0.04 wt% (can be neglected in this study due to very low concentrations at the surface). Also, the ratio of the surface concentration to the bulk concentration for Si tends to be high compared to that of Mn and Cr. A 30-fold increase in the concentration of Si was observed at the surface compared to its bulk value, which was higher than a 6-fold increase for Mn and a 3-fold increase for Cr.

XPS analyses were performed on the steel substrate to determine the possible oxides that might have been segregated over the surface. Intense peaks of Fe 2p_{3/2}, O 1s and Mn 2p_{3/2} were observed with non-intensive Cr 2p_{3/2} peaks at binding energy ranges between 500 and 750 eV as depicted in Figure 4.4.

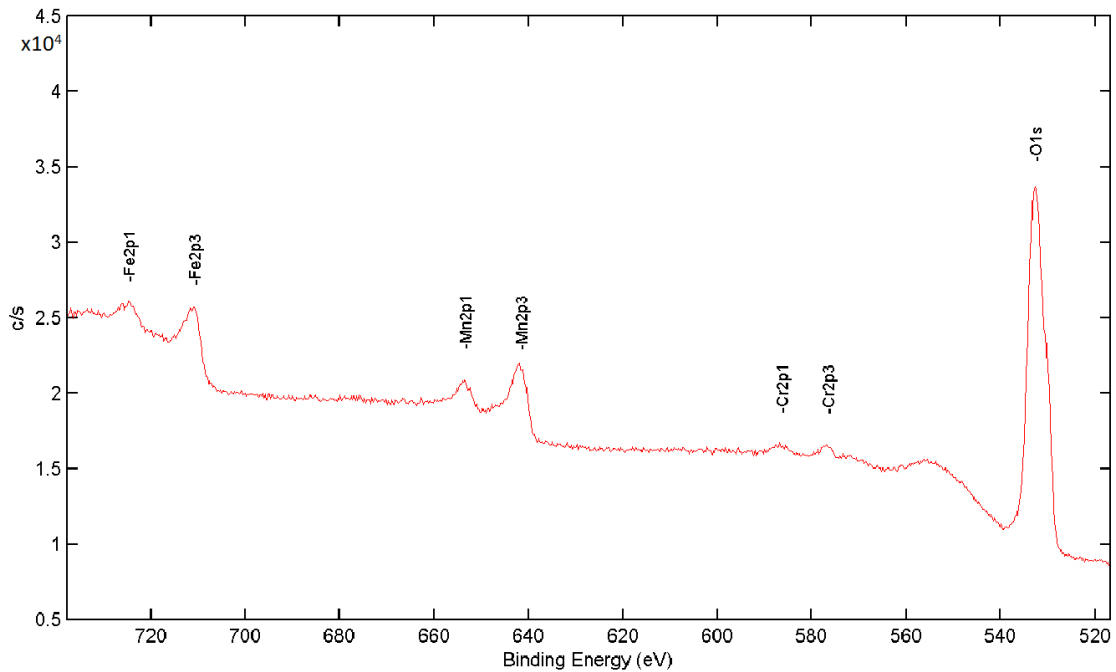


Figure 4.4: XPS spectrum of an untreated DP800 substrate (BE - 500 to 750 eV)

At lower spectral regions (BE - 40 to 120 eV), Si 2p spectra along with secondary peaks of Fe, Mn and Cr (3s and 3p peaks) were observed at very low intensities depicted in Figure 4.5.

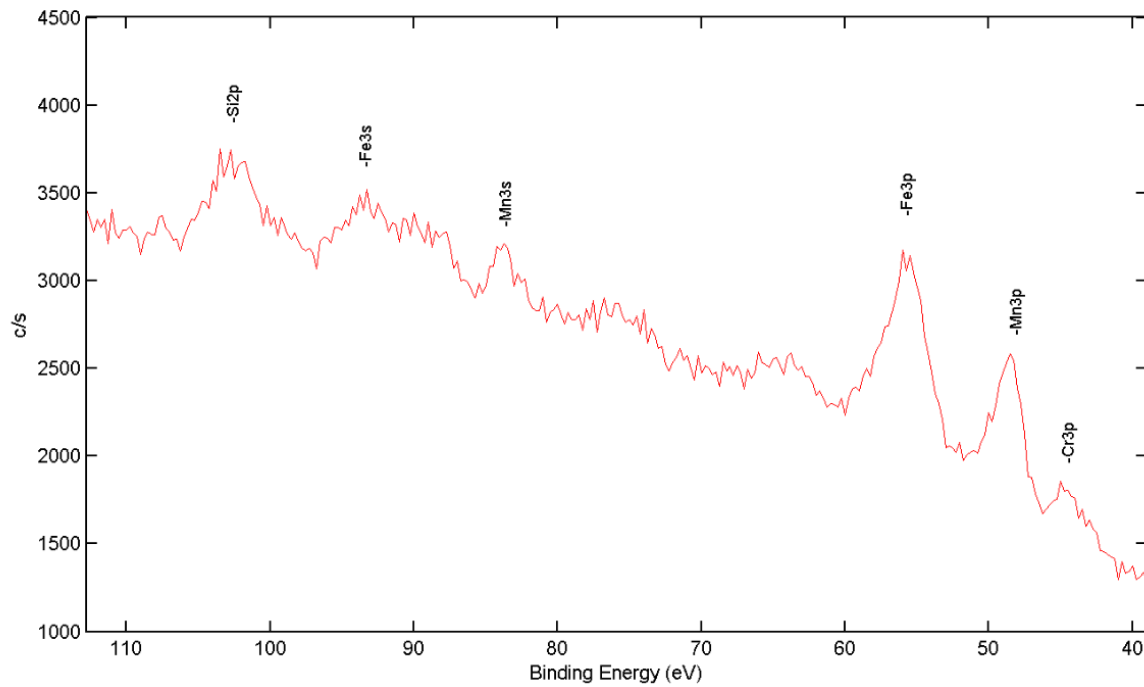


Figure 4.5: XPS spectrum of an untreated DP800 substrate (BE - 40 to 120 eV)

Table 4.1 shows the binding energies of major alloying elements and oxide spectra,

Table 4.1: Binding energies of the corresponding XPS spectra of individual elements

Elements	Binding energy (eV)
Fe 2p _{3/2}	710.3
O 1s	529.6 (O ²⁻) 532.1 (OH ⁻)
Mn 2p _{3/2}	641.2
Si 2p	102.0
Cr 2p _{3/2}	576.0

NIST database [35] was used to determine the possible oxide types at the binding energy values of the corresponding spectral peaks of the alloying elements. Mn 2p_{3/2} spectrum at a binding energy of 641.2 eV along with O 1s spectrum at 529.6 eV might correspond to Mn-based oxides (possible MnO) along the surface. 2p_{3/2} spectrum of Fe at 710.3 eV might suggest iron oxides at the surface with the likelihood of hematite (Fe₂O₃) at the surface. Other low intensity spectra like Cr 2p_{3/2} and Si 2p_{3/2} along 576.0 eV and 102.0 eV might suggest the segregation of chromium oxides (Cr₂O₃) and silicon based oxides (SiO₂) segregated over the surface.

Based on the results obtained from SEM/EDX, GDOES and XPS analyses, the following observations can be made,

- The observations of Mn-Si rich clusters and Mn rich particles from SEM and EDX analyses were similar to the studies reported by Shin et al. [36], who worked on dual phase steels with slightly different bulk concentrations of major alloying elements (Mn and Si). Mn enrichments were found both along the grains and the grain boundaries, possibly due to its grain boundary diffusion and diffusion through vacancies in the crystal lattice of α -iron during annealing [37], characterised by its high concentration in the bulk (section A.2). This was also

evident from GDOES measurements where the enrichments of Mn was higher than that of other alloying elements at the surface. Si enrichments were found mostly along the grain boundary regions, possibly due to the easy diffusion path for Si through these regions to segregate over the surface. Interatomic diffusion of Si might have been less likely due to its lower concentrations in the bulk.

- Higher concentrations of Si were observed compared to Cr along the grain boundaries, even though their concentration in the bulk is comparable. This might be attributed to the high permeability of oxygen to penetrate through the grain boundaries to react with Si in the bulk to form Si-based oxides at those regions. Lower Gibbs free energy of oxide formation and higher affinity of Si towards oxygen to form an oxide compared to Cr might be some possibilities (section A.2).
- XPS spectra of the untreated DP800 substrates might suggest the presence of MnO, SiO₂, Fe₂O₃ and Cr₂O₃ on the surface, determined from the binding energies of their 2p spectra. Possibilities of SiO₂ as a surface oxide is less likely due to its weak 2p spectrum at lower binding energy ranges (Figure 4.5). Studies by Suzuki et al. [11] predicted the type of surface oxides formed at lower oxygen potentials in various Mn-Si added high strength steels with different Si/Mn weight ratios during recrystallisation annealing. The study predicted the selective oxidation of Mn-Si based ternary oxides at decreasing weight ratios, which eventually changes to MnO at very low ratios. Since the steel used in this study corresponds to a low Si/Mn ratio (Si wt% / Mn wt% \approx 0.11), surface oxides might be predominantly Mn rich with some Mn-Si rich ternary oxides. This might be consistent with EDX analyses which showed Mn and Si enriched oxides along the grain boundaries, which might suggest the presence of Mn-Si rich ternary oxides at those regions. Also, the binding energy values for Mn 2p_{3/2} and Si 2p peaks might be comparable with studies by Grosvenor et al. [38] who determined the XPS spectra of the possible surface oxides, Mn₂SiO₄ and MnSiO₃, as ternary oxides on general AHSS. The spectra provided Mn 2p_{3/2} peaks at binding energies of around 641.5 eV and Si 2p peaks along 102.1 eV.
- Low intensity peaks of Cr 2p_{3/2} (576.0 eV) and 3p (43.1 eV) might suggest possible chromium oxides (possible Cr₂O₃) scattered at low amounts over the surface. Strong Fe 2p_{3/2} peaks along 710.3 eV were also detected which might suggest a thin iron oxide layer over the surface due to exposure of the steel sample to air.

A complex surface oxide morphology present on the surface of the DP800 substrate makes it difficult to determine the final surface characteristics of the substrate after the electrolytic cleaning and acid etching steps. This might be attributed to the variations in the dissolution rates of different types of oxide segregated over the surface. This might further induce partial or complete dissolution of the surface oxides and therefore shall influence the coating adhesion properties, which will be discussed later in the upcoming sections.

4.1.2. Effect of electrolytic alkaline cleaning

As discussed earlier in Section 2.1.1, two different electrolytic cleaning procedures were considered for analysis: anodic and cathodic cleaning processes. Infrared spectroscopy was performed on the two different electrolytically cleaned samples with an untreated and degreased DP800 substrate as a reference to check the presence of any hydrocarbons present on the surface as contaminants depicted in Figure 4.6.

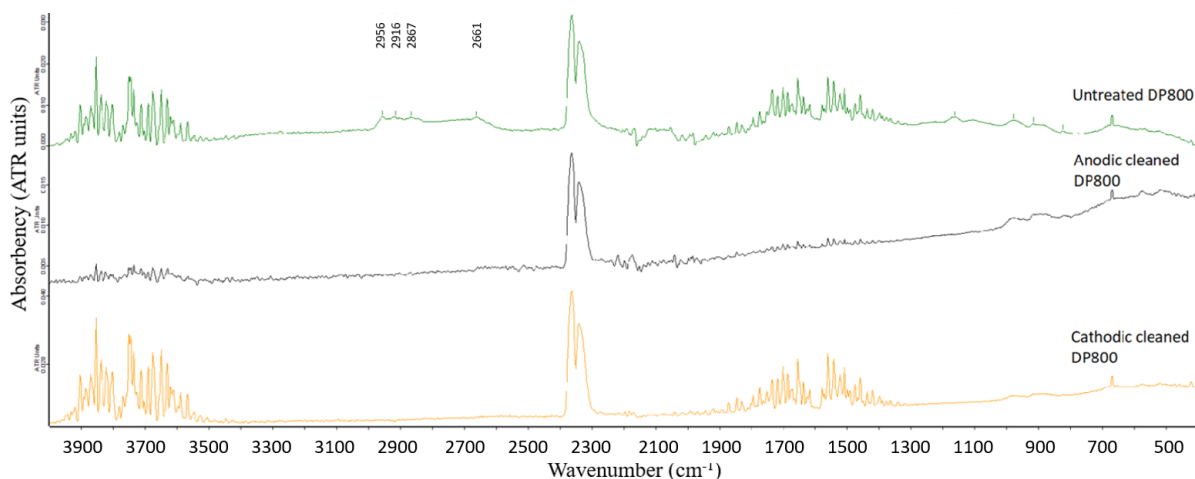


Figure 4.6: Comparative IR spectra of untreated (green spectrum), anodic cleaned (black spectrum) and cathodic cleaned (yellow spectrum) DP800 samples

Peaks along wavenumbers between 2800 to 3000 cm^{-1} (2956 cm^{-1} , 2916 cm^{-1} and 2867 cm^{-1}) were observed for an untreated reference DP800 substrate which seem to disappear for anodic and cathodic cleaned DP800 substrates. Studies by Hassel et al. [21] performed infrared spectroscopy over low carbon steel samples contaminated with certain hydrocarbon impurities and observed peaks along the aforementioned wavenumber range as the vibrational frequencies of C-H bonds tend to occur at this particular absorption spectrum. The first peak (2956 cm^{-1}) might correspond to CH_3 and the other two peaks (2916 and 2867 cm^{-1}) might correspond to CH_2 vibrational modes, suggesting an aliphatic hydrocarbon was initially present on an untreated DP800 substrate. Absence of these peaks in the electrolytically cleaned substrates might suggest that both the electrolytic cleaning techniques were effective enough in the removal of organic residues present as contaminants over the surface of the substrate. However, additional surface effects were observed between an anodic cleaned and a cathodic cleaned sample (see Figure 4.7).



Figure 4.7: Discolouration of a cathodic cleaned DP800 compared to an anodic cleaned DP800 sample

Deposits were observed over the surface when the discoloured part was analysed using SEM as shown in Figure 4.8.

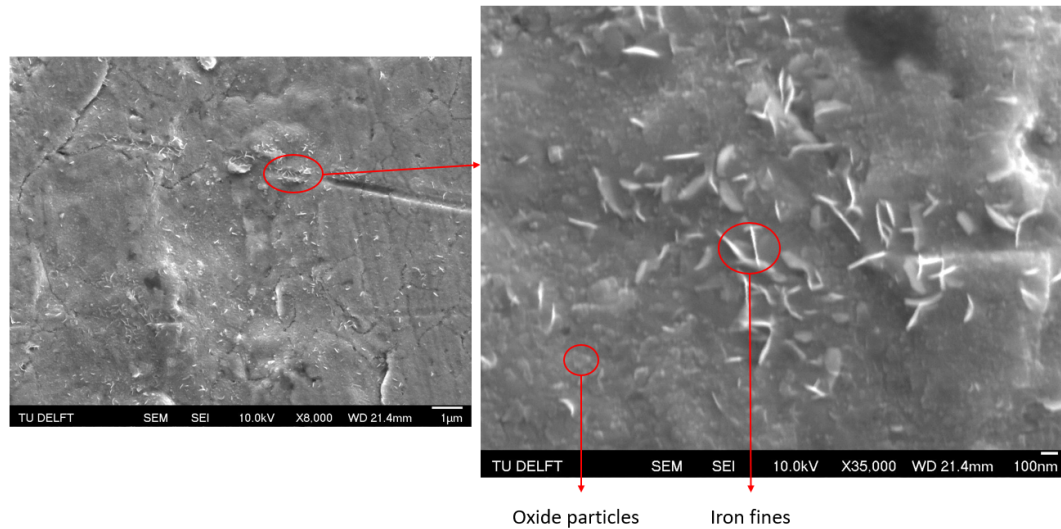


Figure 4.8: SEM image on the discoloured part over a cathodically cleaned DP800 substrate

These 'newly formed' deposits were present over the surface of the underlying steel substrate as the particles of oxides were clearly visible beneath the deposits. These deposits were examined using EDX analyses which showed no enrichments of any alloying elements other than iron (Figure B.2).

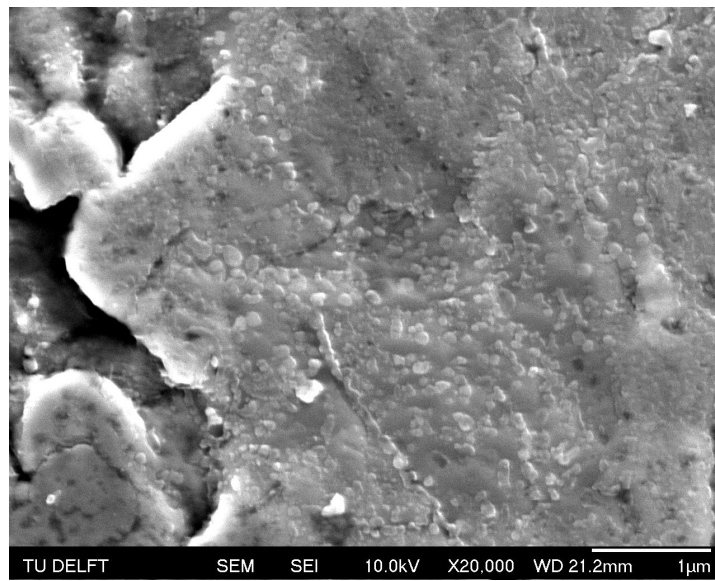
Hassel et al. [21] observed a kind of redeposition of iron fines taking place on a cathodically cleaned full hard steel sheet due to which a decrease in the surface wettability was observed from contact angle measurements. The source of these iron fines may have originated from the alkaline cleaning bath as discussed in Section 2.1.1, which classified them as the major drawback of implementing cathodic cleaning process as a surface treatment for steel substrates. Thus, the most likely possibility of the presence of deposits over the substrate may correspond to iron fines which might have redeposited over the surface from the alkaline cleaning bath.

To observe changes in the surface wettability due to varying surface characteristics of a cathodically cleaned substrate, sessile drop experiments were performed with demineralised water as a reference liquid. This might provide an idea on further adhesion properties of the treated substrate. Table 4.2 shows the changes taking place in the contact angle of demineralised water droplet on a cathodically cleaned sample compared to an untreated and an anodic cleaned sample.

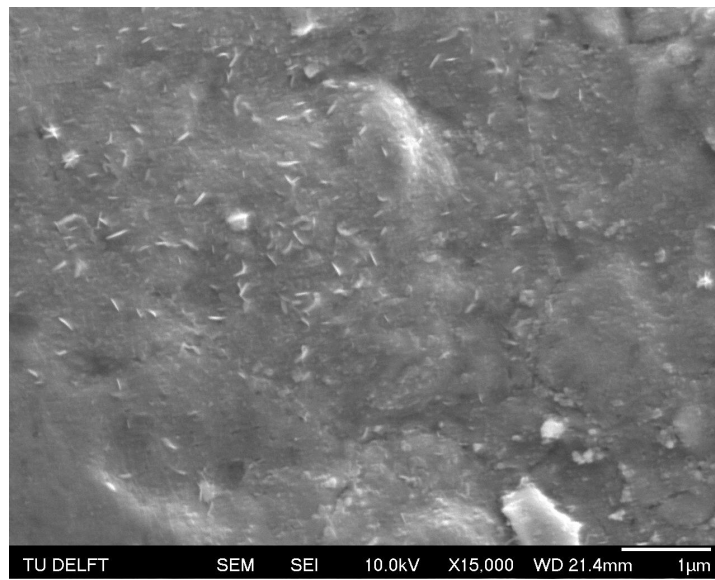
Table 4.2: Variations in contact angle measured between an untreated DP800 substrate with electrolytically cleaned DP800 substrates

DP800 Substrates	Contact angle of water (deg.)
Untreated	$76.3^\circ \pm 1.0^\circ$
Cathodic cleaned	$44.0^\circ \pm 2.9^\circ$
Anodic cleaned	$39.5^\circ \pm 1.6^\circ$

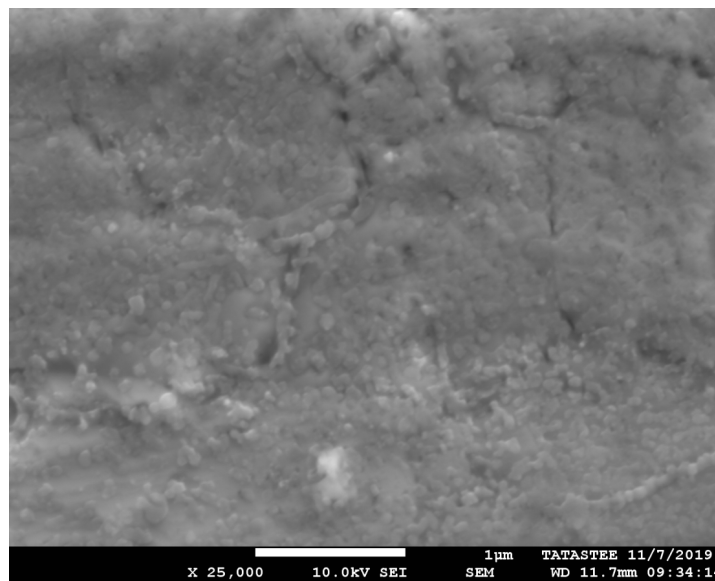
The presence of iron fines over the surface of the cathodically cleaned substrate has shown to influence the surface wettability of the substrate. This is evident by a slightly greater contact angle of water compared to an anodic cleaned substrate. The higher the contact angle of the liquid droplet, the lower the work of adhesion between the surface and the droplet and the lower is its surface wettability (Section 3.4). Anodic cleaning was proven to be the most effective way of removing organic residues and contaminants from the surface of the steel substrate as no such iron fines were observed on the surface of an anodic cleaned DP800 substrate (Figure 4.9c).



(a)



(b)



(c)

Figure 4.9: Comparative surface morphologies of electrolytic alkaline cleaned DP800 substrates - (a) Untreated DP800, (b) Cathodic cleaned DP800, (c) Anodic cleaned DP800

The surface oxide morphology of an anodic cleaned DP800 substrate appears to be similar to that of an untreated DP800 substrate with particles of oxides dispersed evenly throughout the surface and with oxide clusters along the grain boundaries (Figure B.3). GDOES depth profile measurements were performed to observe the changes in the composition of the surface due to the anodic pre-cleaning step. Figure 4.10 depicts the comparative GDOES depth profile results between an untreated DP800 substrate and an anodic cleaned DP800 substrate for the major alloying elements of the DP800 substrate.

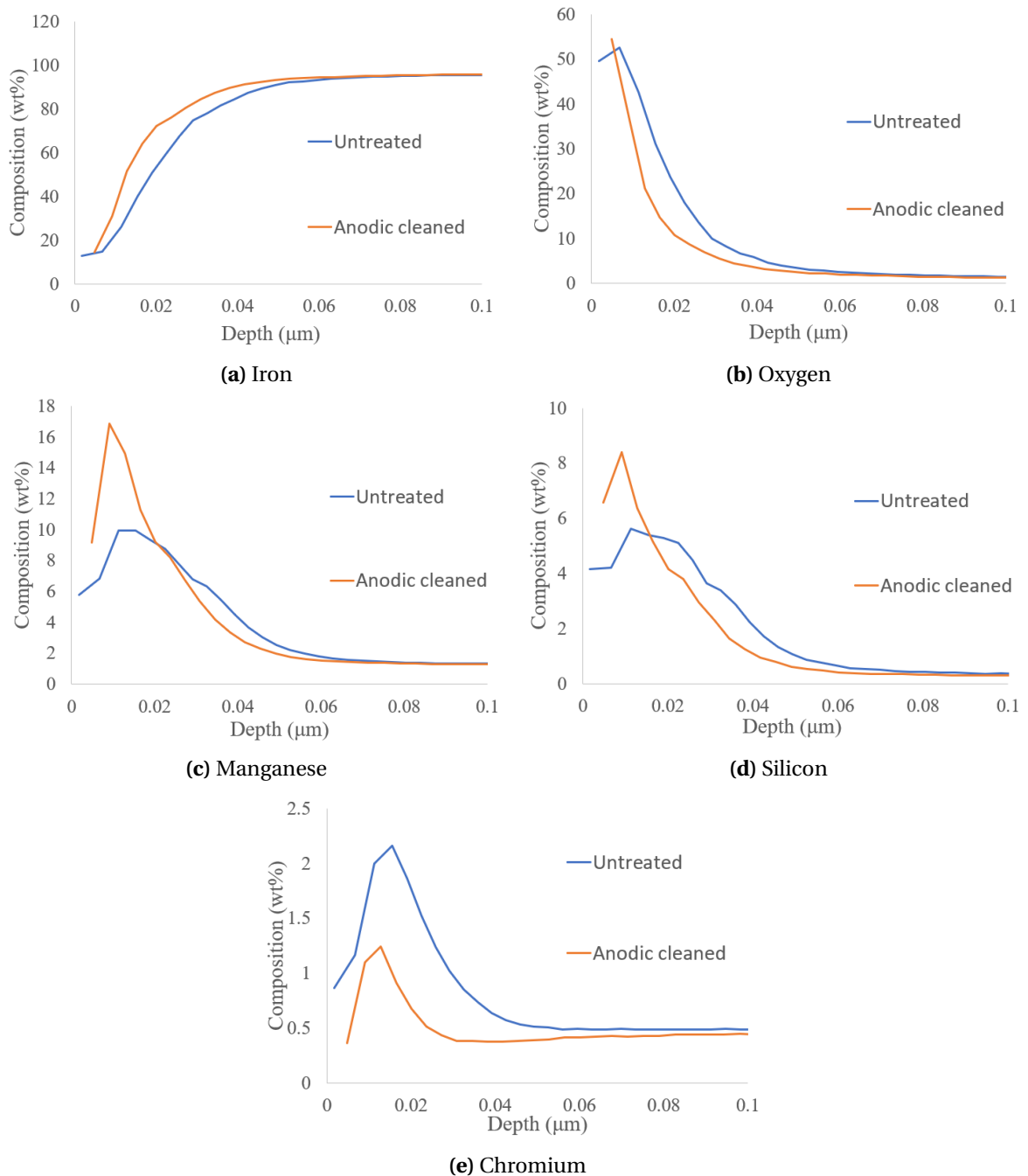


Figure 4.10: Comparative GDOES depth profile results of untreated and anodic cleaned DP800 substrates - (a) Fe, (b) O, (c) Mn, (d) Si, (e) Cr

Vertical shifts (concentrational shifts) in the peak values of Cr were observed in the GDOES analysis

where Cr enrichments tend to decrease from an initial 2 wt% to about 1.25 wt% during anodic cleaning. Also, an increase in the Mn concentration from 10 wt% to about 17 wt% and Si concentration from 6 wt% to about 8 wt% was observed. Horizontal shifts (depth up to which the enrichments are present) were observed for Cr and O from an initial 50 nm for an untreated sample to about 30 nm from the surface for an anodic cleaned sample. However, no major changes were observed for Mn and Si, if horizontal shifts were considered.

To obtain a clear idea on the horizontal and vertical shifts for the corresponding alloying elements, XPS analyses were performed on anodic cleaned samples and compared with an untreated sample. First, the 2p_{3/2} spectra of Fe, Mn, Cr and 1s spectrum of O were compared for both untreated and anodic cleaned substrates which occurs at binding energy values between 500 and 750 eV. Figure 4.11 shows the comparative spectrum of an untreated and anodic cleaned DP800 substrates at binding energies between 500 and 750 eV.

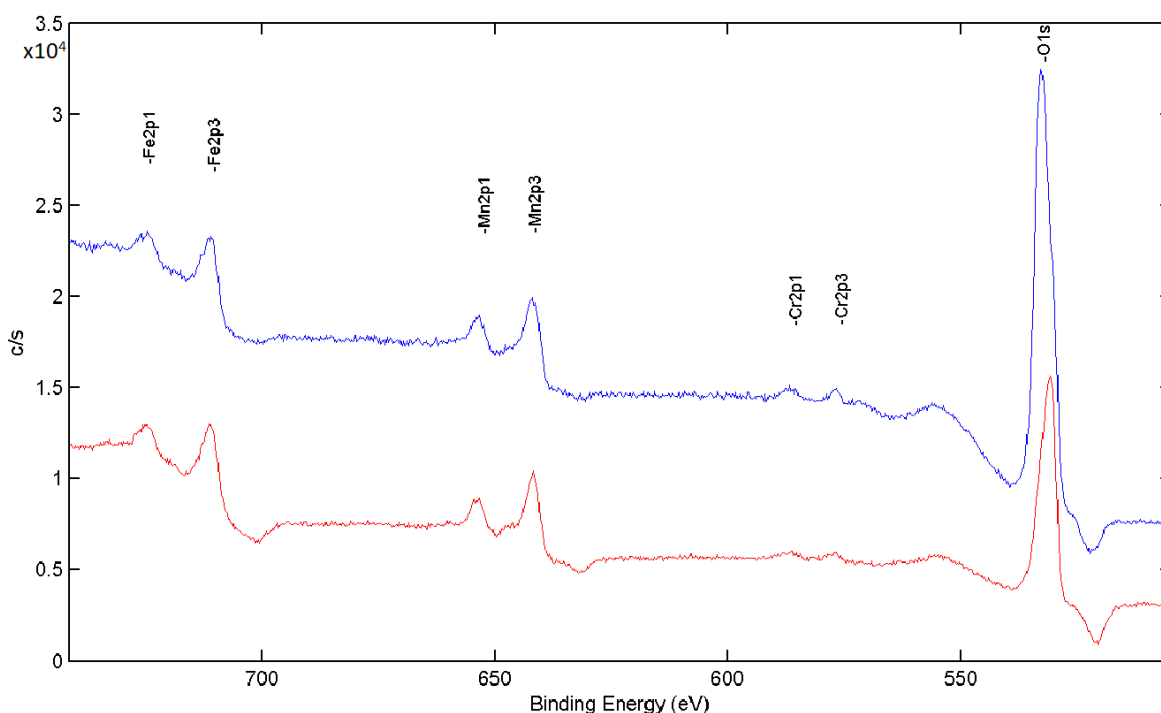


Figure 4.11: Comparative XPS analysis of untreated DP800 and anodic cleaned DP800 substrates (BE - 500 to 750 eV) - dark blue spectrum corresponds to untreated DP800 and the red spectrum corresponds to anodic cleaned DP800

The binding energies of the corresponding elements in the 2p_{3/2} region with 1s spectra of O is given in Table 4.3.

Table 4.3: Comparative binding energies of the spectra obtained in Figure 4.11

Elements	Binding energy (eV)	
	Untreated DP800	Anodic cleaned DP800
Fe 2p _{3/2}	710.3	710.0
O 1s	529.6 (O ²⁻)	530.0 (O ²⁻)
	532.1 (OH ⁻)	532.1 (OH ⁻)
Mn 2p _{3/2}	641.2	641.0
Cr 2p _{3/2}	576.0	576.2

Even though there seems to be no significant change in the binding energies between the two spectrum, a slight shift in the peak intensity of O 1s spectra was observed in Figure 4.11. This might correspond to a reduction in the hydroxide peak which occurs at binding energies between 531.5 to 532 eV corresponding to the formation of iron hydroxides due to the exposure of steel in air. Water vapours in air tend to react with iron at the steel surface to form hydroxides of iron. Overlap of the two bands (OH^- and O^{2-} bands) tend to occur due to close binding energy values between them.

Thus, no significant changes between an untreated and anodic cleaned DP800 substrates were observed between 500 to 750 eV spectral range. Therefore, secondary 3p and 3s peaks of Mn, Fe and Cr along with 2p spectra of Si were compared at binding energies between 40 and 120 eV as depicted in Figure 4.12.

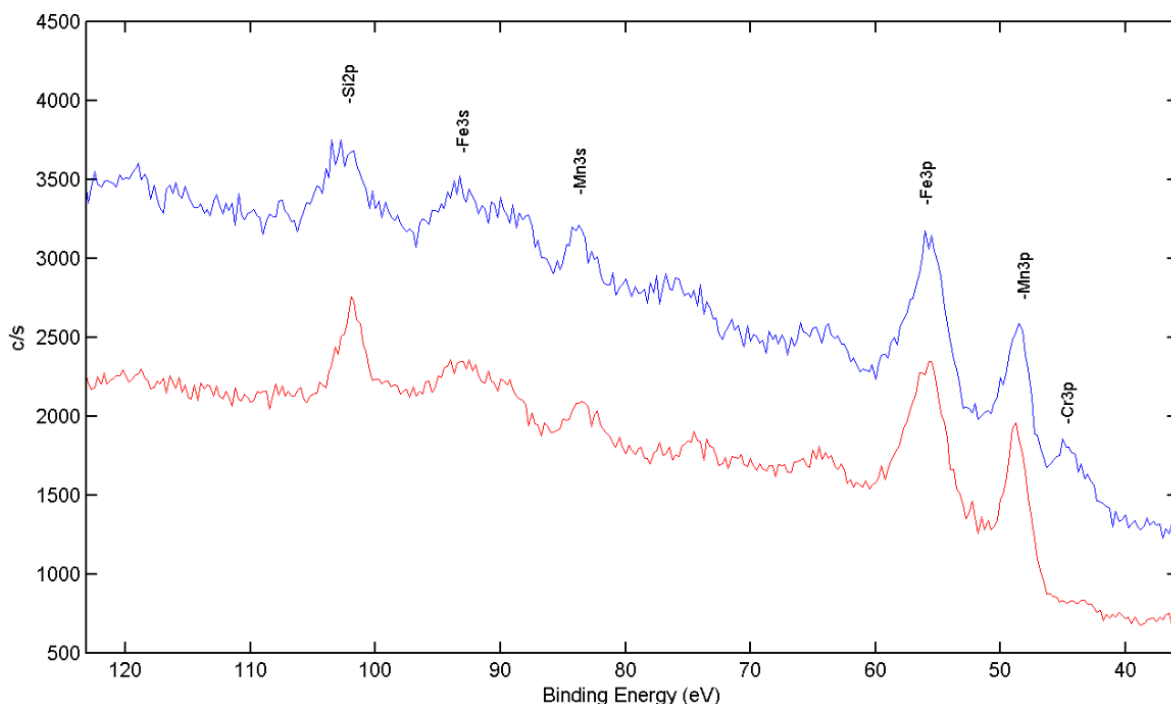


Figure 4.12: Comparative XPS spectra of untreated DP800 and anodic cleaned DP800 substrates (BE - 40 to 120 eV) - dark blue spectrum corresponds to untreated DP800 and the red spectrum corresponds to anodic cleaned DP800

The binding energies of the corresponding Si 2p and Cr 3p spectra are given in Table 4.4.

Table 4.4: Comparative binding energies of the spectra obtained in Figure 4.12 (Si and Cr)

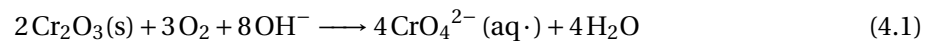
Elements	Binding energy (eV)	
	Untreated DP800	Anodic cleaned DP800
Si 2p	102.0	101.4
Cr 3p	43.1	Not detected

Figure 4.12 shows that the initial Cr 3p peak which was present at a binding energy of about 43.1 eV for an untreated DP800 was not observed in an anodic cleaned DP800 substrate. Significant changes in the spectra of other alloying elements were not observed in this case.

Binding energy values for of the 2p_{3/2} and 3p spectra of Cr might suggest the presence of chromium oxide (Cr_2O_3) over the surface of an untreated DP800 substrate. Anodic cleaned sample did not

produce a Cr 3p peak over the surface, suggesting the possibilities of dissolution of chromium oxide. This result is also consistent with GDOES measurement (Figure 4.10e) where a reduction in chromium enrichments were observed for an anodic cleaned DP800 sample.

During the anodic pre-cleaning step, the steel substrate is subjected to an alkaline solution at high pH values of about 13.8 (calculated from the concentration of NaOH in the solution which is 27 g/L). Studies have shown that oxidative dissolution of chromium oxides tend to take place in alkaline solutions where Cr(III) oxidises to Cr(VI) which tends to form chromates (CrO_4^{2-}) from Equation 4.1, which might tend to dissolve into the alkali media [39],



Thus, the chromium oxides might have been dissolved during the anodic cleaning step. However, reasons for the increasing concentrations of Mn and Si from GDOES measurements cannot be explained properly (Figure 4.10c and Figure 4.10d). It might have been due to inaccuracy in the GDOES measurements or compensating for higher concentrations of Mn and Si for decreasing Cr concentration at the surface.

To summarize, electrolytic pre-cleaning steps tend to affect the surface morphology as follows,

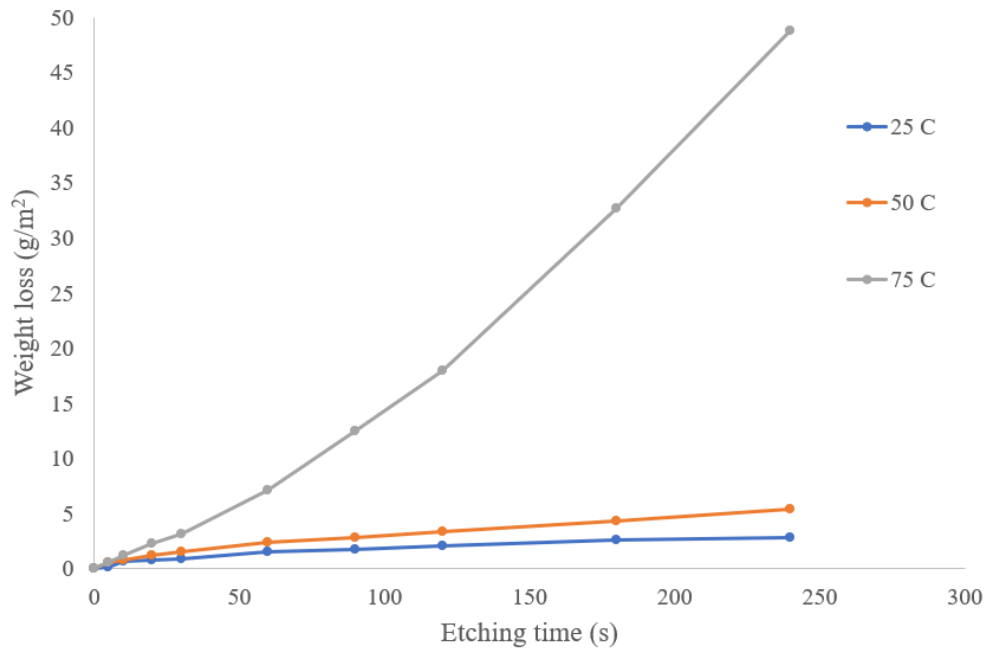
- Both the cathodic and anodic cleaning processes tend to remove hydrocarbon contaminants from the surface of the DP800 substrate effectively.
- Discolouration of the sample was observed during cathodic cleaning. The cleaning step seems to deposit additional iron fines over the surface which might be detrimental to the surface wettability compared to an anodic cleaned substrate, as evident from contact angle measurements.
- Surface oxides still remain intact during the anodic cleaning process except chromium oxide which might dissolve due to an oxidative dissolution process in alkali media.
- Higher surface concentrations of Mn and Si were observed during anodic cleaning for which no clear explanation was derived.

Thus, further improvement in the surface characteristics of the DP800 substrate was required to reduce the effects of surface oxides on the coating adhesion properties of the steel substrate. This was done by a subsequent sulphuric acid etching process which will be discussed in Section 4.1.3.

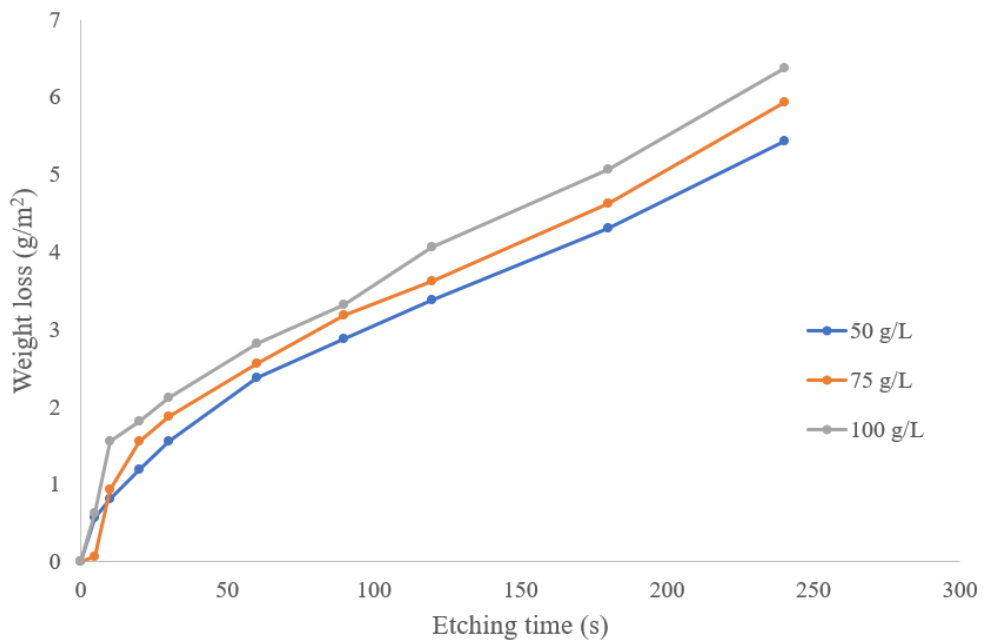
4.1.3. Effect of sulphuric acid etching

The next step in the surface pre-treatment process involves acid etching to further dissolve the oxides present on the surface of the substrate. Here, the anodic cleaned substrates were immersed in a constantly agitated solution of dilute H_2SO_4 at various immersion times to observe the changes taking place in the surface morphology of the substrate.

Preliminary weight loss analysis was conducted in this study before the surface investigations were performed. This was done to study the relationship between the specific reaction rate (k) with respect to temperature and concentration of the acid bath and to verify whether the relation is consistent with the Arrhenius relationship, as discussed earlier in Section 2.1.2. This relation will be useful in further optimisation of the acid etching process. Here, the acid concentration was kept constant and the weight loss was investigated with respect to increasing temperature and vice-versa. The plots in Figure 4.13 gives a clear idea on how temperature and concentration changes affect the rate of dissolution of the specimen.



(a)



(b)

Figure 4.13: Weight loss of acid etched DP800 substrates with respect to (a) increasing acid bath temperature (in °C), (b) increasing acid bath concentration (in g/L)

The weight loss tends to be more rapid with increasing acid temperature as shown in Figure 4.13a, suggesting high dissolution rates at high acid bath temperatures. Acid concentration seems to have a minor effect on the dissolution rate as compared to the effect of acid bath temperature (see Figure 4.13b).

The reaction rates for both the cases were determined from Equation 2.5 to make a rough estimate

on the material removal as a function of etching time (see Table 4.5 and Table 4.6).

Table 4.5: Dissolution rates for acid etched DP800 substrates with increasing acid bath temperature (in °C)

Temperature (°C)	Concentration (g/L)	Dissolution rate $\times 10^{-7}$ (cm/s)
25	50	3.75 ± 0.76
50	50	6.24 ± 1.25
75	50	17.3 ± 1.41

Table 4.6: Dissolution rates for acid etched DP800 substrates with increasing acid concentration (in g/L)

Temperature (°C)	Concentration (g/L)	Reaction rate $\times 10^{-7}$ (cm/s)
50	50	6.24 ± 1.25
50	75	5.78 ± 1.16
50	100	8.80 ± 2.00

Taking an example of a DP800 sample etched at 25 °C in a 50 g/L acid bath (see Table 4.5), the dissolution rate is 3.75×10^{-7} cm/s or 3.75 nm/s. Assuming that the oxide thickness is around 120 nm for the sample, which was observed from GDOES depth profile plots in Figure 4.3a, a minimum etching time of 32s might be required to remove any surface oxides for the given acid bath parameters. However, variations in the surface oxide composition and oxide morphology might correspond to a non-uniform dissolution of surface oxides during etching. Therefore, surface analyses were performed to study the dissolution of surface oxides as a function of etching time. For this, the concentration of the dilute H₂SO₄ bath was kept constant (50 g/L). Temperature was varied between 25°C and 50°C to investigate the surface at higher dissolution rates of etching. Three different observations were made after the etching step,

- Surface morphology
- Variations in surface composition
- Surface reoxidation

Surface morphology

The changes in the surface morphology of acid etched DP800 substrates were observed using SEM analysis. Figure 4.14 shows the SEM images depicting the changes in surface morphology taking place in a 25°C dilute H₂SO₄ bath.

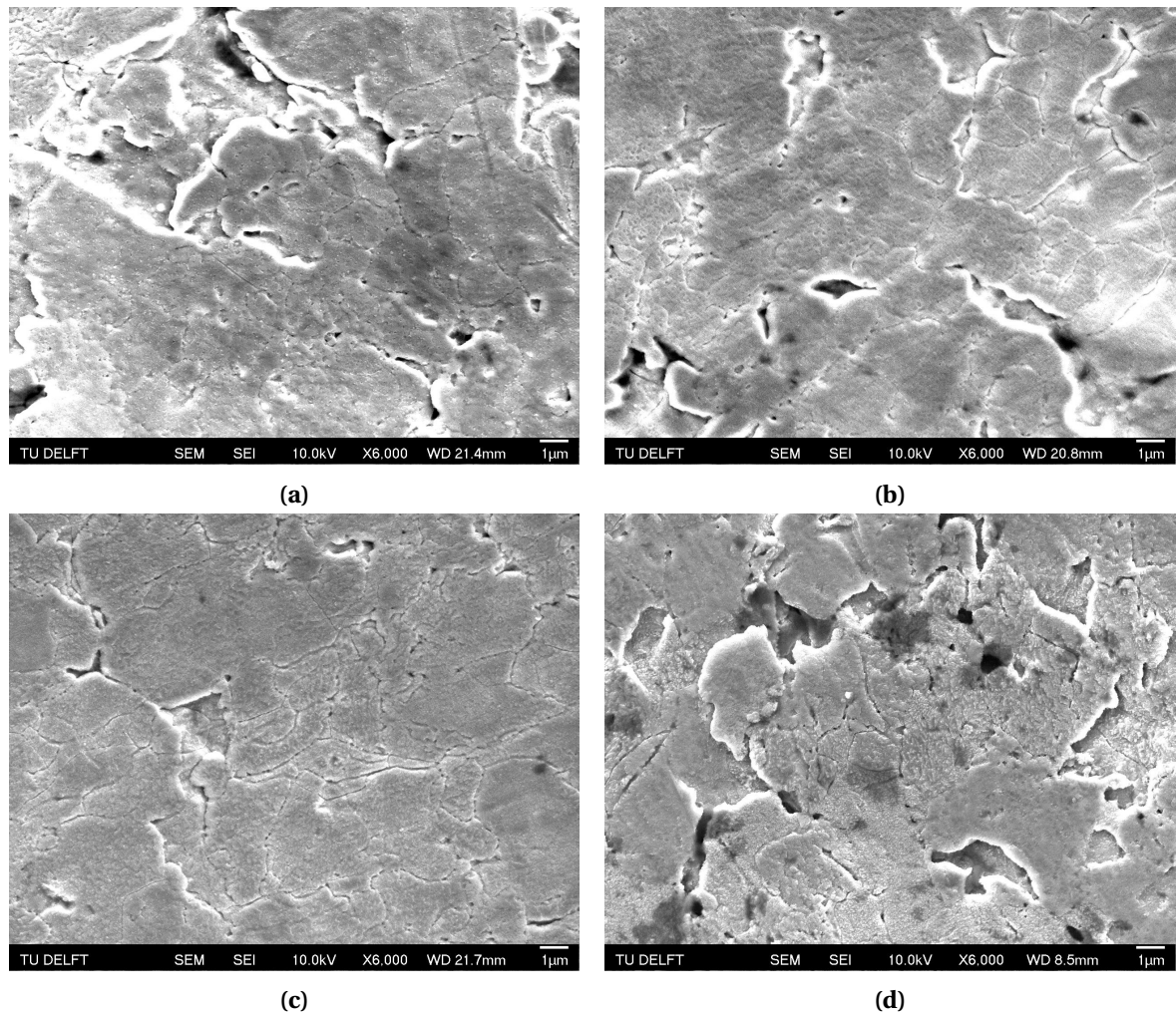
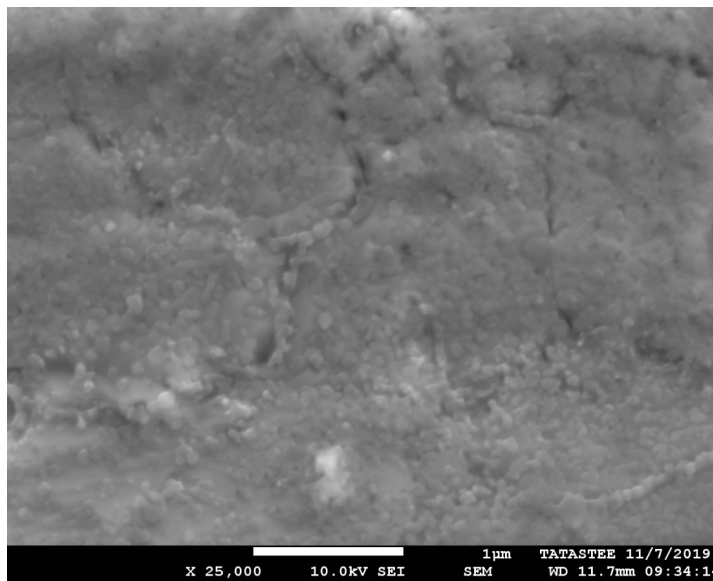


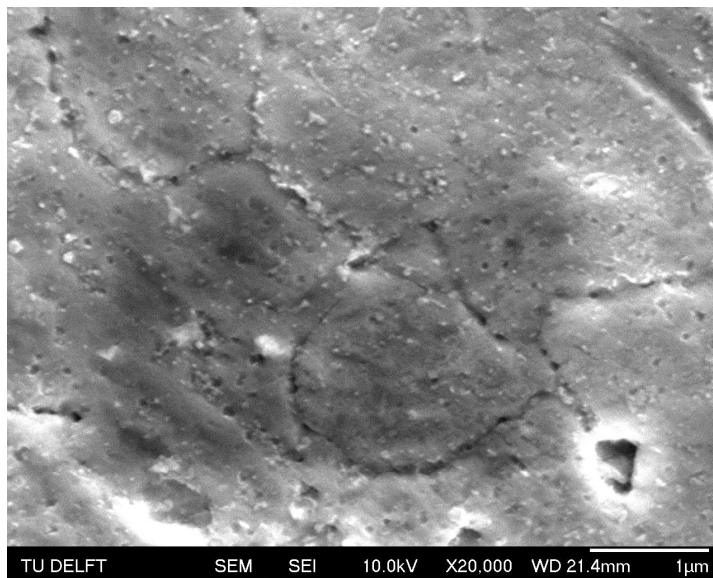
Figure 4.14: Surface changes taking place in a DP800 substrate with increasing etching time in a 25°C dilute H₂SO₄ bath - (a) 10s, (b) 30s, (c) 60s, (d) 120s

At shorter etching times (Figure 4.14a and Figure 4.14b) the surface seems to have a smooth texture with the grain boundaries not clearly visible. At higher etching times (Figure 4.14c and Figure 4.14d) the grain boundaries became more clear. An initial surface roughening over the grains were also observed, characterised by surface ruggedness over the sample.

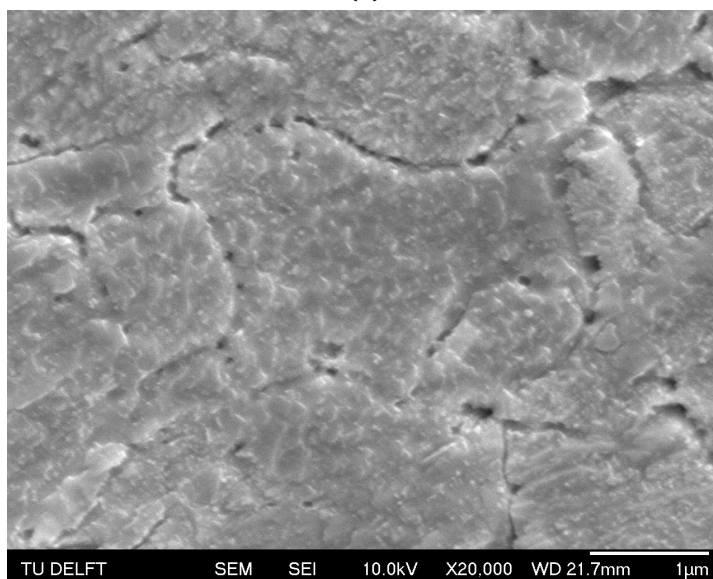
Higher magnifications revealed smaller particles over the grains and discontinuous cluster of particles along the grain boundaries over the surface of the samples etched at a shorter etching time (Figure 4.15b). The size of the particles (about 20 nm on an average) tends to be less than that of the particles present in a non-etched substrate which is anodic alkaline cleaned (about 100 to 150 nm on an average) as shown in Figure 4.15a. The discontinuity in the clusters is characterised by the presence of these oxides only along certain preferred locations along the grain boundaries. As the etching time progressed, the grains became rougher and the particles and clusters tend to disappear. Figure 4.15c shows the roughening of grains taking place at a higher etching time.



(a)



(b)



(c)

Figure 4.15: Disappearance of particles and clusters taking place with increasing etching time (25°C dilute H_2SO_4 bath) - (a) Anodically cleaned DP800 (0s acid etched), (b) 10s acid etched, (c) 60s acid etched

EDX analyses on the particles in Figure 4.15b revealed high atomic fractions of Mn and the discontinuous clusters with high Mn and Si atomic fractions (Figure B.4). However, the oxygen concentration was not detected properly along the particles due to the high interaction volume for the X-rays incident on the substrate as stated earlier in Section 4.1.1. But it was detected along the grain boundary regions. Presence of particles and clusters after etching at shorter etching times might suggest that the surface oxides are partially dissolved during the process, attributed by size reduction in the particles and discontinuity in the clusters present over the surface compared to a non-etched substrate (Figure 4.15a and Figure 4.15b). Also, the detection of oxygen enrichments only along the grain boundary regions by EDX might suggest that the grain boundary oxides might have been initially thicker than the oxide particles. This might correspond to the densification of oxides of alloying elements, preferably at the grain boundary regions, as grain boundaries tend to be the easiest and the most favourable path for the diffusion of alloying elements and oxygen atoms towards the surface (section A.2).

Another interesting observation made during the study was the non-uniformity in the surface roughness as certain preferred grains appeared to be rough after etching. This effect was usually observed at higher etching times (Figure 4.14d) accompanied by grain boundaries becoming much more clear on the surface. The effect was intense when the rate of dissolution of the substrate was increased by raising the acid bath temperature to 50°C. Figure 4.16 shows the changes observed in the surface morphology with increasing etching time in a 50°C dilute H₂SO₄ bath.

Higher magnifications revealed the difference in the surface ruggedness of certain grains on the etched sample, where rough grains were clearly differentiated with smooth grains. Figure 4.17 shows the difference between smooth and rough grains over an acid etched DP800 substrate.

Such significant variations in the roughness of individual grains might be attributed to different corrosion rates of different phases formed after the annealing process of DP800 substrates. DP steels are composed of a matrix of ferritic phase containing small islands of a secondary phase which is usually martensite, although small amounts of retained austenite and bainite might also be a possibility (as discussed in Section 1.1). Each phase corresponds to different crystal structures, different compositions of alloying elements and thus, might also differ in their corrosion properties as well. Studies reported by Si et al. [40] and Fushimi et al. [41] suggest the formation of micro-galvanic corrosion cells formed over the surface of DP steels due to lesser corrosion potential of the softer ferritic matrix in the substrate than the martensitic phase in an acidic environment. The ferritic matrix in contact with its adjacent martensitic grains are known to act as sacrificial anodes in an acidic environment, thus preferentially dissolving ferrite over martensite on the substrate. This might explain the reason behind the non-uniformity in the corrosion rates of different grains over the steel substrate.

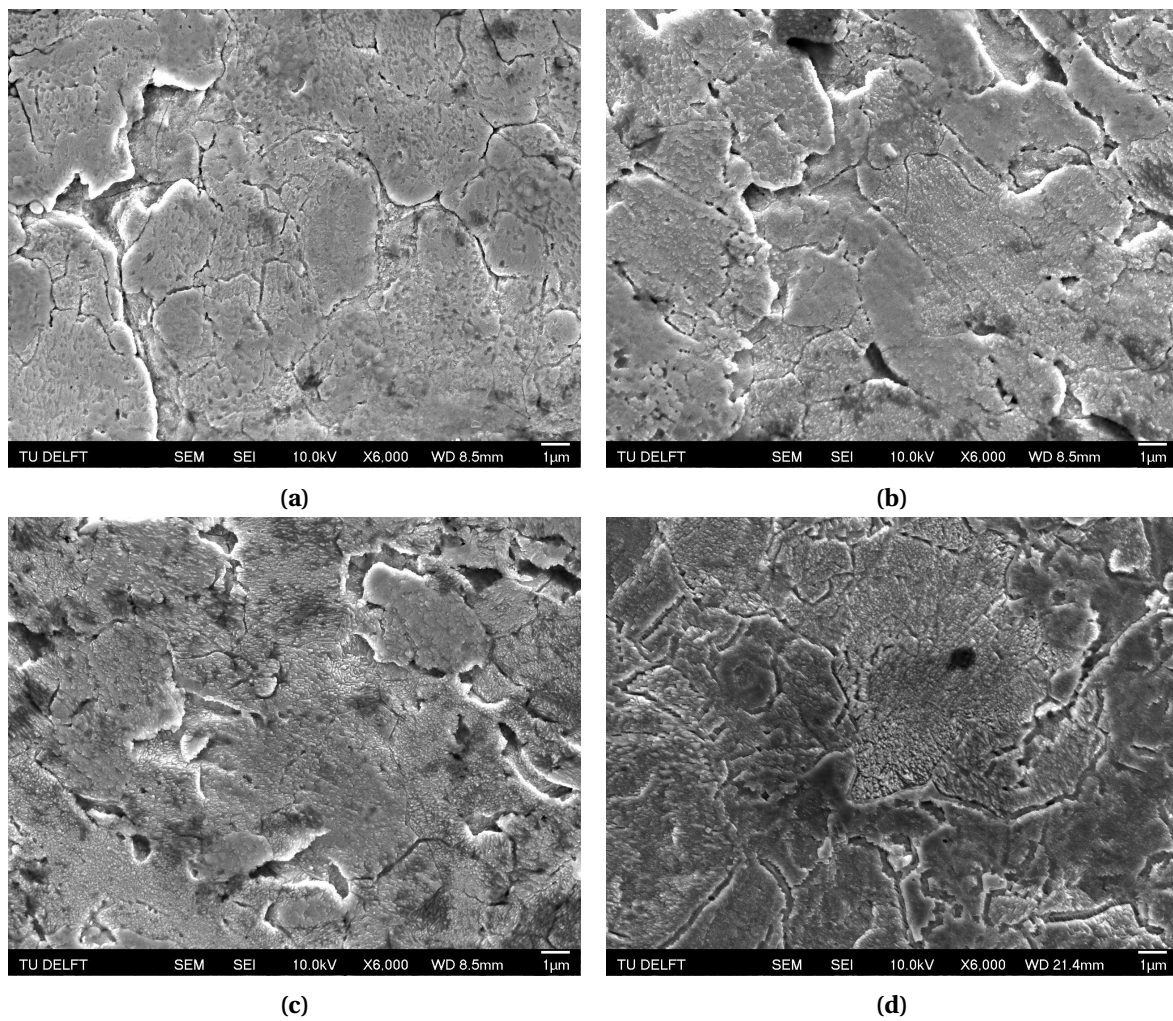


Figure 4.16: Non-uniform surface roughness observed in a DP800 substrate with increasing etching time (50°C dilute H₂SO₄ bath) - (a) 10s, (b) 30s, (c) 60s, (d) 120s

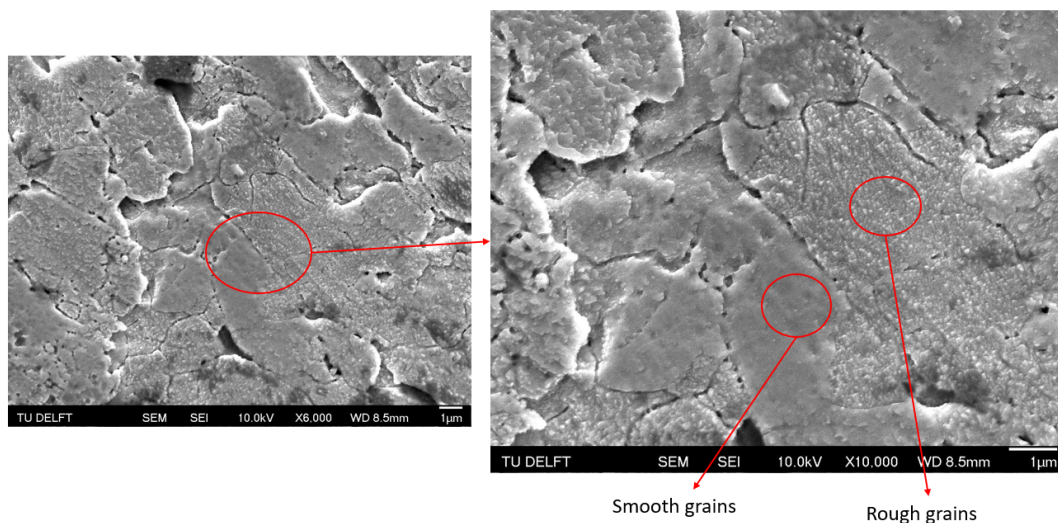


Figure 4.17: Variations in surface roughness between two different grains in a 30s acid etched DP800 substrate (in a 50°C dilute H₂SO₄ bath)

To sum up, the variations in the surface morphology of the substrate takes place in the following order with increasing etching time,

- Partial dissolution of oxide particles may seem to occur at shorter etching times, characterised by size reduction of dispersed particles and discontinuity in cluster of particles observed after etching. The visibility of the grain boundaries were unclear at this stage.
- As the etching time progressed, the remaining particles and clusters disappear and acid attack over the grains seem to initiate, which causes an initial roughening over the surface. Grain boundaries became more clear, suggesting grain boundary dissolution on the surface.
- As the dissolution rate increases due to increasing temperature of the acid bath, certain preferred grains seem to dissolve much faster than the other, which might be related to the micro-galvanic cells formed between ferritic grains and martensitic grains for which the former tends to corrode much faster than the latter.
- Grain boundary dissolution seems to be significant at higher etching rates characterised by the grain boundaries being clearly visible.

To investigate how the changes in the surface morphology affects the surface wettability of the substrate (i.e. related to the surface activation after etching), sessile drop experiments were performed with increasing etching time with demineralised water as a reference liquid droplet. Table 4.7 shows the changes taking place in the contact angle of the liquid droplet with respect to increasing acid etching time,

Table 4.7: Variations in contact angle with increasing etching time for DP800 substrates etched in a 25°C dilute H₂SO₄ bath

DP800 Substrates	Contact angle of water (deg.)
Untreated	76.3° ± 1.0°
Anodic cleaned	39.5° ± 1.6°
Acid etched 10s	30.0° ± 1.8°
Acid etched 30s	29.5° ± 0.7°
Acid etched 60s	29.0° ± 1.4°
Acid etched 120s	22.1° ± 1.4°

We observe that a significant change was observed between the contact angle of an anodic cleaned DP800 substrate and an etched DP800 substrate, suggesting that the surface wettability of the substrate does increase by acid etching. However, no significant change was observed at the initial stages of etching. Only after 120s of etching the substrate, the contact angle seem to change from 29.0° to 22.1°. This might imply that the relative small changes in the surface microstructure do not play such a large role at the start of the etching process. Furthermore, the oxide skin which is typically 120 nm thick is expected to be removed after 30 seconds of etching. To observe the interaction of the etched steel surface with the coating, coating adhesion was investigated using adhesion tests, which will be discussed later in Section 4.2.

Variations in surface composition

As discussed earlier in Section 4.1.1, the surface oxides were enriched with Mn and Si for the clusters along the grain boundary regions and with Mn for particles over the grains. This led to a hypothesis where the presence of ternary Mn-Si oxides (possibly minerals like silicates) were present as cluster

of particles and Mn-rich oxides (most likely MnO) present as dispersed particles. Thus, the dissolution mechanism of silicates and general metallic oxides will be considered in this study.

Crundwell (2014) [42] studied the theory of dissolution mechanism of minerals and metallic oxides in low pH solutions, for which the study described the mechanism of transfer of oxide or silicate anions and metal cations within the solution. The interface between the surface of the solid and the solution is based on the Bockris-Devanathan-Muller model of the electrical double layer where the layer is divided into two different regions (see Figure 4.18),

- A Helmholtz double layer between the surface of the solid and the Outer Helmholtz Plane (OHP) which represents an array of adsorbed charged species (with water molecules). The potential difference tends to be high across this interface.
- A Gouy-Chapman layer between the OHP and the bulk of the solution. The potential difference across this layer tends to be very low.

The driving force for the ions to move towards the solution to react with H^+ or adsorbed water molecules is the potential difference across the Helmholtz layer. Figure 4.18 represents the dissolution phenomena of a solid MA in acidic solutions where M represents the metal species and A represents the bonded species (oxides or silicates).

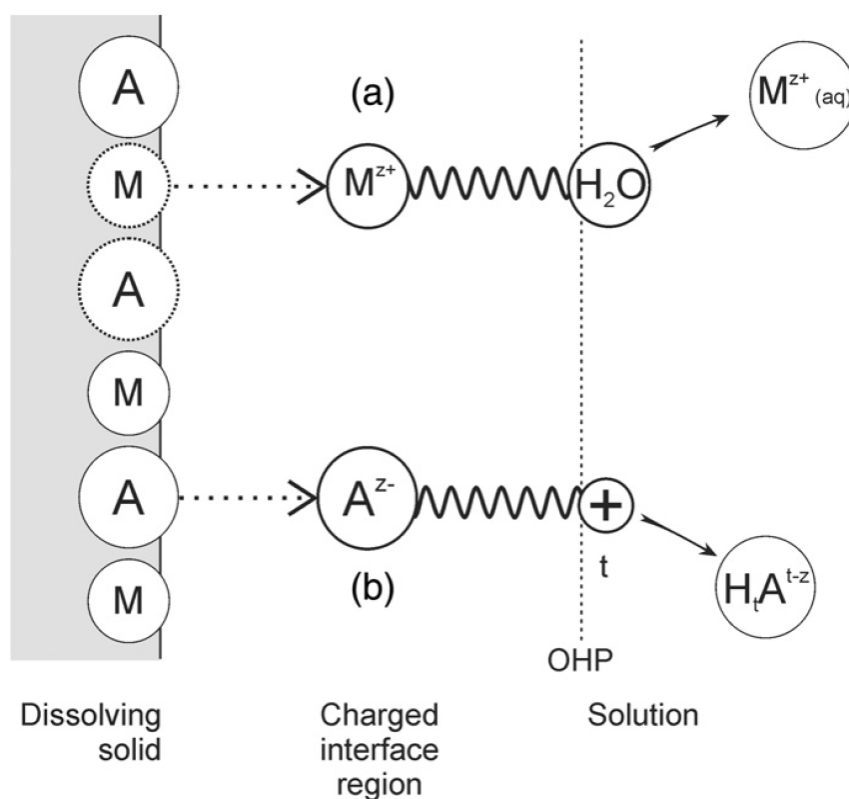


Figure 4.18: Charge transfer taking place across the Helmholtz double layer - (a) Transfer of metal species by adsorbed water molecules to form cations in the aqueous solution (M^{Z+}), (b) Removal of the bonded species (A) by the attack of H^+ ions to form anions in aqueous solution - Crundwell et al. [42]

Two simultaneous steps take place during the dissolution mechanism of MA,

- The bonded metal species M separates from the surface to form a metal cation M^{z+} which reacts with the adsorbed water molecules at the Helmholtz layer to get transferred into the solution.
- The A species, which due to the breaking of bonds with the M species, forms an anion A^{z-} which reacts with H^+ ions at the Helmholtz layer to form a complex which dissolves into the solution.

Since the study deals with the effect of surface changes on the coating adhesion of PVD deposited zinc, the dissolution of surface oxides were measured using surface compositional GDOES depth profile analyses and XPS analyses. Figure 4.19 depicts the changes in the composition of major alloying elements with respect to increasing depth for substrates etched at various etching times in a 25°C dilute H_2SO_4 bath.

GDOES measurements show clear decrease in the enrichments of Mn and Si over the surface characterised by the vertical shift in their peak concentrations. Here, the reference is taken as an untreated DP800 substrate. Mn tends to decrease from an initial concentration of 10 wt% to about 3.5 wt% and Si tends to decrease from 6 wt% to about 2 wt% from the reference as seen from Figure 4.19c and Figure 4.19d. Also, the etching time does not seem to influence the concentrations of Mn and Si over the surface, as the concentrations of Mn and Si remained the same for all etching times. The enrichments of Cr decreased from an initial 2 wt% to about 1 wt% from the reference sample but no changes between an anodic cleaned and an acid etched sample was observed. The same trend was observed for oxygen concentration at the surface (Figure 4.19b) where peak concentrations of about 50 wt% to 60 wt% remained unchanged with acid etching.

Apart from the vertical shifts, horizontal shifts were also observed in the plots, which correspond to changes in the depths. Figure 4.19c to Figure 4.19e indicate that the enrichments of alloying elements such as Mn, Si and Cr were initially present upto depths of about 50 nm after which they reach their concentrations in the bulk. However, after acid etching the depths tend to decrease to lower values of about 10 nm on the surface. The same trend can be observed for oxygen where its high concentration region, which was initially observed at 50 nm depth from the surface (see Section 4.1.1), shifted to about 20 nm.

The vertical and horizontal shifts in the concentrations of Mn and Si after acid etching might be correlated with the dissolution of Mn-Si rich and Mn-rich surface oxides as discussed earlier through studies reported by Crundwell [42]. The elements tend to reach their bulk values at the surface after the oxide dissolution. This might explain the constant surface concentrations of Mn and Si for all the etching times. However, the partial dissolution of oxides (as observed from Figure 4.15b) at shorter etching times was not verified using this method. This might be due to a resolution problem in GDOES. GDOES computes the average surface composition of elements on a large surface area (spot size ≈ 5 mm diameter). Therefore, relative small changes in the surface oxide morphology might not affect the average composition on a larger scale.

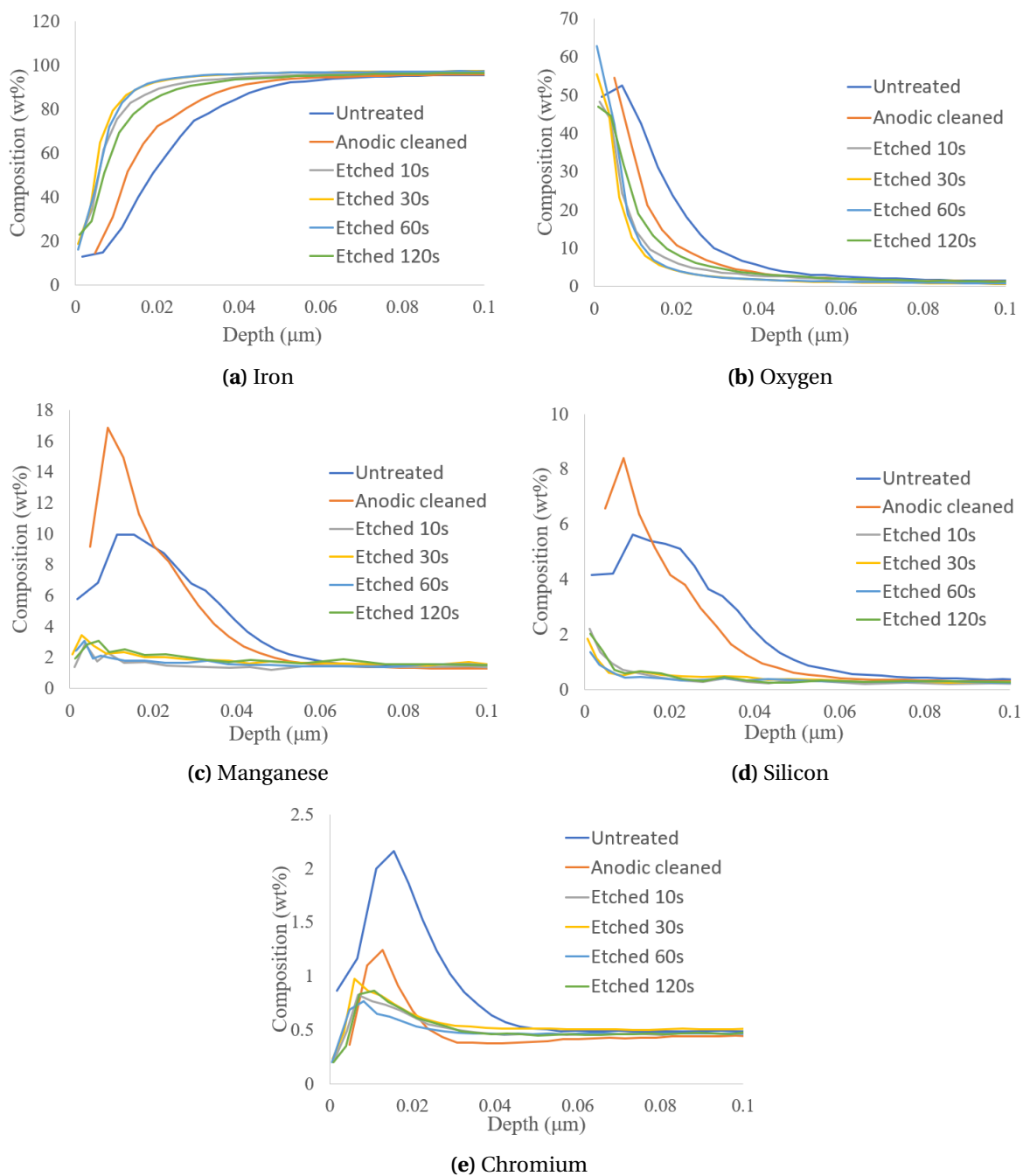


Figure 4.19: Comparative GDOES depth profile results of untreated, anodically cleaned and acid etched DP800 substrates - (a) Fe, (b) O, (c) Mn, (d) Si, (e) Cr

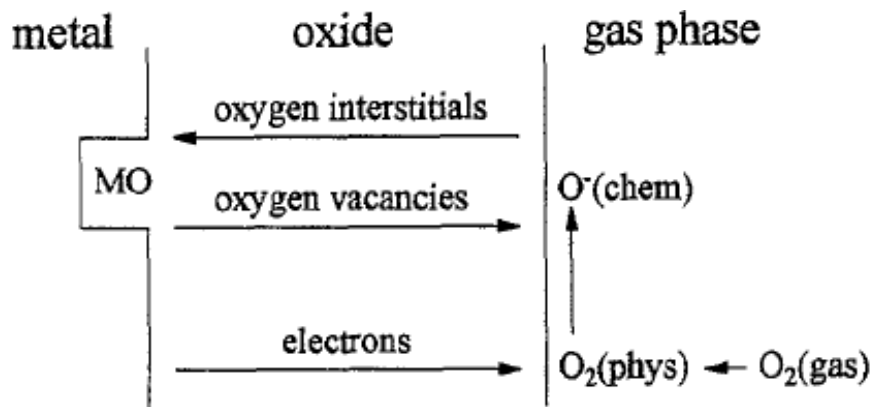
After the dissolution process, a slight enrichment of the major alloying elements (Mn, Si, and Cr) were still present at smaller depths regardless of the etching time. This might suggest an external driving force that makes the solute atoms diffuse towards the surface to form enrichments. However, the substrates were not subjected to very high temperatures to thermally activate the solute atoms for diffusion towards the surface. Instead, the samples were exposed to air at room temperatures after the etching process (GDOES depth profile measurements were taken after 14 days of exposure). Figure 4.19b depicts high oxygen concentrations at the surface, present upto depths of about 20 nm even though the etching seems to have removed the surface oxides. This might explain a certain phenomenon that relates to surface reoxidation of the base metal after the etching step.

Surface reoxidation

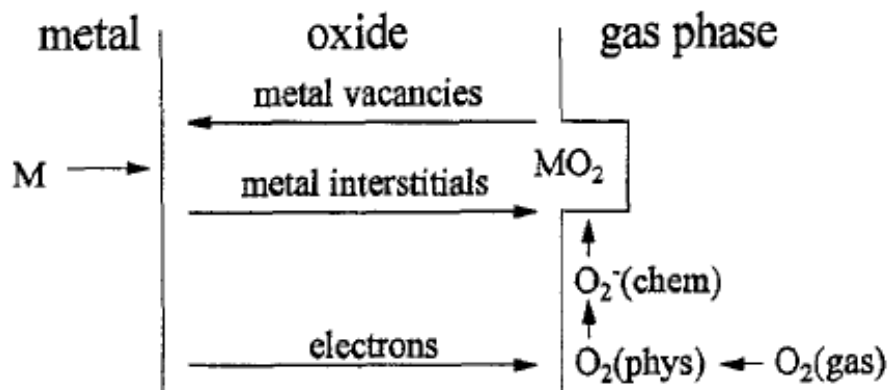
Studies by Martin et al. [43] and Grosvenor et al.[44] suggested the formation of metal oxides at low temperatures by Cabrera-Mott theory of oxidation. The studies reported that an initial physisorption of oxygen gas over the bulk metal will act as electron acceptors from the metal to give chemisorbed O_2^- anions. This forms covalent bonds with the metal cations to form an initial monolayer of oxide. The transfer of electrons from the metal surface to the oxide is prevalent and is driven by a contact potential, called Mott potential, that exists between the bulk metal and the adsorbed oxygen at the interface. This contact potential initiates tunneling of electrons through the oxide layer, maintaining an electric field across the oxide layer. Until this field diminishes, two different processes take place,

- Transport of metal cations from the bulk metal to the oxide surface as interstitials at the oxide/gas interface to form a vacancy in the bulk metal
- Transport of oxygen anions at the metal/oxide interface as interstitials to form vacancies at the oxide surface

A brief overview of the initial steps of low temperature oxidation of metals is given in Figure 4.20,



(a) Transport of metal cations as interstitials at the oxide/gas interface



(b) Transport of oxygen anions as interstitials at the metal/oxide interface

Figure 4.20: Building up of layers of oxide over the bulk metal at low temperatures by Cabrera-Mott theory of oxidation - Martin et al. [43]

The presence of surface oxides even after the etching process due to reoxidation was investigated using XPS analyses. Samples were acid etched for 60s in a 25°C dilute H_2SO_4 bath and the analysis

was performed after 20 days. Figure 4.21 depicts a comparative spectra between an acid etched DP800 (etched for 60s), anodic cleaned DP800 substrate and an untreated DP800.

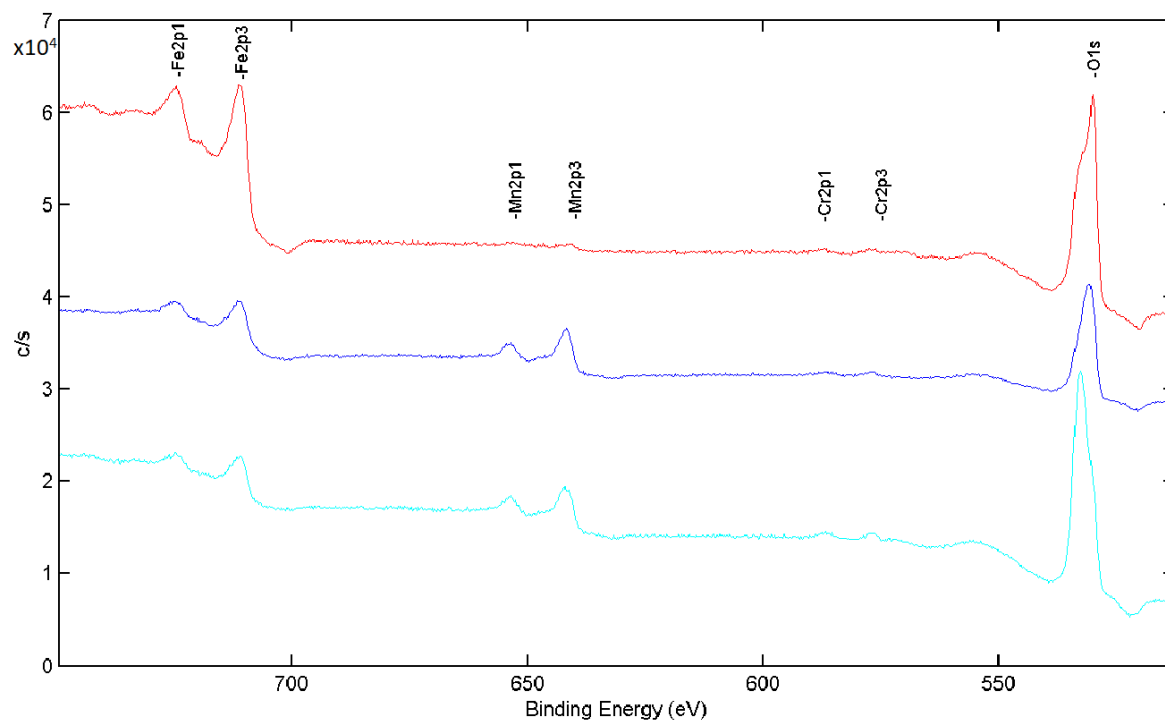


Figure 4.21: Comparative XPS spectra of anodic cleaned DP800, untreated DP800 and acid etched DP800 taken 20 days after the treatment (BE - 500 to 750 eV) - red spectrum corresponds to acid etched DP800 substrate, dark blue spectrum corresponds to anodic cleaned DP800 and cyan spectrum corresponds to untreated DP800

Intense Fe 2p_{1/2} and 2p_{3/2} and O 1s peaks were observed for an acid etched DP800 substrate compared to an untreated or anodic cleaned substrates. The binding energy values of the corresponding Fe 2p_{3/2} and O 1s peaks are given in Table 4.8,

Table 4.8: Binding energies of Fe 2p_{3/2} and O 1s on an acid etched DP800 substrate etched for 60s in a 25°C dilute H₂SO₄ bath

Elements	Binding energy (eV)
Fe 2p _{3/2}	710.3
O 1s	530.0 (O ²⁻)
	532.4 (OH ⁻)

Peaks of major alloying elements such as Mn 2p seem to have non intensive peaks along the spectrum compared to an anodic cleaned or untreated sample, evident from Figure 4.21. The same trend was observed in case of Si 2p peaks at lower binding energy values and secondary Mn 3p and 3s peaks as depicted in Figure 4.22.

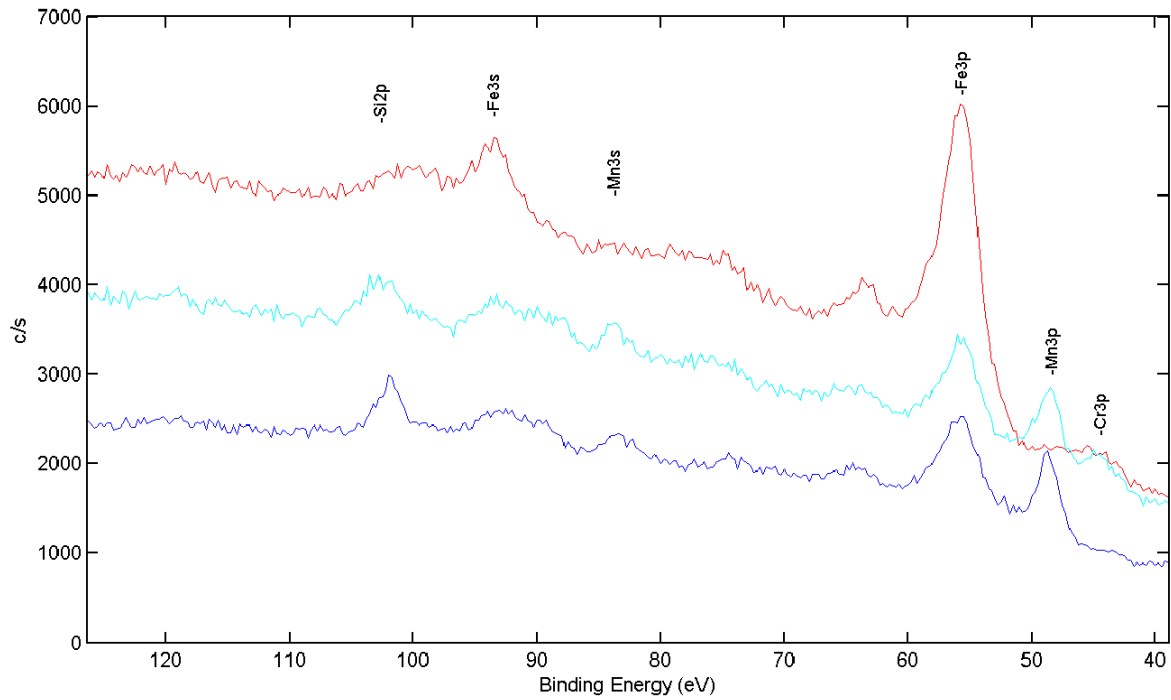


Figure 4.22: Comparative XPS spectra of anodic cleaned DP800, untreated DP800 and acid etched DP800 taken 20 days after the treatment (BE - 40 to 120 eV) - red spectrum corresponds to acid etched DP800 substrate, dark blue spectrum corresponds to anodic cleaned DP800 and cyan spectrum corresponds to untreated DP800

The binding energies of the corresponding minute peaks of Mn 2p_{3/2}, Si 2p and Cr 2p_{3/2} are given in Table 4.9.

Table 4.9: Binding energies of alloying elements on an acid etched DP800 substrate etched for 60s in a 25°C dilute H₂SO₄ bath

Elements	Binding energy (eV)
Mn 2p _{3/2}	640.8
Si 2p	101.3
Cr 2p _{3/2}	576.8

Strong primary peak intensities of Fe 2p and O1s along with secondary Fe 3s and 3p peaks might suggest that a thin layer of iron oxide (possibly hematite (Fe_2O_3) from the binding energy values [35]) was formed due to reoxidation after the acid etching step. This is consistent with the GDOES depth profile results (Figure 4.19a and Figure 4.19b), where the concentrations of iron and oxygen predominated at the surface compared to other major alloying elements. However, the oxygen concentrations remained the same regardless of the etching pre-treatment step.

The reduction in the peak intensity of Mn, Cr and Si 2p peaks might be correlated to the reduction in the enrichments of Mn and Si from their GDOES plots as shown in Figure 4.19c and Figure 4.19d. This might suggest an effective dissolution of surface oxides that were initially present on an untreated DP800 substrate. However, due to their low concentrations in the bulk compared to iron and very low thermal energy available at room temperatures for their diffusion towards the surface to form an oxide, they tend to segregate at low amounts, as evident from their surface concentrations from GDOES depth profile results. Thus, their oxides were vaguely detected using XPS analysis.

Thus, surface activation of the steel due to acid etching will always tend to form an oxide skin. This oxide layer continues to build up over the surface with constant exposure. Attempts were made to track the surface wettability of the steel surface with respect to increasing exposure times (Appendix C). However, no proper trend was obtained between the contact angle of the liquid droplet and the exposure time of the steel surface for which the method seems to be ineffective for analysis.

4.1.4. Effect of corrosion inhibitor

Corrosion inhibitors are added to the acid bath to reduce the effects of over-etching, as discussed earlier in Section 2.1.2. This will reduce further attack of H^+ ions over the bare metal substrate after the oxides are dissolved in the acid bath by the adsorption of inhibitor molecules over the metal substrate. In this study, the effect of corrosion inhibitors on the surface wettability of the etched substrate will be studied, as the adsorption of inhibitor molecules over the surface might tend to influence the coating adhesion properties of the substrate.

Preliminary weight loss analysis was performed to check the inhibition efficiency of the inhibitor used. Figure 4.23 shows the comparative weight loss analysis taking place with increasing etching time for inhibited and uninhibited samples etched in a dilute H_2SO_4 bath at $50^\circ C$.

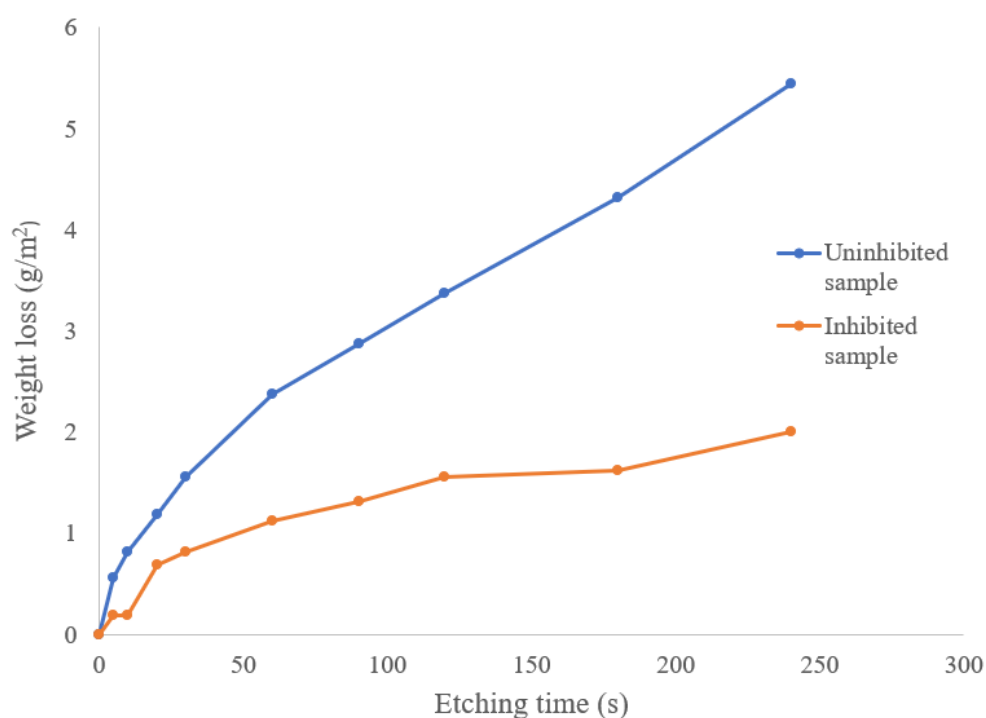


Figure 4.23: Comparative weight loss results for inhibited and uninhibited samples etched in dilute H_2SO_4 bath at $50^\circ C$

Dissolution rate of the inhibited and uninhibited samples were obtained from Equation 2.5. Inhibition efficiency was calculated by comparing the relative dissolution rates of both the samples as given in Equation 4.2,

$$\eta = \frac{DR_{\text{uninhibited}} - DR_{\text{inhibited}}}{DR_{\text{uninhibited}}} \times 100 \quad (4.2)$$

where,

η - Inhibition efficiency (%)

$DR_{\text{uninhibited}}$ - Dissolution rate of uninhibited sample (cm/s)

$DR_{\text{inhibited}}$ - Dissolution rate of inhibited sample (cm/s)

An inhibition efficiency of about 59% was achieved for the given inhibitor concentration (Section 3.1). Even though the effect of inhibitor was observed by reduced dissolution rates, its effect on the coating adhesion properties of the steel samples were investigated by surface wettability analysis. Thus, sessile drop experiments were performed on the inhibited surface with increasing etching time to observe changes in the contact angle of the liquid droplet (demineralised water) over the surface. Table 4.10 shows the changes taking place in the contact angle of water with increasing etching time for an inhibited surface.

Table 4.10: Variations in contact angle with increasing etching time for DP800 substrates etched in a 25°C dilute H_2SO_4 bath with 150 $\mu\text{L/L}$ inhibitor

DP800 Substrates	Contact angle of water (deg.)
Untreated	$76.3^\circ \pm 1.0^\circ$
Anodic cleaned	$39.5^\circ \pm 1.6^\circ$
Acid etched 10s with inhibitor	$40.4^\circ \pm 1.4^\circ$
Acid etched 30s with inhibitor	$40.9^\circ \pm 0.6^\circ$
Acid etched 60s with inhibitor	$52.9^\circ \pm 1.4^\circ$
Acid etched 120s with inhibitor	$64.1^\circ \pm 2.2^\circ$

Table 4.10 suggests that the contact angle of the liquid droplet increases with increasing etching time. This is inconsistent with the results obtained for an uninhibited steel (see Table 4.7). This can be explained by the added inhibitor in the acid bath, due to which adsorption of inhibitor molecules might have taken place on the surface during etching. These molecules might have hindered the wetting of the liquid droplet over the steel for which an increase in the contact angle was observed. To verify the presence of inhibitor over the etched samples, a comparative surface analysis was performed for samples etched at shorter etching time (say 30s) and higher etching time (say 120s). Figure 4.24 represents the comparative SEM images between the inhibited and uninhibited samples.

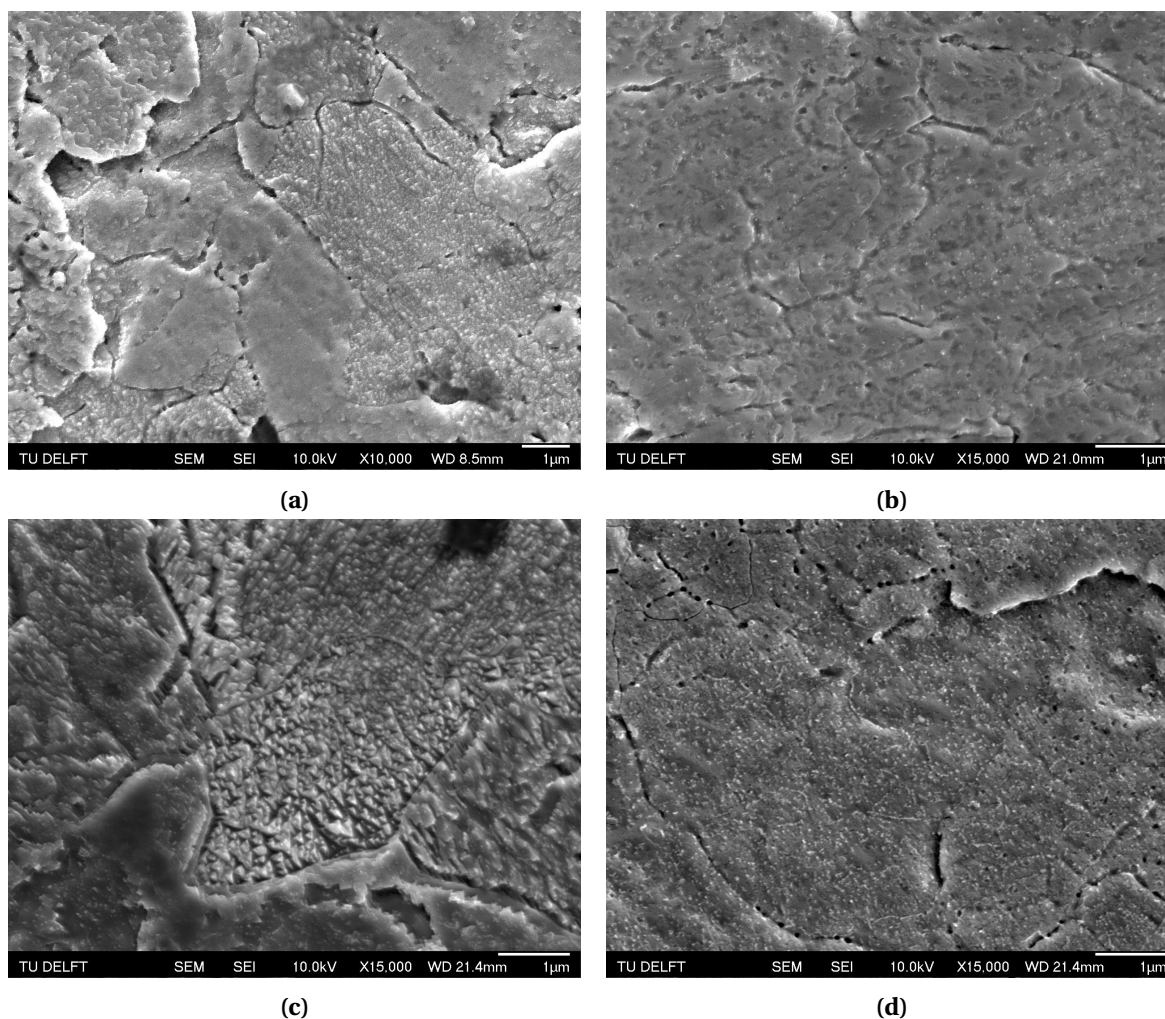


Figure 4.24: Comparative analysis of uninhibited and inhibited DP800 samples - (a) Etched for 30s without an inhibitor, (b) Etched for 30s with an inhibitor, (c) Etched for 120s without an inhibitor, (d) Etched for 120s with an inhibitor

Figure 4.24b and Figure 4.24d suggest that the acid attack on the steel surface was not so prominent compared to the uninhibited samples in Figure 4.24a and Figure 4.24c. Another interesting observation is the presence of additional nano-sized particles over the surface as shown in Figure 4.25 for a sample etched for 120s in a dilute H_2SO_4 bath with an inhibitor. These particles were 10 to 20 nm in size, spread uniformly over the surface of the sample. Thus, EDX analyses failed to characterise these particles from the steel substrate, as they were detected with Fe, Mn and C enrichments similar to that of an uninhibited acid etched sample (Figure B.5). Since a thiourea derivative was used (an organic molecule which contains one atom of sulphur), sulphur was also investigated. However, no enrichments of sulphur were observed. GDOES depth profile analyses were also performed to investigate changes in the composition of individual elements over the substrate at higher resolutions. However, no such changes were observed between an uninhibited sample and a inhibited sample as shown from GDOES plots of carbon and sulphur as shown in Figure 4.26a and Figure 4.26b.

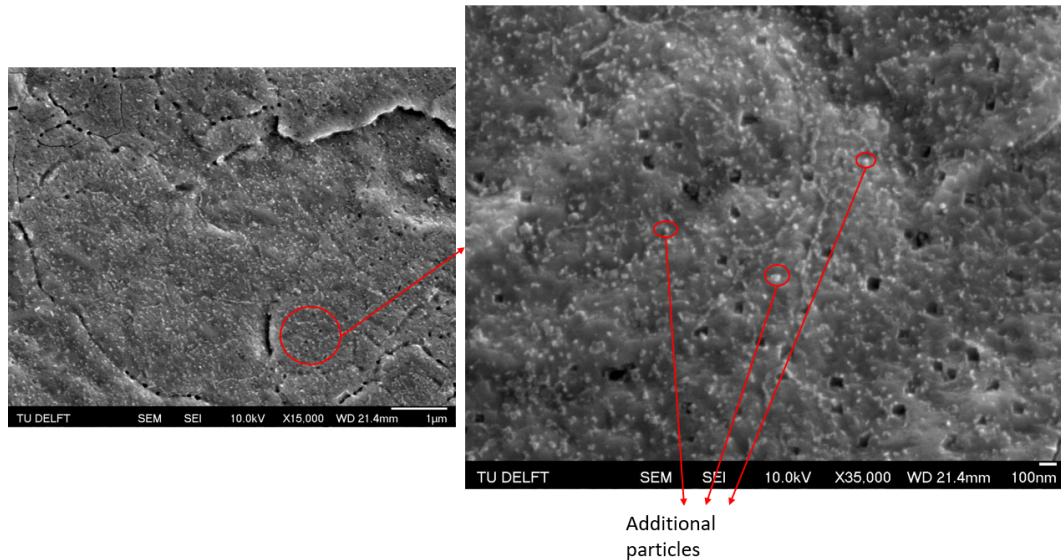


Figure 4.25: Presence of nano-scale particles over the surface after etching with dilute H_2SO_4 at 50°C with $150 \mu\text{L/L}$ inhibitor for 120s

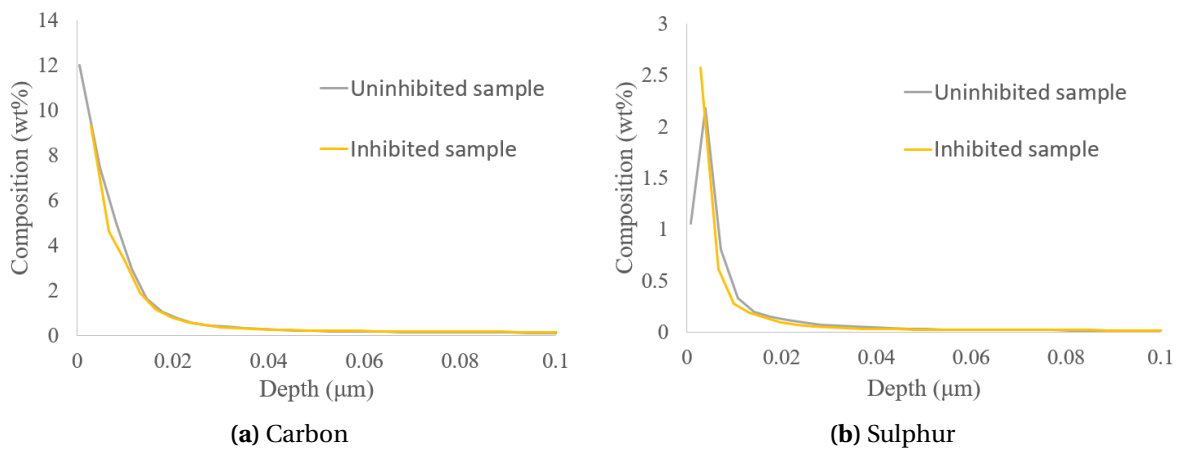


Figure 4.26: Comparative GDOES depth analysis of (a) Carbon, (b) Sulphur compositions at the surface between uninhibited and inhibited DP800 samples

Thus, the composition of additional particles over the surface was difficult to detect using surface compositional techniques. However, the particles can be speculated as adsorbed inhibitor particles over the surface, attributed to changes in the dissolution rate and surface wettability of the samples after acid etching with an inhibitor.

Surface wettability analysis also suggested a gradual rise in the contact angle of the liquid droplet with increasing etching time. This can be correlated with an increase in the surface coverage of the particles adsorbed per unit surface area with increasing etching time as observed from SEM images (Figure 4.24b and Figure 4.24d).

The dissolution of an oxide particle from the surface might create an adsorption site for the inhibitor molecules. As the etching time progresses, the adsorbed molecules might nucleate over these sites to grow as particles. Eventually, the surface coverage of these particles might tend to increase with increasing etching time, as the number of adsorption sites created by the surface increases with

more surface oxide particles being dissolved.

The effect of corrosion inhibitors was investigated to regulate the acid etching process so that acid attack on the metal surface can be minimised. This might be helpful in retarding the diffusion of H^+ ions through the grain boundary regions to ensure minimisation of intergranular corrosion and hydrogen embrittlement at higher dissolution rates. However, a decrease in the surface wettability due to the adsorption of inhibitor molecules over the surface, making it incompatible for coating adhesion properties. Thus, a pre-sputter process might be necessary after the etching process to remove the adsorbed inhibitor molecules from the surface, which will be discussed in Section 4.2.4.

4.2. Analysis of coated DP800 samples

In this section, samples were coated using the PVD deposition method and analysed for coating adhesion performance. First a minimum required sputter intensity and minimum substrate temperature were determined to obtain good coating adhesion properties. Then the effect of the pre-treatment steps on the adhesion performance was observed. Adhesion tests were performed for analysis. SEM/EDX analyses were performed on delaminated parts. Thus, an overview of the results from these analyses will be discussed.

4.2.1. Minimum required sputter intensity

Untreated DP800 substrates were sputtered in the argon ion sputtering unit, which was implemented within the PVD chamber as an initial surface pre-treatment process to remove contaminants and surface oxides. For this, steel plates of about 17 cm x 10 cm surface were taken for which the sputter time was varied at a constant sputter power of 200 W. The steel strip was placed in a cart of dimensions 33 cm x 17 cm which forms a total surface to be sputtered, i.e., $0.056m^2$. Plasma sputter intensities were calculated as follows,

$$I = \frac{Pt}{A} \quad (4.3)$$

where,

I = Plasma sputter intensity in J/m^2

P = Sputter power used (W)

t = Time taken for the plasma etching process (s)

A = Total surface covered for sputtering (m^2)

The minimum required sputter intensity was first determined for an untreated DP800 steel substrate. Plasma sputter intensities were varied by changing the sputter time. After the sputter treatment, the cart is immediately passed over the VDB where the coating deposition took place. Adhesion tests were performed on coated samples for which the samples were cut into 4 strips - 3 strips for BMW test and 1 strip for OT test. The specifics of both the tests were discussed already in Chapter 3. The results of the adhesion tests are given in Table 4.11,

Table 4.11: Adhesion test results on coated DP800 substrates pre-treated with decreasing plasma sputter intensity (A/B/C in BMW test correspond to BMW test results for 3 strips, A, B and C)

DP800 Substrate	Plasma Sputter intensity (kJ/m ²)	0T test	BMW Test	Overall result
20180502A 21	2679	OK	0/0/0	OK
20190807B	2357	OK	0/0/0	OK
20180424A 33	2250	NOK	0/1/4	NOK
20190812A	1714	OK	1/0/2	NOK
20180424A 32	1607	NOK	1/4/4	NOK
20180420B 30	804	NOK	1/1/1	NOK

BMW and 0T tests reveals a transition between 2357 kJ/m² and 2250 kJ/m² from OK adhesion to NOK adhesion. Thus, a minimum sputter intensity of about 2300 kJ/m² was required to obtain a good coating adhesion. This corresponds to about 650s of sputter time required for a 200 W sputter power.

Due to the sputtering process, the temperature of the sputtered samples increases before coating deposition. This temperature increase plays a role in the coating adhesion performance of the samples, which will be discussed in the next section.

4.2.2. Effect of substrate temperature on coating adhesion

The study aims at reducing the minimum sputter intensity required to obtain a good adhesion. At low sputter intensities, the substrate temperature will be low before the coating deposition takes place. As discussed earlier in Section 2.2, low substrate temperatures might not favour good coating adhesion on the substrate. Thus, the coating adhesion performance as a function of substrate temperatures was investigated to determine the minimum substrate temperature required to obtain a good coating adhesion.

First, the substrate temperature was plotted as a function of sputter time to determine the increase in the substrate temperature with sputtering. This was measured using a thermocouple welded to the substrate (see Figure 4.27).

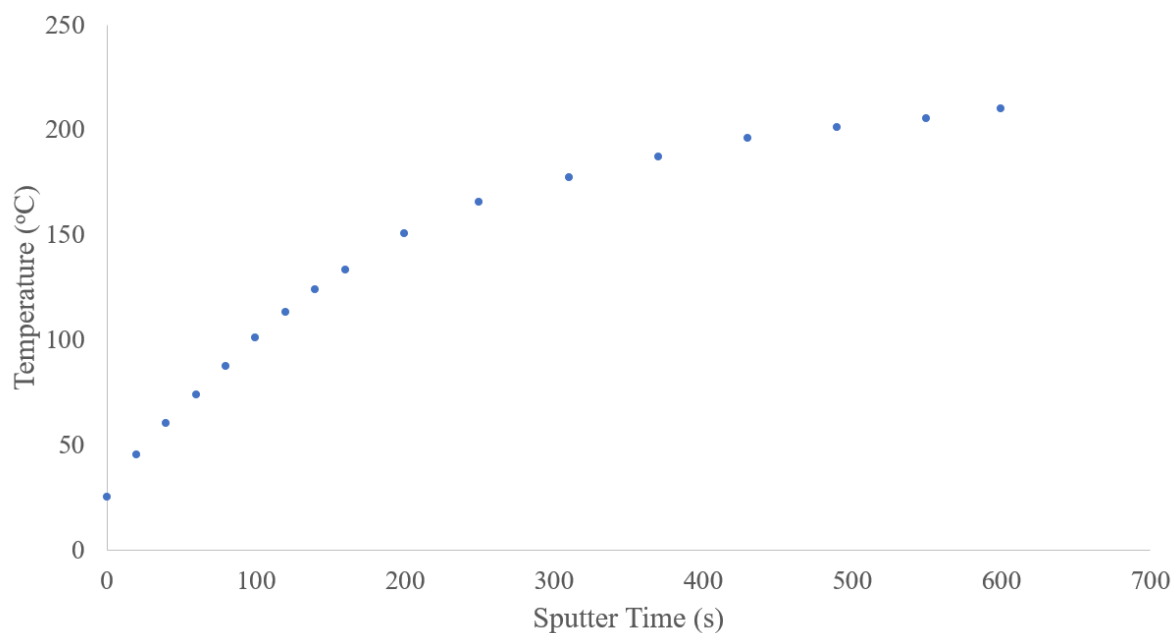


Figure 4.27: Temperature evolution of the substrate with increasing sputter time for a sputter power of 200 W

Then, untreated DP800 samples were sputtered at a constant power of 2500 kJ/m^2 which favours a good coating adhesion when applied in a single run. It corresponds to a substrate temperature of about 220°C (see Figure 4.27). However, to coat the sample at the desired substrate temperature, the sample was made to wait after sputtering till it has reached 20°C below the desired temperature. Then a sputtering of about 1 min was performed to eliminate any surface oxides present due to reoxidation of the samples, as it was known to take place at even high vacuum environment (10^{-4} mbar) [44]. The pre-sputter eventually increases the substrate temperature to the desired value. Then the samples were immediately coated by passing it over the VDB. The strip speed was maintained at 1 m/min. Table 4.12 shows the adhesion test results obtained with increasing substrate temperature.

Table 4.12: Adhesion test results of DP800 substrates coated at increasing substrate temperatures

DP800 Substrate	Sputter power (W)	Sputter time (s)	Sputter intensity (kJ/m^2)	Substrate temperature ($^\circ\text{C}$)	OT test	BMW Test	Overall result
20190930A	200	720	2571	110	NOK	1/1/1	NOK
20190927A	200	720	2571	120	NOK	1/1/1	NOK
20190930B	200	720	2571	131	NOK	1/1/1	NOK
20191001A	200	720	2571	141	NOK	1/1/1	NOK
20191001B	200	720	2571	147	OK	1/1/1	NOK
20191003A	200	720	2571	162	OK	0/0/0	OK

BMW and OT tests suggest OK adhesion for a substrate coated at a temperature of 162°C but NOK for a substrate temperature below 147°C . Thus, substrate temperature of at least 147°C was required to obtain a good coating adhesion over the substrate. Final coating microstructures of these samples were obtained using SEM images to determine the cause of de-adhesion taking place at lower substrate temperatures. Figure 4.28 depicts the microstructural evolution of the coating material taking place with respect to increasing substrate temperature,

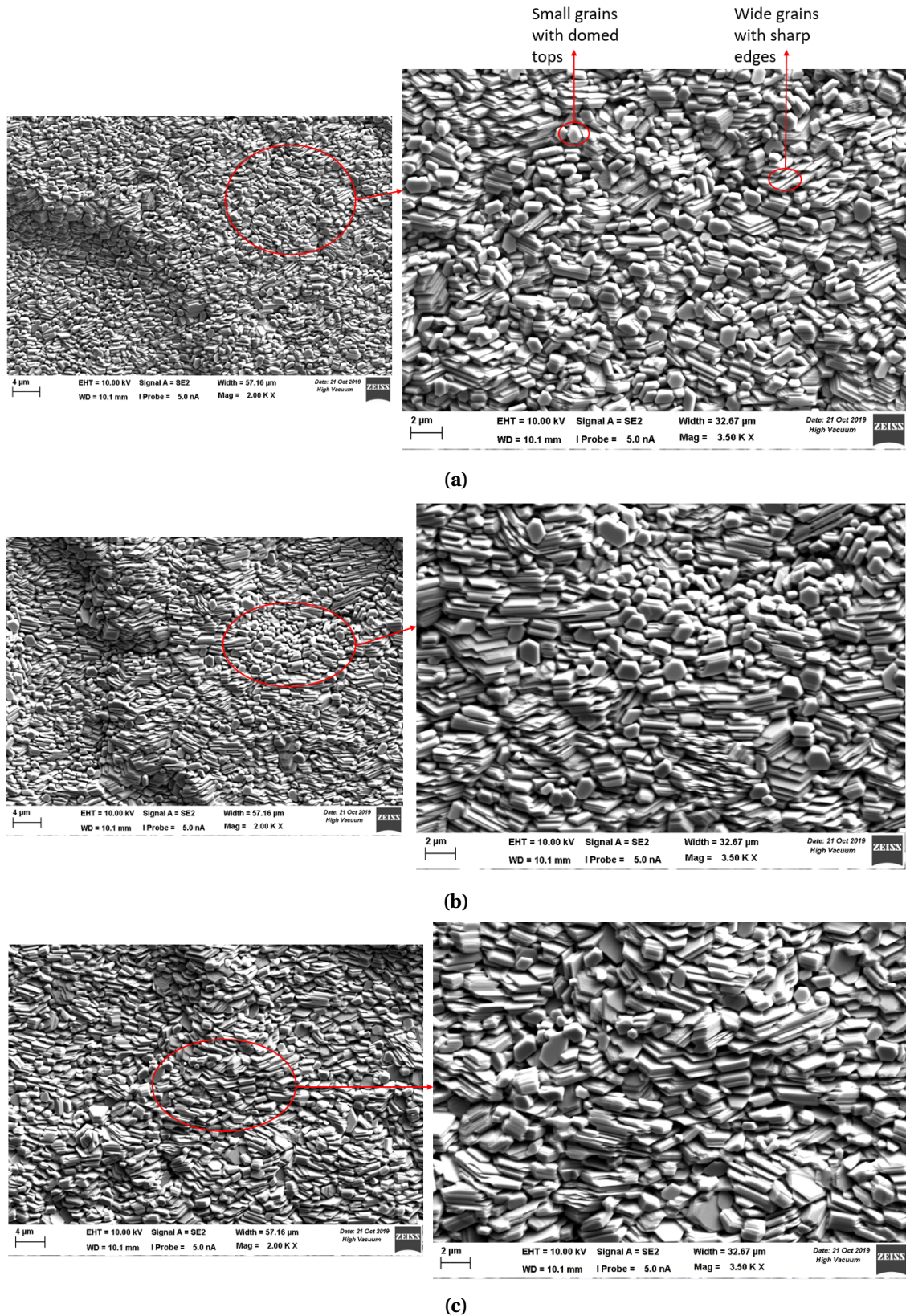


Figure 4.28: Microstructural evolution of the coating material with increasing substrate temperature - (a) Coated at 120°C, (b) Coated at 141°C, (c) Coated at 162°C

Figure 4.28 suggests that increasing substrate temperature changes the final crystallographic struc-

ture of the coated sample from smaller grains with domed tops (Figure 4.28a) to wider grains with sharp edges (Figure 4.28c).

To summarize, two different results were obtained regarding the coating adhesion performance and homogeneity of the final coating microstructure with increasing substrate temperature.

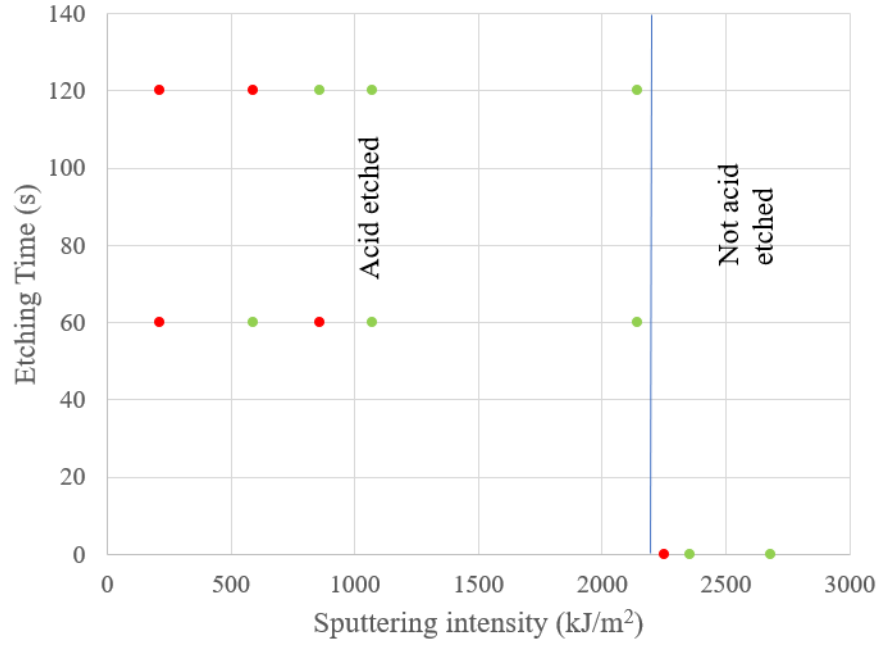
- Higher substrate temperatures provide better coating adhesion. This might correspond to the mobility of the vapour atoms towards the surface which requires that the surface is also at a relatively higher temperature so that the adsorbed vapour atoms have a higher surface diffusivity. This might in turn increase the flux of vapour atoms uniformly distributed over the surface as discussed by Hass et al. [29] and Thornton et al. [30].
- Homogeneity of the final coating microstructure was obtained at higher substrate temperatures. This was verified from studies by Thornton et al. [30] who reported a transition in the grain structure of coatings deposited using electron beam evaporation (an atomistic vapour deposition technique) over substrates with increasing substrate temperature. This transition might have produced inhomogeneity in the final coating microstructure at low temperatures.

4.2.3. Effect of surface pre-treatment process on coating adhesion

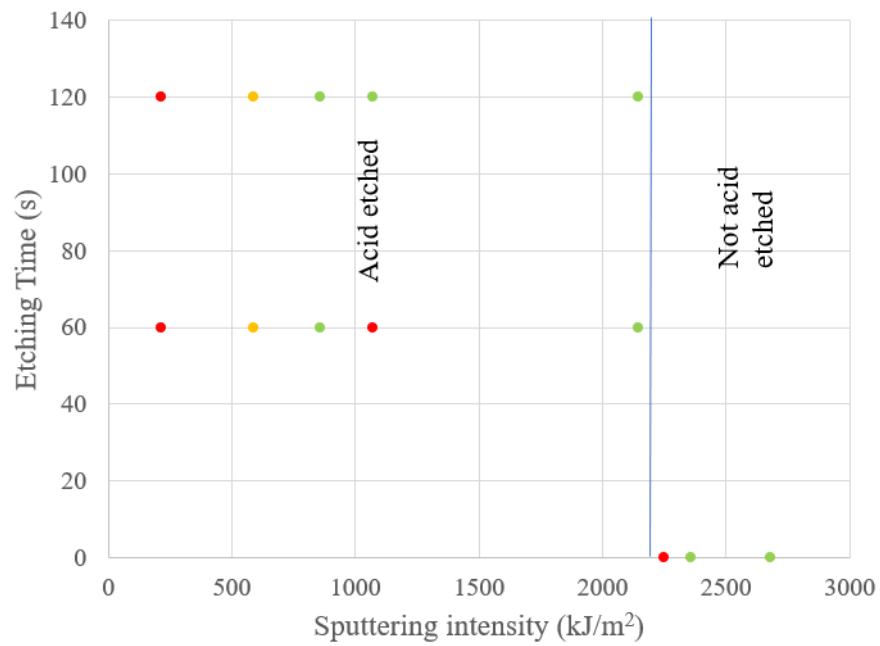
PVD coating depositions were performed on anodic alkaline cleaned DP800 steel substrates which were pre-treated by an acid etching step for which the quality of adhesion of the final coating will be discussed in this section.

The samples were initially etched in a 25°C dilute H₂SO₄ bath in a different laboratory. The acid treated DP800 plates were transferred to the PVD chamber, located in another laboratory, for the sputtering process and coating deposition. During the transfer process, the samples were exposed to air. To prevent this, the samples can be sealed in vacuum packs so that the exposure time is minimised. To remove an initial reoxidised layer, a pre-sputter was done for different samples by decreasing the sputter intensities for each sample starting from 2150 kJ/m² as the main aim of this study is to reduce the sputter intensity as much as possible. An infrared heater was used to heat up the steel substrates in case of lower sputter intensities (<1000 kJ/m² which corresponds to about 300s of sputtering for a sputter power of 200 W) to enable a proper coating adhesion. For this, a constant substrate temperature was maintained for all the acid etched samples after sputtering (200°C). Immediate coating deposition was done after the sputtering process and adhesion tests were performed on the coated samples.

The initial adhesion tests were performed without a vacuum sealing procedure and thus, the samples were exposed to air. Acid etching time versus sputtering intensity plots were made to investigate the transition from a good (OK) to bad (NOK) coating adhesion. Figure 4.29 shows the plots for OT and BMW test results, for which the green dots correspond to OK adhesion, red dots correspond to NOK adhesion and yellow dots corresponds to OK/NOK.



(a)



(b)

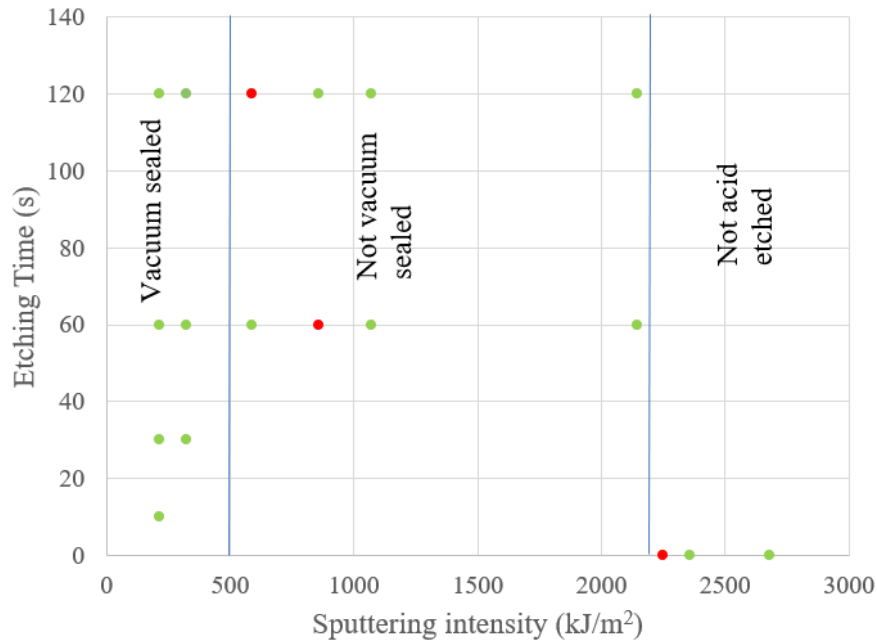
Figure 4.29: Etching time vs Sputter intensity plots for DP800 samples etched in a 25°C dilute H₂SO₄ bath - (a) 0T test results, (b) BMW test results

The plots in Figure 4.29 suggest that a threshold value was reached at a sputter intensity of around 800 kJ/m^2 for which acid etching provided OK adhesion. Below 800 kJ/m^2 provided inconsistent results, for which the adhesion was either OK/NOK or NOK. Thus acid etching provided a reduction in the sputter intensity from an initial 2300 kJ/m^2 to 800 kJ/m^2 , thus showing its effectiveness as a surface pre-treatment step.

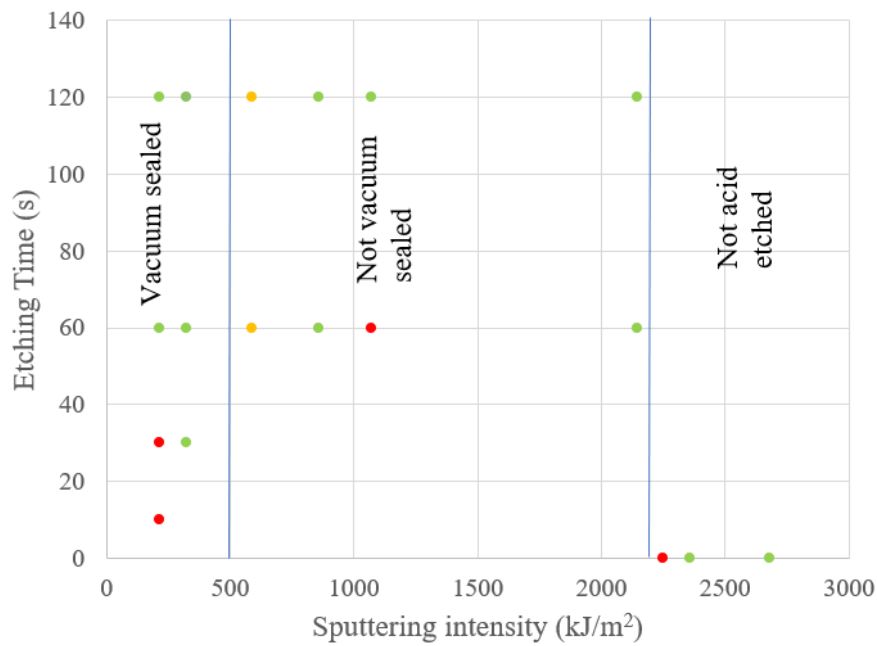
A further reduction in the sputter intensity was required and thus the samples were vacuum sealed before coating. This was done to check whether lower sputter intensities were achieved by retarding the effects of surface reoxidation. Therefore, the etched samples were covered in an aluminium foil, vacuum sealed and then transferred. The sealing was then removed and a thermocouple was welded over the sample to track its temperature during infrared heating. Then the samples were placed on a cart and transferred into the PVD chamber for coating deposition, which took in total of about 8 minutes of air exposure.

A pre-heating was performed using the infrared heater, as the samples were to be sputtered at lower intensities. Two different sputter intensities were used namely, 214 kJ/m^2 and 321 kJ/m^2 (which corresponds to 1 min and 1.5 min of sputter time at 200 W of sputter power respectively). Coating deposition was performed over the steel strips and adhesion tests were done. A comparative plot between vacuum sealed strips and exposed strips was made for acid etching time versus sputtering intensity. Figure 4.30 shows the changes taking place due to the vacuum sealing method.

Plots in Figure 4.30 shows a clear improvement in the coating adhesion with the vacuum sealing method even though the surface was exposed to air for a maximum of 8 min during the process. This might suggest that the reoxidation rate tends to be very slow due to which longer exposure times of even 8 min seems to provide a good coating. However, the transfer of samples took place between two laboratories. This might explain the reason behind the bad coating adhesion results for samples which were not vacuum sealed.



(a)



(b)

Figure 4.30: Comparative acid etching time vs Sputter intensity plots for adhesion tests with and without vacuum sealing etched in a 25°C dilute H₂SO₄ bath - (a) OT test results, (b) BMW test results

At shorter etching times (10s and 30s), the BMW test results provided NOK adhesion even after the vacuum sealing method was used. To investigate the possible reasons for the NOK adhesion obtained, the delaminated part was investigated under SEM/EDX analyses. Figure 4.31 shows the part where the delamination took place for a strip etched for 10s.

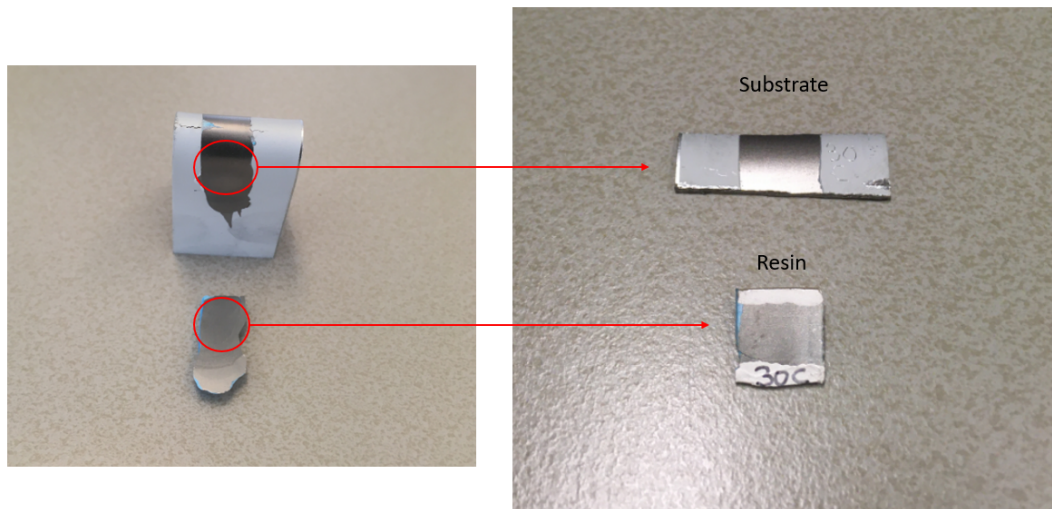


Figure 4.31: Delaminated part of the BMW test results of a strip etched for 10s in a 25°C acid bath and sputtered at 214 kJ/m²

The delamination consists of two different parts - a substrate part and an adhesive (resin) part, as shown in Figure 4.31. The SEM images of the corresponding substrate part and the resin part are shown in Figure 4.32,

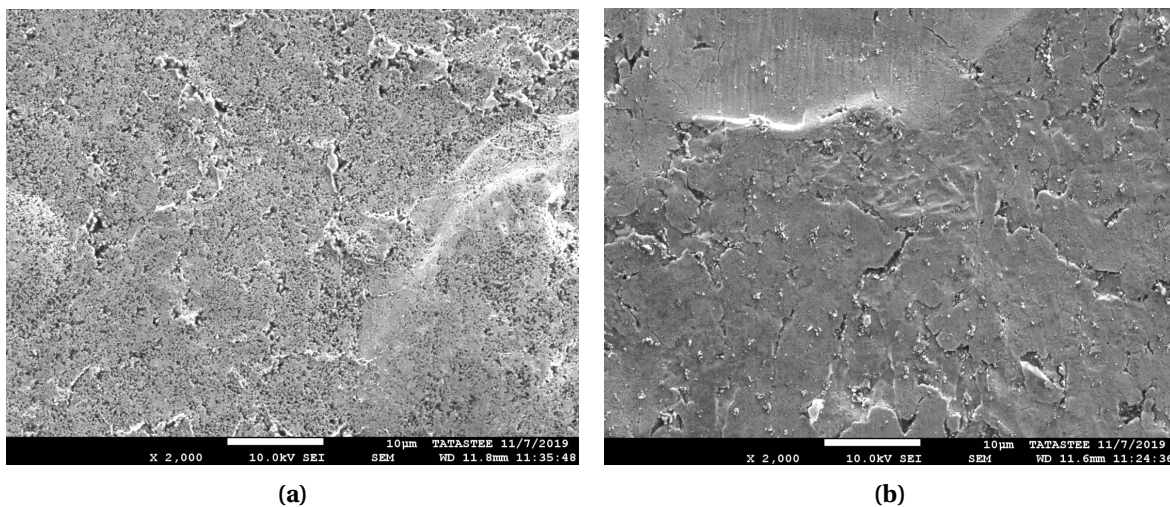


Figure 4.32: SEM images of the delaminated parts - (a) Resin part, (b) Substrate part

First the adhesive part was investigated, which was mostly covered with the delaminated zinc (see Figure 4.32a). At higher magnifications, flake-like substances were observed at certain regions (see Figure 4.33). The number of flakes present per unit surface area on the adhesive was low, due to which there were difficulties in detecting the flakes.

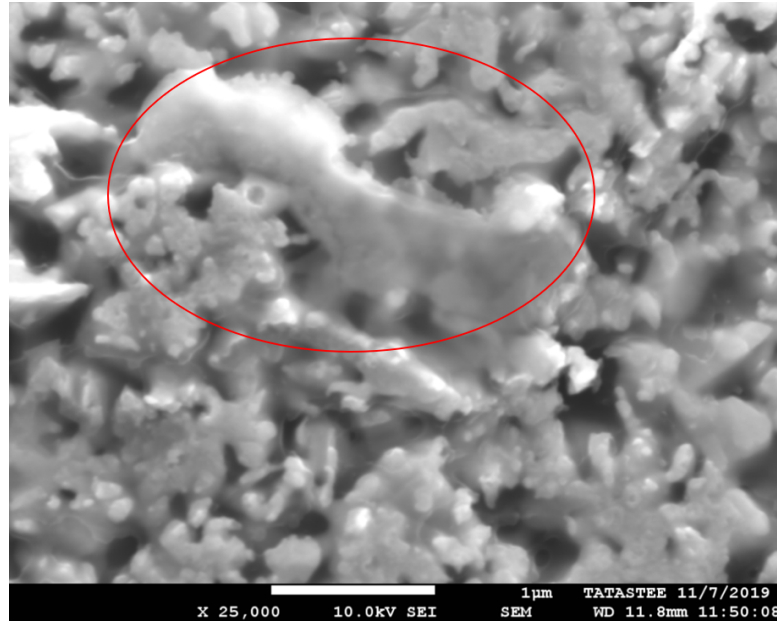


Figure 4.33: SEM image of a flake-like substance over the adhesive part

EDX analyses over the flakes (Figure B.6) revealed the presence of iron. The most likely explanation for the presence of these flakes might be attributed to the BMW testing process, where the bending of the steel strips might have torn off the underlying steel substrate at its topmost surface, producing flakes of iron over the adhesive. Subsequently, the substrate part was investigated using SEM/EDX analyses at higher magnifications as shown in Figure 4.34 to check whether there are other causes that influence the coating adhesion. The substrate was analysed using EDX analyses which revealed high atomic fractions of Mn and Si over the grain boundary regions with more oxygen concentrations (Figure B.7).

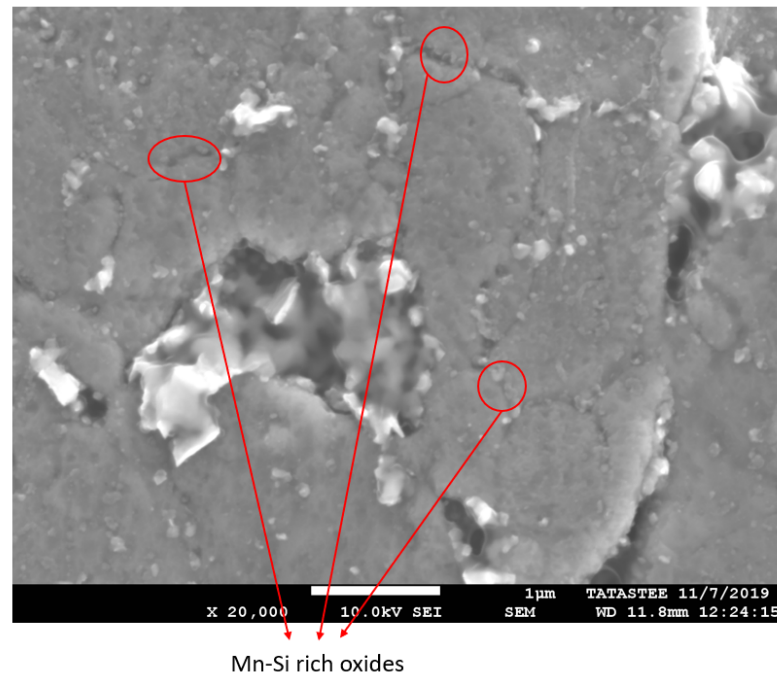


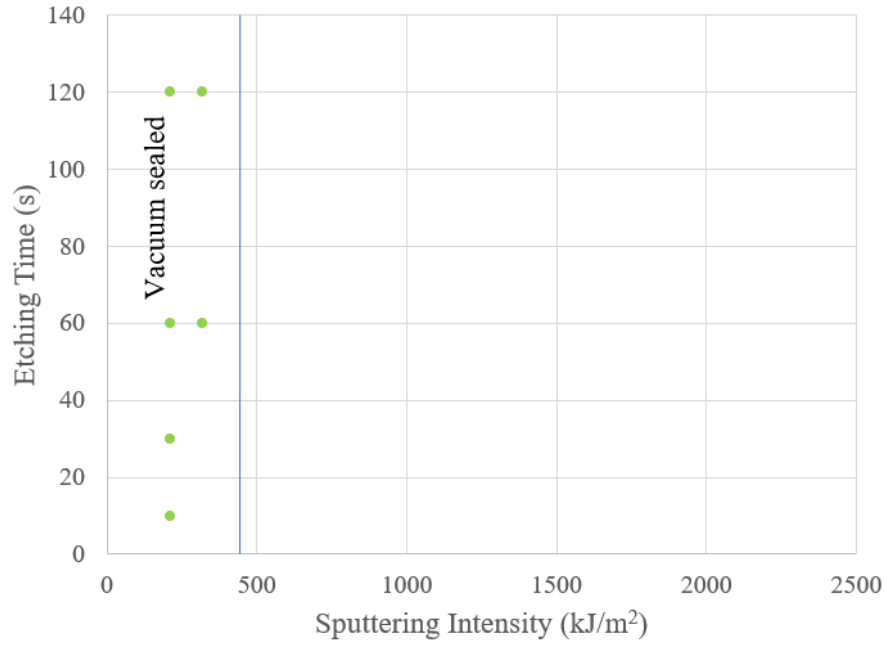
Figure 4.34: SEM image of the substrate part at higher magnifications

Two possible explanations can be derived for the bad coating adhesion at shorter etching times and lower sputter intensities,

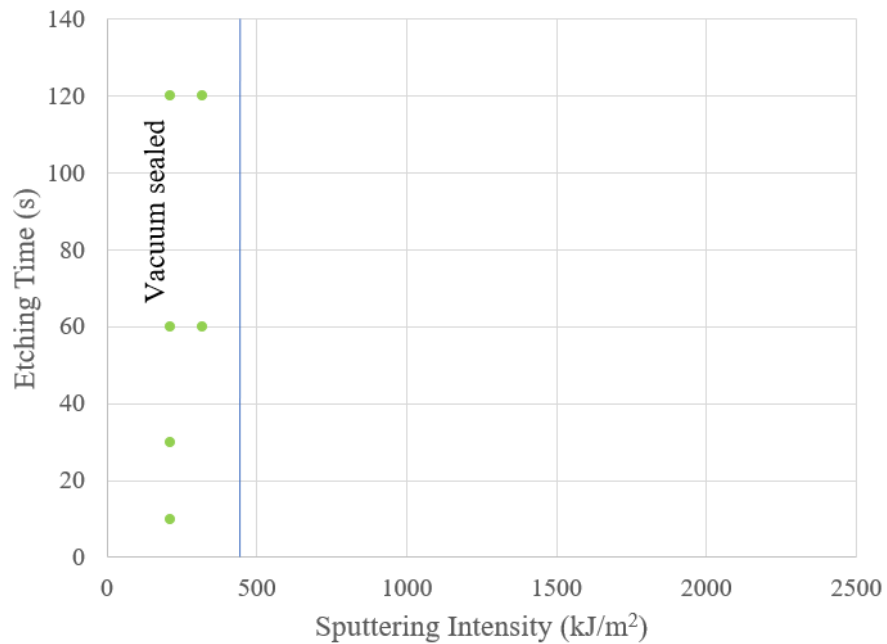
- A partial dissolution of oxides might have taken place at shorter etching times due to which small particles and discontinuous clusters were observed over the surface Figure 4.15. Thus, after a low intensity sputtering step, the oxides may not have been removed completely as the sputter rate tends to be around 0.15 to 0.33 nm/s as stated before in Section 3.2.1. Assuming an average sputter rate of about 0.2 nm/s, 214 kJ/m² of sputter intensity, which corresponds to 1 min of sputtering at 200 W of sputter power, might have only removed 12 nm of depth from the surface of the substrate which might not be enough to remove the remaining surface oxides present over the surface. This can be confirmed with increasing the sputter intensity to 321 kJ/m² (corresponding to 1.5 min of sputtering at 200 W) where OK adhesion was obtained at even 30s of etching time.
- Acid attack on the grains initiated only at higher etching times (60s and 120s) for which the grains appeared rough as discussed earlier in Section 4.1.3. The higher the surface roughness, the higher the surface area available for the contact of zinc vapours on the substrate and thus the better will be the coating adhesion. Thus, surface roughness might have played a role on the coating adhesion of zinc vapours over the surface of the steel substrate.

Therefore, two factors might be involved in obtaining good coating adhesion - surface oxide dissolution and surface roughness. These two factors can be achieved at higher dissolution rates (by increasing the acid bath temperature), where the surface oxides tend to dissolve completely at the surface with grain roughening even at shorter etching times. Figure 4.35 shows the results of adhesion tests with vacuum sealing for strips etched in a 50°C dilute H₂SO₄ bath at various etching times.

Plots in Figure 4.35 confirm that even shorter etching times of 10s provided OK coating adhesion for a sputtering intensity of 214 kJ/m² suggesting that acid etching seems to be an effective surface pre-treatment step in reducing the required sputter intensity from 2300 kJ/m² to 214 kJ/m² which corresponds to a reduction in the sputter intensity by more than a factor of 10.



(a)



(b)

Figure 4.35: Etching time vs sputter intensity plots for vacuum sealed for DP800 samples etched in a 50°C dilute H₂SO₄ bath - (a) 0T test results, (b) BMW test results

Further investigations were performed on the variation of surface morphology of the final coating microstructure at different etching times, to check whether the changes in the surface characteristics of the base substrate might affect the final coating microstructure. Figure 4.36 shows the surface morphologies of the final coating microstructure with increasing etching time for substrates etched in a 25°C dilute H₂SO₄ bath.

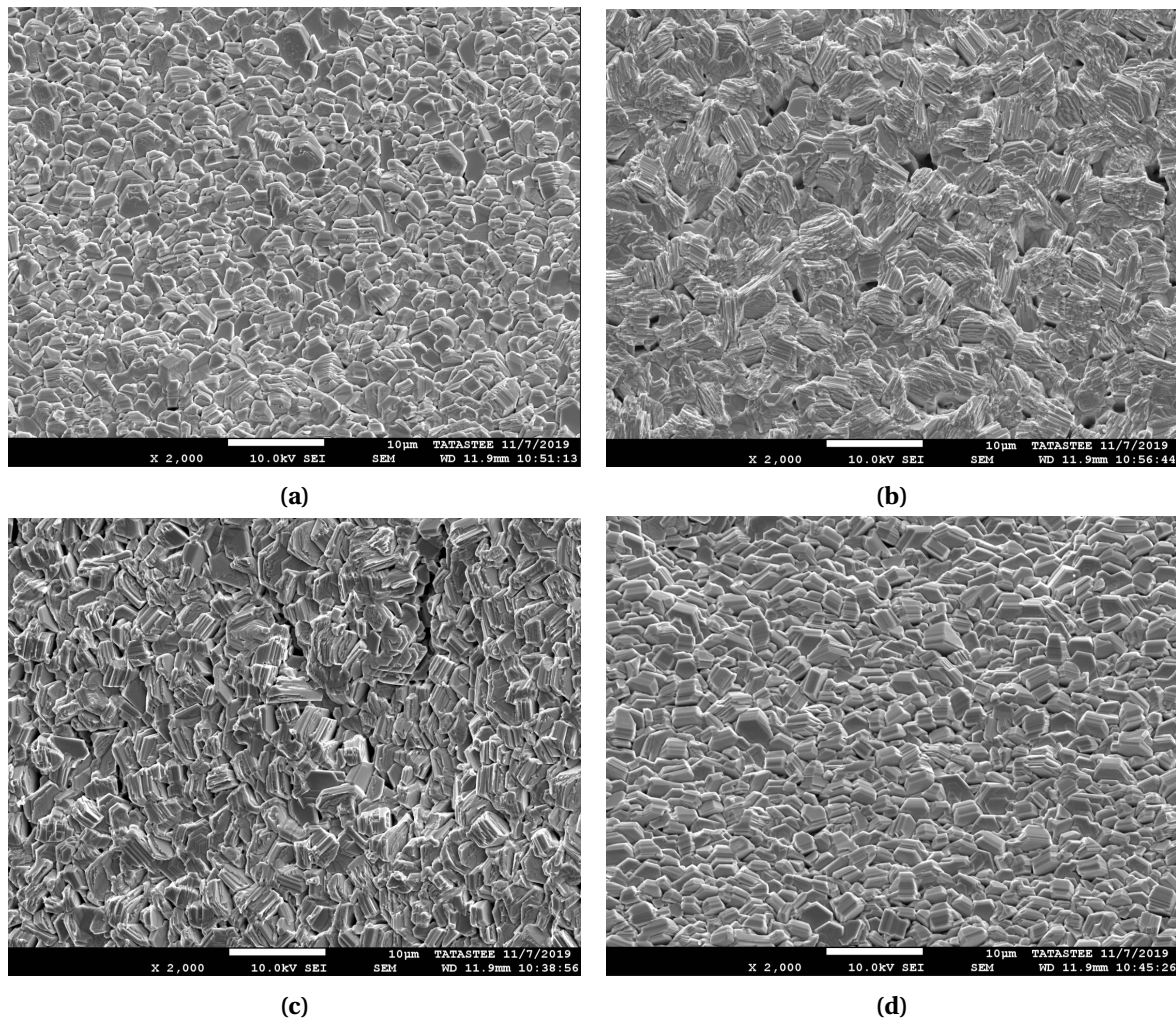
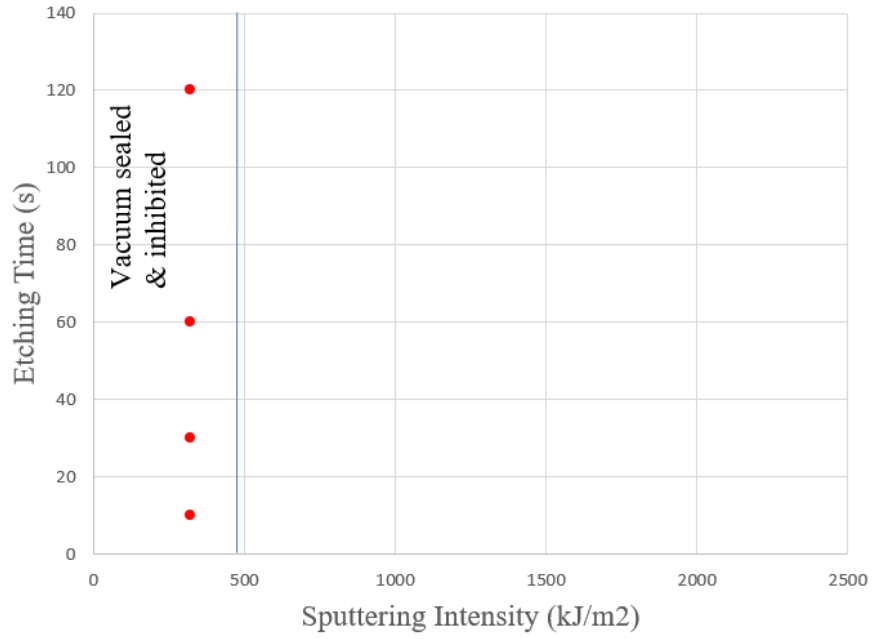


Figure 4.36: Surface morphology of the final coated microstructure of DP800 substrates etched at different etching times in a 25°C dilute H_2SO_4 bath - (a) Etched 10s, (b) Etched 30s, (c) Etched 60s, (d) Etched 120s

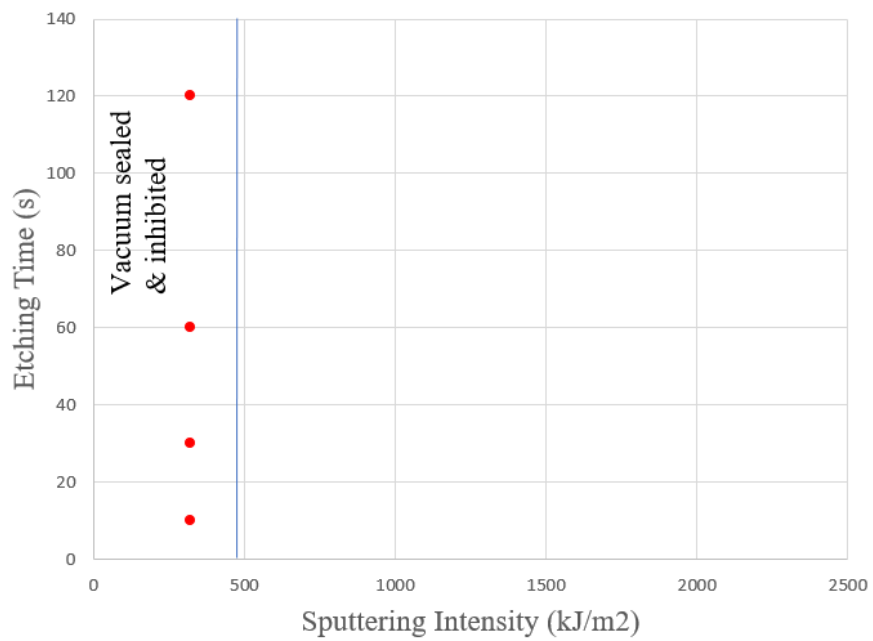
The surface morphology of the zinc crystals seems to be homogeneous irrespective of the etching time. As stated earlier, the temperature of the substrate before the coating deposition was always maintained at about 200°C irrespective of the method of etching. Also, the homogeneity of the crystals seem to depend entirely on the substrate temperature (Section 4.2.2) [30]. This might suggest that the acid etching time does not seem to affect the homogeneity of the final coating microstructure on the substrate.

4.2.4. Effect of corrosion inhibitor during the pre-treatment process on coating adhesion

Addition of corrosion inhibitors after the acid etching process were tested for coating adhesion of zinc vapours over the surface after a pre-sputter step. Here the steel strips were treated in a dilute H_2SO_4 bath at 50°C with the addition of 150 $\mu\text{L}/\text{L}$ inhibitor in the acid bath, after an anodic pre-cleaning step. The strips were immediately transferred into vacuum packs and placed in the PVD chamber for which an allowance of 8 min was considered as exposure time, as explained in Section 4.2.3. The sputter intensity was maintained at 321 kJ/m^2 (corresponding to 1.5 min of sputter time at 200 W of sputter power) to remove any reoxidised layer along with the adsorbed inhibitor molecules over the surface of the steel strip. Coating deposition on the steel strips was performed for which the adhesion test results were obtained from plots in Figure 4.37



(a)



(b)

Figure 4.37: Acid etching time vs Sputter intensity plots for inhibited samples etched in a 25°C dilute H₂SO₄ bath with 150 μL/L inhibitor - (a) OT test results, (b) BMW test results

Adhesion results suggested that a sputter intensity of 321 kJ/m^2 was not enough to provide OK coating adhesion. However, OK adhesion was achieved even at sputter intensities lower than 321 kJ/m^2 for uninhibited samples (Figure 4.30 and Figure 4.35).

Surface analyses were performed for different sputter intensities on samples etched for 120s in a dilute H_2SO_4 bath at 50°C with an inhibitor, to check whether increasing the sputter intensities tend to remove the particles adsorbed on the surface (which were speculated as inhibitor particles from Section 4.1.4). Figure 4.38 shows the SEM images of inhibited samples sputtered with increasing sputter intensities.

Figure 4.38 shows that increasing the sputter intensity gradually removes the adsorbed inhibitor particles, characterised by their absence after 428 kJ/m^2 of sputtering. Thus, higher sputtering intensities might be needed to remove the adsorbed inhibitor particles completely from the surface. But the study focuses on decreasing the required sputter intensity as much as possible. Hence, the addition of an inhibitor during the acid etching pre-treatment might not be feasible for this research study.

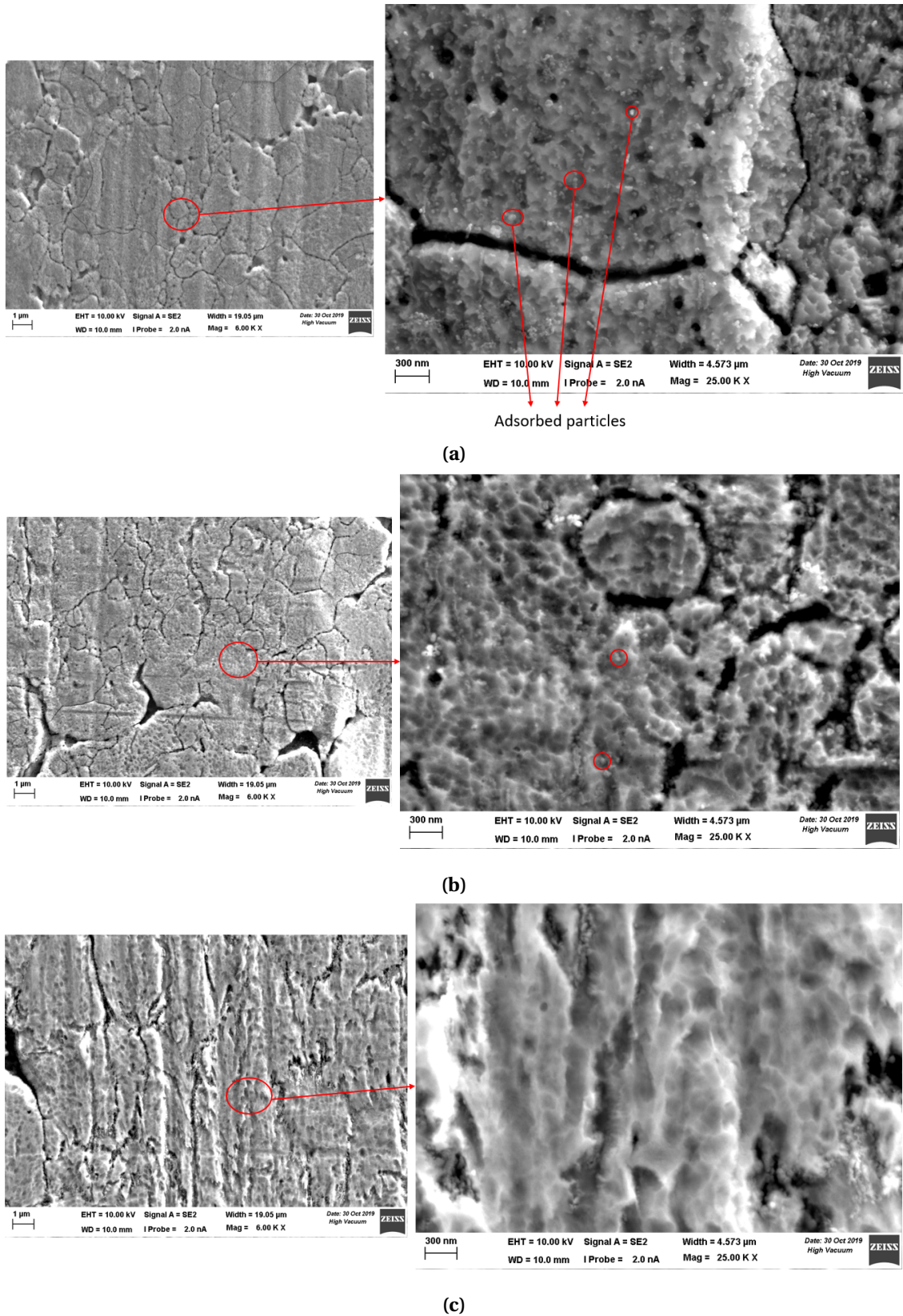


Figure 4.38: Inhibited samples etched for 120s in dilute H_2SO_4 bath at 50°C with $150 \mu\text{L/L}$ inhibitor with increasing sputter intensity - (a) 107 kJ/m^2 , (b) 214 kJ/m^2 , (c) 428 kJ/m^2

5

Conclusions

In the present work, a new surface pre-treatment step was investigated for zinc coating deposition using PVD for cold rolled and annealed DP800 steels-. The study shows that a combination of electrolytic alkaline cleaning and sulphuric acid etching might prove to be an effective surface pre-treatment step as it tends to minimise the required sputter intensity by more than a factor of 10 to provide a good coating adhesion. The effect of these two pre-treatment steps on the surface characteristics and coating adhesion properties of DP800 steel are summarised in this chapter as follows,

- Two types of electrolytic alkaline cleaning were discussed; cathodic and anodic cleaning. Anodic cleaning seems to be more effective than cathodic cleaning as the latter was characterised by discolouration and presence of iron fines over the surface which tends to reduce its surface wettability (Hassel et al. [21]). Surface oxides on anodic cleaned samples remained intact except chromium oxides, which might have undergone a oxidative dissolution in the alkali media.
- Low temperature acid etching (25°C) at shorter etching times seem to partly dissolve the surface oxides and grain boundaries being partly visible, as observed using SEM and EDX analyses. Increasing the etching time roughened the grains after complete surface oxide dissolution with grain boundaries clearly visible due to acid attack.
- Surface oxide dissolution was characterised by a reduction in surface enrichments from 10 wt% to 3.5 wt% for Mn and 6 wt% to 2 wt% for Si along with a decrease in the depth of enrichments for Mn, Si and O from 50 nm to about 10 to 20 nm from the surface, as observed from GDOES depth profile plots. The dissolution was carried out in a dilute sulphuric acid bath at 25°C.
- Increasing the dissolution rate of etching by increasing the acid bath temperature (50°C) dissolved preferential grains over the surface which might correspond to the faster dissolution rates of ferrite over martensite, forming a micro-galvanic cell. Significant grain boundary dissolution was also observed, suggesting that the acid attack was severe on the grain boundary regions.
- Coating deposition performed on acid etched samples seem to have reduced the minimum sputter intensity required from 2300 kJ/m² to about 800 kJ/m² to give OK coating adhesion. A surface reoxidation process might have taken place due to the exposure of steel substrates to air, which formed a thin oxide layer . This layer might have required 800 kJ/m² of sputtering to be removed from the surface before coating.

- Surface reoxidation was evident from XPS spectrum and GDOES plots which suggested the presence of a thin passive iron oxide layer (possibly Fe_2O_3) over the surface even after the acid etching step.
- Retarding the surface reoxidation by a vacuum sealing method reduced the minimum required sputter intensity from 800 kJ/m^2 to a mere 214 kJ/m^2 to obtain OK coating adhesion. The rate of formation of an oxide layer after acid etching might be very low as an allowance of even 8 min exposure time provided OK coating adhesion.
- Low temperature acid etching provided NOK coating adhesion at shorter etching times for a sputter intensity of 214 kJ/m^2 . This might correspond to two effects; partial dissolution of oxides and the absence of rough grains at shorter etching times. These factors were achieved by increasing the dissolution rates of acid etching (by increasing the acid bath temperature) which provided OK adhesion at even shorter etching times for the given sputter intensity.
- Addition of a corrosion inhibitor during the etching process seem to have reduced the surface wettability with increasing etching time as the surface coverage of inhibitor particles (which was speculated) increased, as observed by SEM analyses. Coating adhesion tests on the inhibited samples provided NOK adhesion even at higher etching times and a slightly higher sputter intensity used (321 kJ/m^2) after vacuum sealing. As OK adhesion was obtained for uninhibited samples even at lower sputter intensities (214 kJ/m^2), the addition of corrosion inhibitors in the acid bath was undesired.
- Increasing the substrate temperature before coating deposition seem to increase the coating adhesion properties and homogeneity of the final coating microstructure. A minimum threshold value was obtained at about 147°C above which the coating adhesion performance was good. Also, the homogeneity of the final coating microstructure increased with increasing substrate temperature.

6

Recommendations

- The study was restricted to only one type of steel; DP800, which has a unique surface oxide morphology. Investigating the pre-treatment steps on DP steels of different compositions and processed through different annealing cycles can be performed as a future work.
- Alternating current electrolytic alkaline cleaning can be investigated in the future to study its effect on the surface characteristics of the steel substrate.
- Variations in Mn and Si enrichments for anodic cleaned samples were observed for which no clear explanations were derived. A more detailed study on the effect of anodic cleaning on compositional changes at the surface of the steel can be performed.
- Effects of hydrogen embrittlement and intergranular corrosion due to diffusion of H^+ ions into the steel and grain boundary cracks after etching can be studied in the future, as the corrosion aspects of the steel were not considered in this study.
- Feasibility studies on implementing the pre-treatment step in a continuous line can be performed. Strip speeds can be increased and the effect of spray cleaning instead of immersion using dilute sulphuric acid solutions can be investigated in the future. Also, further reduction in the etching times can be performed by increasing the acid temperature, as the fundamental kinetics of dissolution remain unchanged.

A

Ellingham diagram and Diffusion of alloying elements

A.1. Ellingham diagram - Possible region for RTF process

Depending upon the annealing cycle that the steel is processed through, selective oxidation of major alloying elements takes place. Typical soak temperatures during annealing of DP800 steels was around 800-850 °C for which possible selective oxidation of major alloying elements in the steel like Mn, Si and Cr took place in the RTF during the reduction of FeO. This is determined by Ellingham diagram which is a plot that describes the stability of metal oxides as a function of temperature. It determines the standard Gibbs free energy of oxide formation for metals with dependence on the oxygen potentials and the temperature that they are subjected to. Figure A.1 depicts a standard Ellingham diagram with the possible region at which the RTF process is held during the annealing cycle.

Thus, any metal oxide formation below the circled region tend to have a negative Gibbs free energy, suggesting a favourable reaction for the formation of oxides and vice-versa. Hence, in this study, the formation of Cr, Mn and Si based oxides were more favourable as they are the major alloying elements for the DP steel used. External oxidation of these surface oxides might correspond to a RTF process at low oxygen potentials (lower dew point temperatures).

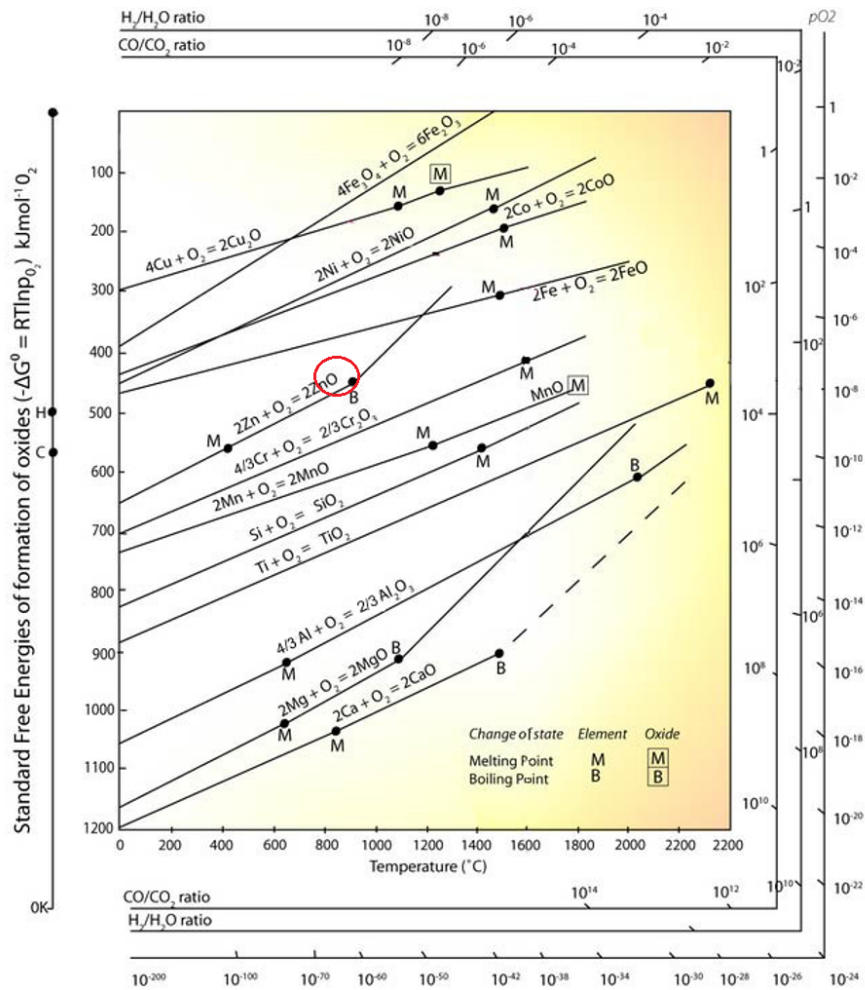


Figure A.1: Ellingham diagram - The circled region might correspond to standard annealing region for RTF processes as determined by Melfo (2007) [9]

A.2. Diffusion of alloying elements

Assuming a soak temperature of about 800°C during annealing (as the annealing parameters were unknown for the given DP800 steel), the Gibbs free energy of formation of the major alloying element oxides from Figure A.1 are given in Table A.1.

Table A.1: Gibbs free energy of oxide formation for major alloying elements

Alloying elements	Gibbs free energy of oxide formation (ΔG°) (kJ/mol)
Mn	-620
Si	-707
Cr	-565

According to Fick's first law of diffusion, the flux of atoms diffusing from a high concentration region to a low concentration region depends on its diffusion coefficient and its concentration gradient. Since the concentration gradient of Mn in the DP steel is very high, the concentration of Mn at the surface of the steel substrate will also be high due to thermal activation during annealing. Both interatomic diffusion and grain boundary diffusion of Mn will be favourable in this case due to its high concentration in the bulk. However, Si and Cr are secondary alloying elements in the steel. Their

diffusion tends to be more favourable through grain boundaries as they seem to be the easiest and the most favourable path for diffusion towards the surface. Interatomic diffusion will be the least favourable due to their low concentrations in the bulk.

Transition from selective external to internal oxidation of alloying elements may also depend on the driving force for surface segregation of those elements. This was explained by Wynblatt et al. [45] stating that the enthalpy of segregation of the corresponding solute atoms determines the driving force. This driving force depends on the configurational energies due to the exchange of solute and the solvent atoms between the bulk and the surface and the elastic strain energy involved. Since this topic is out of scope for the present study, a general view can be obtained where the driving force for segregation of Mn was higher, due to which it tends to form external surface oxides along the grains and the grain boundaries during annealing. Si was segregated only along the grain boundaries possibly due to its low driving force for segregation towards the surface. However, high permeability of oxygen to diffuse through the grain boundaries to form Si-based oxides at the sub-surface layers might have shown higher enrichments of Si at the surface (Figure 4.3b).

B

EDX results

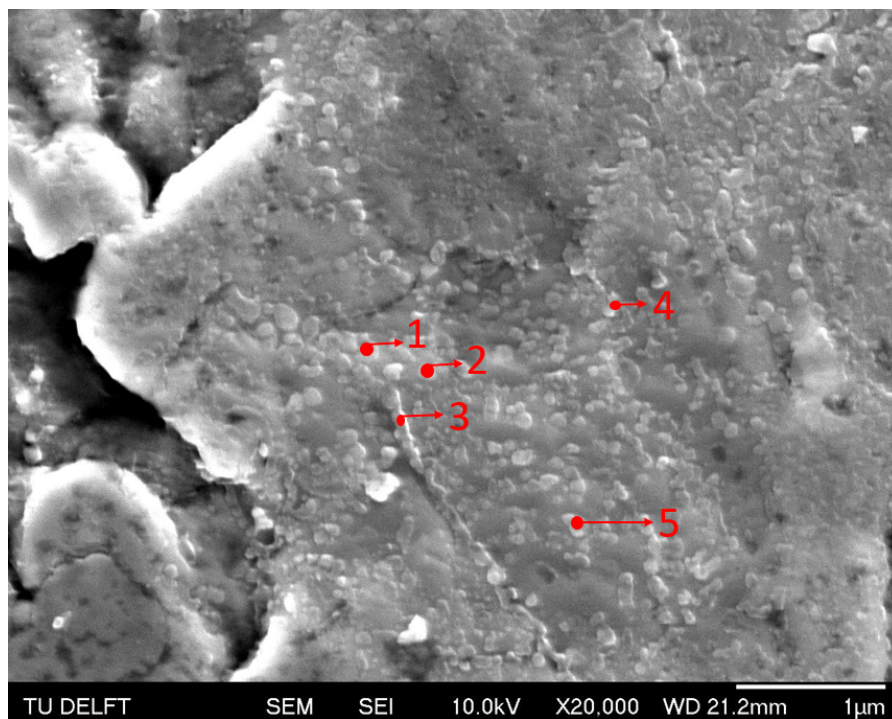


Figure B.1: EDX analysis of untreated DP800 sample

Table B.1: Atomic fractions (At%) of major elements for points in Figure B.1

Pt \ At %	C	O	Si	Cr	Mn	Fe
1	1.7	1.7	1.4	1.5	14.3	79.2
2	3.8	4.5	2.2	1.0	5.2	83.3
3	2.4	7.2	4.1	0.7	11.6	73.6
4	2.8	7.4	4.0	0.9	12.9	71.6
5	3.5	1.6	0.6	0.0	8.8	85.5

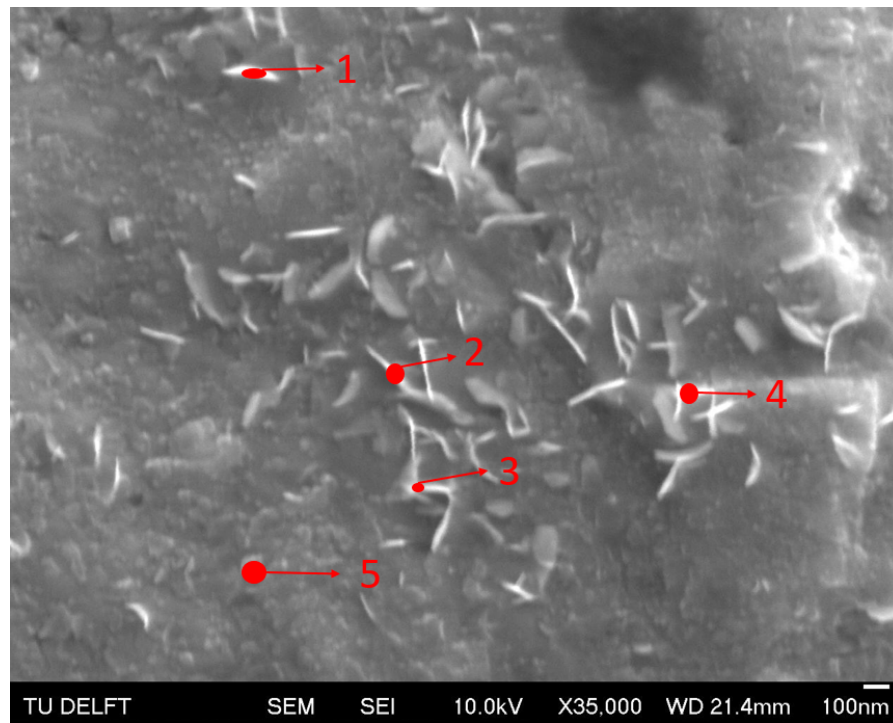


Figure B.2: EDX analysis of a cathodic cleaned DP800 sample

Table B.2: Atomic fractions (At%) of major elements for points in Figure B.2

Pt \ At %	C	O	Si	Cr	Mn	Fe
1	3.3	0.2	0.1	0.9	0.8	94.6
2	3.8	0.2	0.3	0.0	0.9	94.3
3	2.6	0.8	0.7	0.6	0.0	92.5
4	5.4	1.9	0.6	0.3	0.8	90.2
5	2.0	1.2	0.9	0.5	7.9	87.2

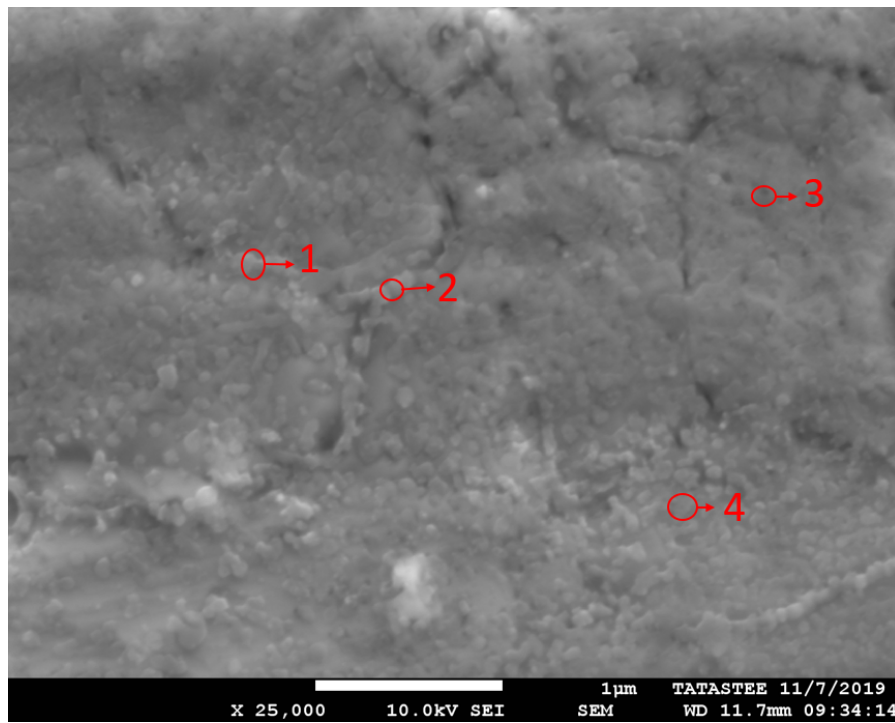


Figure B.3: EDX analysis of an anodic cleaned DP800 sample

Table B.3: Atomic fractions (At%) of major elements for points in Figure B.3

Pt \ At %	C	O	Si	Cr	Mn	Fe
1	2.3	5.8	2.4	0.9	6.9	81.8
2	2.0	6.5	2.6	0.5	7.9	80.6
3	2.7	2.4	1.2	1.5	4.2	87.9
4	2.6	3.6	1.8	0.9	6.0	85.2

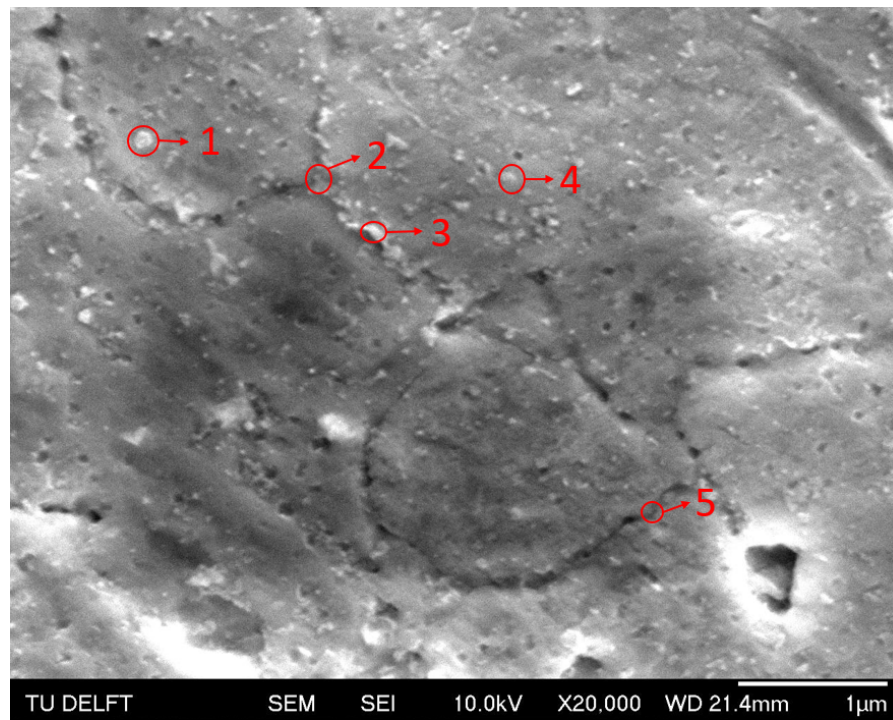


Figure B.4: EDX analysis of an acid etched DP800 sample etched for 10s in a 25°C dilute H_2SO_4 bath

Table B.4: Atomic fractions (At%) of major elements for points in Figure B.4

Pt \ At %	C	O	Si	Cr	Mn	Fe
1	3.3	1.4	0.2	2.8	4.4	87.0
2	1.8	3.3	2.0	0.5	7.9	84.4
3	2.9	2.7	1.5	0.0	7.9	84.0
4	2.6	0.0	0.6	2.0	6.2	88.3
5	0.9	2.6	2.6	0.0	13.8	80.1

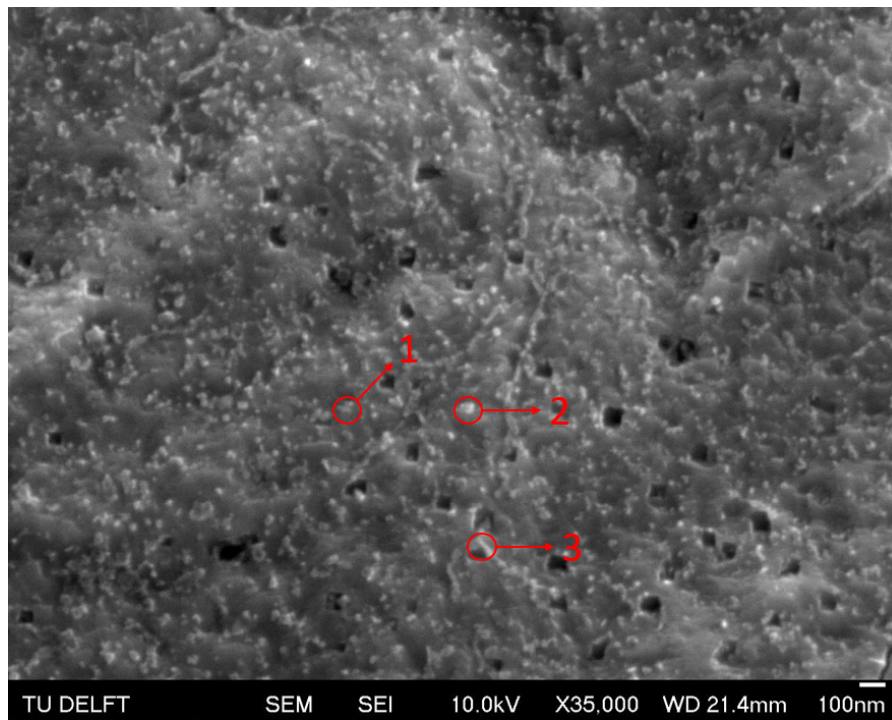


Figure B.5: EDX analysis of an acid etched and inhibited DP800 sample etched for 120s in a 50°C dilute H₂SO₄ bath with 150 μL/L inhibitor added

Table B.5: Atomic fractions (At%) of major elements for points in Figure B.5

Pt \ At %	C	O	Si	S	Cr	Mn	Fe
1	2.4	0.0	0.2	0.3	0.5	0.8	95.5
2	3.4	0.0	0.5	0.0	0.3	3.4	92.0
3	2.4	1.3	0.1	0.2	1.7	2.0	92.1

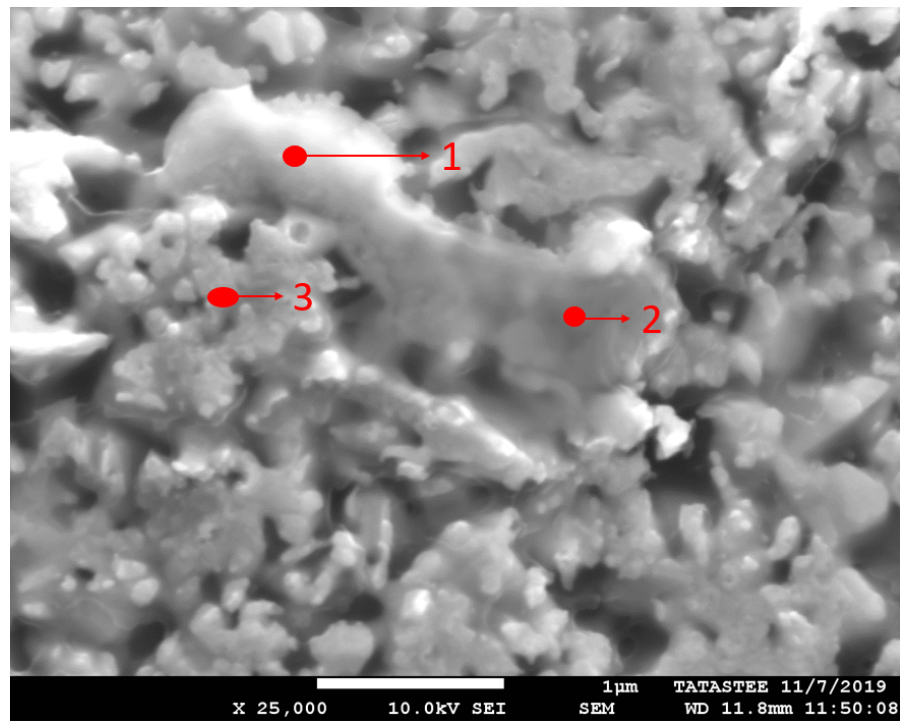


Figure B.6: EDX analysis of a flake-like substance over the adhesive part of the delamination

Table B.6: Atomic fractions (At%) of major elements for points in Figure B.6

Pt \ At %	C	O	Fe	Zn
1	21.2	4.5	35.8	38.5
2	39.2	4.3	18.9	37.6
3	11.6	2.1	1.3	85.0

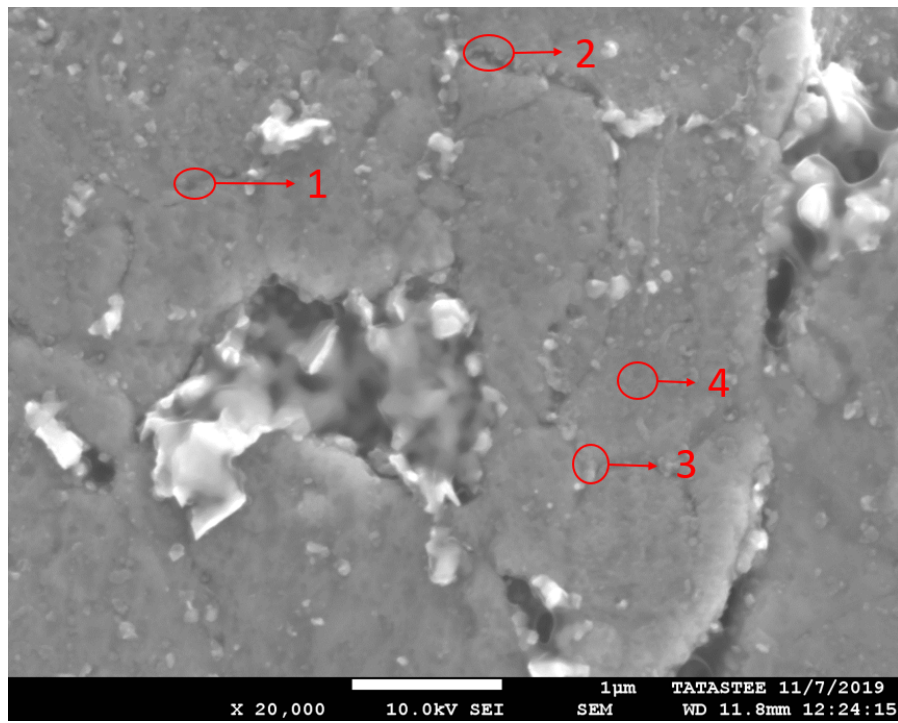


Figure B.7: EDX analysis of the substrate part of the delamination

Table B.7: Atomic fractions (At%) of major elements for points in Figure B.7

Pt \ At %	C	O	Si	Cr	Mn	Fe	Zn
1	2.0	3.6	2.0	0.7	6.7	82.8	2.2
2	2.2	8.1	2.6	0.6	8.3	73.1	4.7
3	2.0	4.6	2.1	0.9	5.4	82.1	2.8
4	2.9	0.0	0.4	0.6	1.6	92.3	2.2

C

Contact angle vs Exposure Time measurements

Effect on the surface wettability of acid etched steel samples was analysed with respect to exposure time to check whether a minimum threshold value for the exposure time can be determined. For this, several steel samples were prepared with anodic alkaline cleaning, etched in a 25°C dilute H₂SO₄ bath for 60s, neutralised with NaOH, rinsed and exposed for the desired amount of time to perform sessile drop experiments with demineralised water as the reference liquid droplet.

A plot was made with respect to the contact angle of the liquid droplet with respect to the exposure times of the steel samples. Figure C.1 depicts the variations in contact angle of the liquid droplet as a function of exposure time.

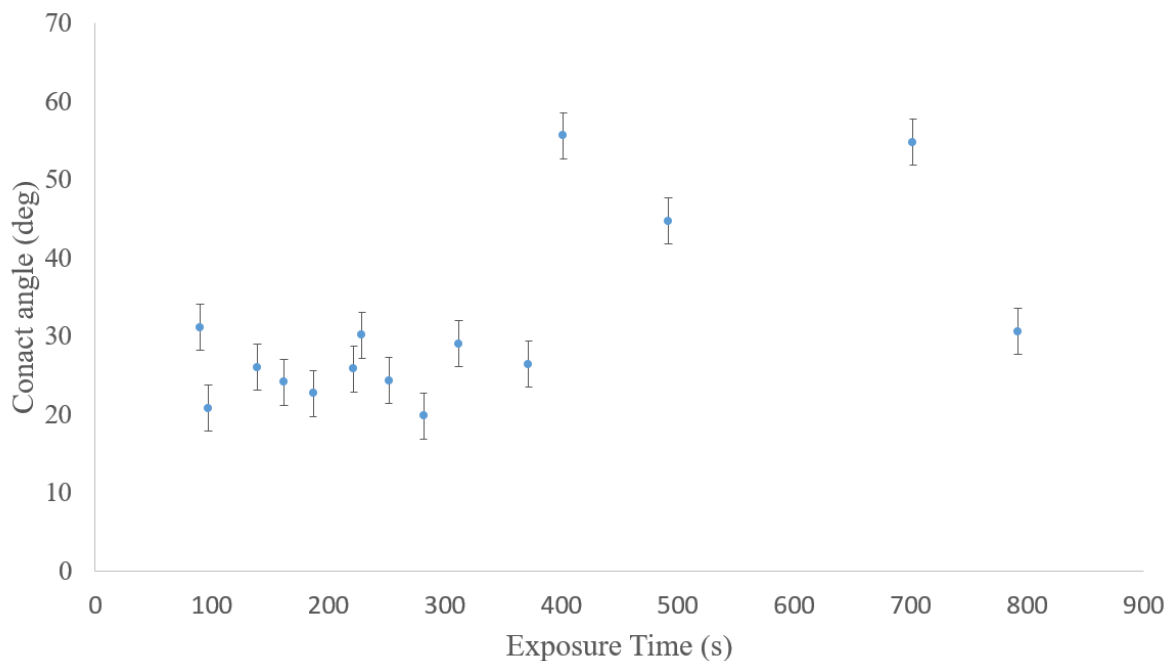


Figure C.1: Contact angle vs Exposure time for DP800 samples etched in a 25°C dilute H₂SO₄ bath for 60s

Figure C.1 shows that higher contact angles were obtained after exposure times of about 400s for

which the steel tends to lose its work of adhesion with the liquid droplet. However, lower contact angles were also obtained after about 750 s of exposure time suggesting better surface wettability of the steel. Inconsistencies in the results were obtained during the measurement due to several factors involved. Samples were changed frequently for different measurements, which might lead to random errors during the measurement. The sessile drop setup allowed only for three contact angle measurements for each sample. Another possibility might correspond to the possible adsorption of a water film during the rinsing process. Thus, contact angle measurements were also performed without a rinsing step after etching and neutralising as shown in Figure C.2.

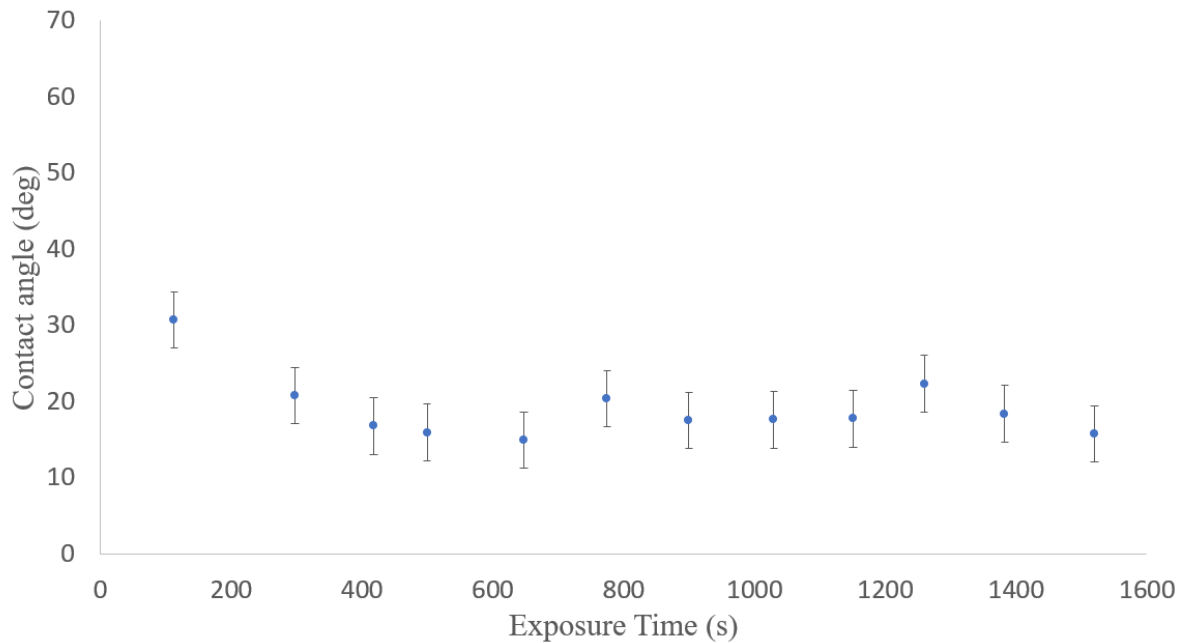


Figure C.2: Contact angle vs Exposure time for DP800 samples etched in a 25°C dilute H₂SO₄ bath for 60s without a rinsing step

The contact angles of the liquid droplet seem to have reduced compared to the values obtained in Figure C.1. However, no proper trend was obtained between the contact angle and exposure times. Thus the sessile drop experiment was not considered a suitable analysis for the determination of a minimum exposure time required for the steel, so that the samples can be transferred from the acid etching step to the PVD coating chamber.

Bibliography

- [1] Carrie M. Tamarelli. AHSS 101: The evolving use of advanced high-strength steel for automotive applications. *Steel Market Development Institute*, page 42, 2011.
- [2] Roumen H. Petrov, Jurij Sidor, and Leo A.I. Kestens. Advanced High-Strength Steels: Microstructure and Texture Evolution. *Encyclopedia of Iron, Steel, and Their Alloys*, (July):70–99, 2016. doi: 10.1081/e-eisa-120050410.
- [3] Enbao Pan, Hongshuang Di, Guangwei Jiang, and Chengren Bao. Effect of heat treatment on microstructures and mechanical properties of hot-dip galvanized DP steels. *Acta Metallurgica Sinica (English Letters)*, 27(3):469–475, 2014. ISSN 21941289. doi: 10.1007/s40195-014-0066-y.
- [4] David K Matlock, John G Speer, Emmanuel De Moor, and Paul J Gibbs. Recent Developments in Advanced High Strength Sheet Steels for. *Jestech*, 15(1):1–12, 2012.
- [5] Marion Calcagnotto, Dirk Ponge, and Dierk Raabe. On the effect of manganese on grain size stability and hardenability in ultrafine-grained ferrite/martensite dual-phase steels. *Metallurgical and Materials Transactions A: Physical Metallurgy and Materials Science*, 43(1):37–46, 2012. ISSN 10735623. doi: 10.1007/s11661-011-0828-3.
- [6] Yun Han, Shuang Kuang, Hua sai Liu, Ying hua Jiang, and Guang hui Liu. Effect of Chromium on Microstructure and Mechanical Properties of Cold Rolled Hot-dip Galvanizing DP450 Steel. *Journal of Iron and Steel Research International*, 22(11):1055–1061, 2015. ISSN 1006706X. doi: 10.1016/S1006-706X(15)30112-6. URL [http://dx.doi.org/10.1016/S1006-706X\(15\)30112-6](http://dx.doi.org/10.1016/S1006-706X(15)30112-6).
- [7] A.R. Marder. The metallurgy of zinc-coated steel. *Progress in Materials Science*, 45(3):191 – 271, 2000. ISSN 0079-6425. doi: [https://doi.org/10.1016/S0079-6425\(98\)00006-1](https://doi.org/10.1016/S0079-6425(98)00006-1). URL <http://www.sciencedirect.com/science/article/pii/S0079642598000061>.
- [8] W Mao. *Oxidation Phenomena in Advanced High Strength Steels: Modelling and Experiment*. PhD thesis, Delft University of Technology, 2018.
- [9] Wanda Melfo. Selective oxidation on AHSS during continuous annealing and the consequences for zinc wettability. *TATA Steel internal report*, 2007.
- [10] I. Parezanović. Selective Oxidation and Segregation in Commercial Steels and Model Alloys (Tools for improving the Surface Wettability by liquid Zn during Hot Dip Galvanizing). 2005: 213, 2005.
- [11] Yoshitsugu Suzuki, Takako Yamashita, Yoshiharu Sugimoto, Sakae Fujita, and Shu Yamaguchi. Thermodynamic analysis of selective oxidation behavior of Si and Mn-added steel during recrystallization annealing. *Tetsu-To-Hagane/Journal of the Iron and Steel Institute of Japan*, 96(1):11–20, 2010. ISSN 00211575. doi: 10.2355/tetsutohagane.96.11.
- [12] P.J.L. Fernandes, R.E. Clegg, and D.R.H. Jones. Failure by liquid metal induced embrittlement. *Engineering Failure Analysis*, 1(1):51–63, 1994.

- [13] J Carpio, JA Casado, JA Álvarez, and F Gutiérrez-Solana. Environmental factors in failure during structural steel hot-dip galvanizing. *Engineering Failure Analysis*, 16(2):585–595, 2009.
- [14] B. Navinšek, P. Panjan, and I. Milošev. PVD coatings as an environmentally clean alternative to electroplating and electroless processes. *Surface and Coatings Technology*, 116-119:476–487, 1999. ISSN 02578972. doi: 10.1016/S0257-8972(99)00145-0.
- [15] MJ Carr and MJ Robinson. The effects of zinc alloy electroplating on the hydrogen embrittlement of high strength steels. *Transactions of the IMF*, 73(2):58–64, 1995.
- [16] S Sabooni, E Galinmoghaddam, HT Cao, RJ Westerwaal, E Zoestbergen, J Th M De Hosson, and YT Pei. New insight into the loss of adhesion of ZnMg-Zn bi-layered coatings on steel substrates. *Surface and Coatings Technology*, 2019.
- [17] E. Bouwens R.J. Westerwaal, C. Commandeur. In-house developed Ar plasma sputter system for surface preparation of steel sheets. *TATA Steel Internal report*.
- [18] Andreas Borst. Acid etching steel substrate pre-treatment for the physical vapor coating deposition. (July), 2018.
- [19] NV Mandich. Surface preparation of metals prior to plating. *Metal finishing*, 101(9):8–22, 2003.
- [20] ASM Handbook. Surface Engineering, vol. 5. *ASM International, Materials Park, OH*, page 240, 1994.
- [21] Achim Walter Hassel, K Bruder, V Denoose, A Hennion, Xavier Vanden Eynde, M Fiorucci, H Oberhoffer, H Baulig, J Gerdenitsch, and M Wolpers. New approaches in electrolytic cleaning of cold rolled steel sheet. *Research Fund for Coal and Steel*, 2011.
- [22] Nabil Zaki. Electrocleaning. *Metal Finishing*, 98(1):134 – 139, 2000. ISSN 0026-0576. doi: [https://doi.org/10.1016/S0026-0576\(00\)80318-9](https://doi.org/10.1016/S0026-0576(00)80318-9). URL <http://www.sciencedirect.com/science/article/pii/S0026057600803189>.
- [23] M. J L Gines, G. J. Benitez, T. Perez, E. Merli, M. A. Firpo, and W. Egli. Study of the picklability of 1.8 mm hot-rolled steel strip in hydrochloric acid. *Latin American Applied Research*, 32(4): 281–288, 2002. ISSN 03270793.
- [24] B. G. Ateya, B. E. El-Anadouli, and F. M. El-Nizamy. The adsorption of thiourea on mild steel. *Corrosion Science*, 24(6):509–515, 1984. ISSN 0010938X. doi: 10.1016/0010-938X(84)90033-7.
- [25] Bogumił Eugeniusz Brycki, Iwona H. Kowalczyk, Adrianna Szulc, Olga Kaczerewska, and Marta Pakiet. Organic Corrosion Inhibitors. In Mahmood Aliofkhaezaei, editor, *Corrosion Inhibitors, Principles and Recent Applications*, chapter 1. IntechOpen, Rijeka, 2018. doi: 10.5772/intechopen.72943. URL <https://doi.org/10.5772/intechopen.72943>.
- [26] I. Singh. Inhibition of steel corrosion by thiourea derivatives. *Corrosion*, 49(6):473–478, 1993. ISSN 00109312. doi: 10.5006/1.3316074.
- [27] Donald M Mattox. *Handbook of physical vapor deposition (PVD) processing - Ch.1:1-5, Ch.6:195-200, Ch.13:523-524*. William Andrew, 2010.
- [28] R.J. Westerwaal E. Bouwens. Custom-made single steel sheet transport system for the PVD process. *TATA Steel Internal report*.

- [29] D. D. Hass, Y. Y. Yang, and H. N.G. Wadley. Pore evolution during high pressure atomic vapor deposition. *Journal of Porous Materials*, 17(1):27–38, 2010. ISSN 13802224. doi: 10.1007/s10934-008-9261-4.
- [30] John A. Thornton. INFLUENCE OF SUBSTRATE TEMPERATURE AND DEPOSITION RATE ON STRUCTURE OF THICK SPUTTERED Cu COATINGS. *J Vac Sci Technol*, 12(4):830–835, 1975. ISSN 0022-5355. doi: 10.1116/1.568682.
- [31] *Cold-rolled DP800-UC*, 2016. URL https://www.tatasteeleurope.com/static_files/Downloads/Automotive/Data%20Sheets/Tata%20Steel%20AM%20-%20CR%20DP800-UC%20-%20datasheet%20EN.pdf.
- [32] American society for testing and materials. standard practice for checking the operating characteristics of x-ray photoelectron spectrometers (e902-88). *Surface and Interface Analysis*, 17(12):889–892, 1991. doi: 10.1002/sia.740171208. URL <https://onlinelibrary.wiley.com/doi/abs/10.1002/sia.740171208>.
- [33] Konrad Terpilowski, Lucyna Hołysz, Diana Rymuszka, and Robert Banach. Comparison of contact angle measurement methods of liquids on metal alloys. *Annales UMCS, Chemia*, 71:89, 05 2016. doi: 10.17951/aa.2016.71.1.89.
- [34] Georgios M Kontogeorgis and Sören Kiil. *Introduction to applied colloid and surface chemistry, Ch.2:10-18, Ch.3:39-43, Ch.4:74-76*. Wiley Online Library, 2016.
- [35] *NIST XPS DATABASE*. URL https://srdata.nist.gov/xps/main_search_menu.aspx.
- [36] K S Shin, S H Park, S H Jeon, D C Bae, and Y M Choi. Characterization of the Galvanizing Behavior Depending on Annealing Dew Point and Chemical Composition in Dual-Phase Steels Characterization of the Galvanizing Behavior Depending on Annealing Dew Point and Chemical Composition in Dual-Phase Steels. (November 2009), 2016.
- [37] V. Irmer and M. Feller-Kniepmeier. Diffusion of manganese in α -iron single crystals of different purity. *Journal of Physics and Chemistry of Solids*, 33(11):2141 – 2148, 1972. ISSN 0022-3697. doi: [https://doi.org/10.1016/S0022-3697\(72\)80244-0](https://doi.org/10.1016/S0022-3697(72)80244-0). URL <http://www.sciencedirect.com/science/article/pii/S0022369772802440>.
- [38] A. P. Grosvenor, E. M. Bellhouse, A. Korinek, M. Bugnet, and J. R. McDermid. XPS and EELS characterization of Mn₂SiO₄, MnSiO₃ and MnAl₂O₄. *Applied Surface Science*, 379:242–248, 2016. ISSN 01694332. doi: 10.1016/j.apsusc.2016.03.235.
- [39] Barbara Zydorczak, Peter M. May, Danielle P. Meyrick, David Bátka, and Glenn Hefter. Dissolution of Cr₂O₃(s) and the behavior of chromium in concentrated NaOH solutions. *Industrial and Engineering Chemistry Research*, 51(51):16537–16543, 2012. ISSN 08885885. doi: 10.1021/ie302096e.
- [40] Yongchao Si. Dissolution Behavior of Dual Phase Steel during Pickling. *United States Steel Corporation, Research and Technology Center*, 2018.
- [41] K Fushimi, K Yanagisawa, T Nakanishi, Y Hasegawa, T Kawano, and M Kimura. Electrochimica Acta Microelectrochemistry of dual-phase steel corroding in 0.1 M sulfuric acid. *Electrochimica Acta*, 114:83–87, 2013. ISSN 0013-4686. doi: 10.1016/j.electacta.2013.09.162. URL <http://dx.doi.org/10.1016/j.electacta.2013.09.162>.

- [42] F. K. Crundwell. The mechanism of dissolution of minerals in acidic and alkaline solutions: Part I - A new theory of non-oxidation dissolution. *Hydrometallurgy*, 149:252–264, 2014. ISSN 0304386X. doi: 10.1016/j.hydromet.2014.06.009. URL <http://dx.doi.org/10.1016/j.hydromet.2014.06.009>.
- [43] M Martin and E Fromm. Low-temperature oxidation of metal surfaces I. 258:7–16, 1997.
- [44] A P Grosvenor. Examination of the oxidation of iron by oxygen using X-ray photoelectron spectroscopy and QUASES TM. 565:151–162, 2004. doi: 10.1016/j.susc.2004.06.210.
- [45] P. Wynblatt and R. C. Ku. Surface energy and solute strain energy effects in surface segregation. *Surface Science*, 1977. ISSN 00396028. doi: 10.1016/0039-6028(77)90462-9.